DESIGN AND USE OF A TWO-DIMENSIONAL PROPORTIONAL COUNTER IN A STUDY OF THE BREAKUP AND DECAY OF STATES IN ^{10}B.

by

ALI AKBAR MIRZAI

A THESIS

Submitted to the Faculty of Graduate Studies

in Partial Fulfillment of the

Requirements for the Degree

MASTER OF SCIENCE

Department of Physics

University of Manitoba

Winnipeg, Manitoba 

ISBN 0-315-37288-5

DESIGN AND USE OF A TWO-DIMENSIONAL PROPORTIONAL COUNTER IN A STUDY OF THE BREAKUP AND DECAY OF STATES IN ^{10}B

BY

ALI AKBAR MIRZAI

A thesis submitted to the Faculty of Graduate Studies of the University of Manitoba in partial fulfillment of the requirements of the degree of

MASTER OF SCIENCE

ABSTRACT

A two-dimensional position sensitive proportional counter, for use in conjunction with a surface barrier detector, has been designed and constructed. The main design criteria were to produce a counter of simple construction and readout, low cost, and acceptable spatial resolution in two dimensions. The counter was tested under different conditions of gas pressure, bias voltage, and rate of gas flow. The gas pressure of 0.16 atm and bias voltage between 680 and 720 volts were optimum values in improving the position resolution. The measured intrinsic position resolution (full-width at half maximum) in the vertical and horizontal directions was as 1.4 mm and 1.3 mm respectively.

The proportional counter has been used in a coincidence study of the breakup of states in ^{10}B to measure the branching ratios for gamma and particle (alpha and proton) decay. For this study, the $^{13}C(p,\alpha)^{10}B$ reaction was used with a proton beam from the University of Manitoba Cyclotron at an energy of 40.45 MeV leading to several excited states of ^{10}B.

The energy resolution was greatly improved by calculating the scattering angle and applying a kinematic correction which was made possible by the use of the X-Y counter. The full-width at half maximum (FWHM) of the g.s., which was 0.356 MeV in raw spectrum, was improved to 0.215 MeV.

The gamma-decaying states of ^{10}B resulting in nearly 100% coincidence detection efficiency between the ^{10}B recoil nuclei and alpha particles were used to calibrate the coincidence detection efficiency.

A Monte Carlo simulation was carried out which took into account beam spot size, beam energy resolution and geometric acceptance of detectors. The theoretical coincidence efficiencies were calculated and compared with the experimental ones. The average ratio between the two results for the first three γ-decaying states was calculated as 1.03 ± 0.01 and this value was used as the normalization factor for the Monte Carlo output in measuring the branching ratios of the particle-decaying states.

Levels were examined in the recoil nucleus (^{10}B) up to the 7.47 MeV in excitation energy with the following results.

- The 0.718, 1.74, 2.15 and 3.59 MeV states are purely γ-decaying states, since they are below any particle thresholds.

- The 4.77 MeV state is primarily α-decaying state ($\bar{\beta}_\alpha \sim 97.7 \pm 2.9$ %). The previously reported value for this state is $\beta_\gamma = 0.23 \pm 0.03$ %.

- The 5.16 MeV state is primarily γ-decaying ($\bar{\beta}_\gamma \sim 78.7 \pm 1.7$ %). The previously reported value is $\beta_\gamma = 87.0 \pm 4.0$ %.
The discrepancy of $\sim$ 8 % is attributed to the two neighbouring, i.e. the 5.11 and 5.18 MeV states which are nearly 100 % alpha-decaying. Due to the excitation of these states, they contribute approximately 10 % to the excitation in the region of the 5.16 MeV state.

- The 6.025 MeV state is primarily α-decaying ($\bar{\beta}_\alpha \sim 99.5 \pm 1.1$%).

The previously reported value is $\beta_\gamma \leqslant 0.9$ %

- The 7.47 MeV state is primarily α- and p-decaying state ($\bar{\beta}_\alpha \sim 50.7 \pm 1.8$ % and $\bar{\beta}_p \sim 51.3 + 2.5$ %). Considering the uncertainties in the α- and p- decaying channels, an upper limit of 1-2 % is assigned to the γ-decaying process.

Acknowledgements

I wish to thank my advisor, Dr. W. Falk who proposed the projects described in this thesis and to acknowledge his ideas, assistance and direction concerning the investigations presented in this work.

I would also like to thank Dr. R.A. Aryainejad and Dr. J. Birchall for their collaboration.

I am grateful to all the cyclotron and computer technical staff for their support and helpfulness.

TABLE OF CONTENTS

CHAPTER 1

Introduction

The subject matter presented in this thesis consists of two major parts. In the first part the design and construction of a small two-dimensional position sensitive proportional counter is discussed, suitable for providing position information over an area of about 2 cm x 2 cm. In the second part the use of this proportional counter in a coincidence study of the breakup of states in ^{10}B is presented. The technique of coincidence measurements in conjunction with the position sensitive counter can be used to measure the branching ratios for γ-decaying and particle-decaying states.

The operation of proportional counters depends on the different processes associated with the motion and the interactions of ions and electrons in gases under the influence of electric fields, and the basic laws of the underlying phenomena have been known for decades (Ch. 79), (Ch 84). They have been used as essential tools during various phases of nuclear science: in high-, intermediate-, and low-energy physics and in many other fields of applied research.

Many of the present-day particle-detectors are based on the ionization produced by the passage of a charged particle through a gas. As a result of inelastic collisions, with a resultant transfer of energy from the moving particle to the molecules of the gas, a number of ion

pairs, i.e., positively charged gaseous ions and free electrons, are produced.

A widely used detector is perhaps the resistive-anode proportional counter using charge division and drift time effects to locate the event. The horizontal position information (position along the anode wire) is extracted using resistive charge division techniques and the vertical position information (distance normal to the wire) is extracted by measuring the time difference between the arrival of the signal from the counter and some timing reference, for example the signal from a surface barrier stopping detector. Although these detectors generally do not give submillimeter resolution, they are preferred because of their low cost, simplicity and ability to transmit the detected particles to backing detectors which serve to reduce background events and to improve particle identification.

Some background information dealing with the general considerations and properties of gaseous ionization chambers is discussed in chapter 2.

Chapter 3 deals with the design and construction of the proportional counter including the gas filling and the electrostatic field calculations. Tests of the counter as well as a description of the electronics used during the experiment are discussed. Finally, calibration information, test results of the position resolution and kinematic correction techniques, are also explained in this chapter.

Position resolution provided by the counter was a little worse than 1 mm, which was quite satisfactory for our experiment. Considering the feature of two-body reactions, kinematic broadening will always be present. However, it is possible to improve the energy resolution by calculating the scattering angle and applying a kinematic correction.

Investigation of the reaction $^{13}C(p,\alpha)^{10}B$, was carried out using the counter in a coincidence study of the breakup of states in ^{10}B, to separate γ-decaying states from particle decaying ones, and to measure the branching ratios for gamma, proton and alpha decay. The results of some (p,α) reactions have been interpreted on the basis of the presence of both compound nuclear and direct reaction transitions or alternatively with a pre-compound decay model. At energies comparable to our experiment, the (p,α) reaction of interest was considered to be direct.

Because of the small momentum carried by γ-rays, γ-decaying states result in nearly 100% coincidence detection efficiency between the ^{10}B recoil nuclei and alpha particles passing through the central region of the X-Y counter. These γ-decaying states were used to calibrate the coincidence detection efficiency. A Monte Carlo simulation was carried out in order to determine the dependence of the coincidence detection efficiency on the various geometrical parameters of the experiment, beam properties, and the reaction under consideration. Experimental considerations together with a detailed data analysis and the results achieved are described in chapter 4.

CHAPTER 2

General Considerations and Properties of Gaseous Ionization Chambers

2-1 Energy-Loss Mechanism

A fast charged particle can undergo several different kinds of interactions while it traverses the gaseous medium of a proportional counter. Of the possible different interactions, the probability of occurrence for electromagnetic interactions is much greater than the others, and hence it forms the basis for charged particle detection. Bethe and Bloch have developed the following relativistic quantum mechanical expression for the energy loss due to the highly probable incoherent Coulomb interactions which result in both excitation and ionization of the atom of the medium (Sa 77).

$$\frac{dE}{dx} = -K \frac{Z}{A} \frac{\rho}{\beta^2} \left\{ \ell n \frac{2mc^2\beta^2 E_m}{I^2(1-\beta^2)} - 2\beta^2 \right\}$$

$$K = \frac{2\pi N z^2 e^4}{mc^2} \cdot \qquad (2\text{-}1)$$

where N is the Avogadro number, m and e are the electron mass and charge, Z, A and ρ are the atomic number and mass, and the density of the medium, respectively, and I is its effective ionization potential; z is the charge and β the velocity (in units of the speed of light c) of the projectile. In the electrostatic system of units, and expressing

energies in MeV,

$K=0.154$ MeV g^{-1} cm^2 for unit charge projectiles.

The quantity E_m represents the maximum energy transfer allowed in each interaction, and two-body relativistic kinematics gives

$$E_m = \frac{2mc^2\beta^2}{1-\beta^2} \quad . \tag{2-2}$$

The light elements and heavy ones have different energy losses in a proportional counter and this difference in energy loss is used for particle identification. The restriction for particle identification is that there should be sufficient energy loss of the particles to be detected, otherwise if the proportional counter is too thin or the gas pressure is too low, the energy loss ΔE as compared to the total energy E will be too small and most probably particle identification cannot be carried out effectively. (For details about this section and the other subjects discussed in this chapter, refer to (Sa 77).)

The energy loss of alpha particles having a typical energy of 5.48 MeV, emitted from a ^{241}Am source, while passing through the proportional counter was calculated as follows (Ja 66), (Sa 84). These results compare closely with the values given by the stopping power tables.

- Energy loss in the entrance window 0.538 MeV
- Energy loss in the gas 0.371 MeV
- Energy loss in the exit window 0.592 MeV

Considering the above energy losses, the energy of outgoing α-particles will be 3.979 MeV. It is to be noted that in calculating the above energy losses, the following points were taken into consideration:

- Since the gas was a mixture of argon and methane, the composition law was used for the gas mixture.

- The proportional counter was operating at 0.16 atm pressure during the experiment, therefore the energy loss calculation was based on this reduced pressure rather than atmospheric pressure.

- An average of 6 mm was added to the internal dimension of the counter to get the gas thickness because of the bulge of the windows.

2-2 Delta Ray Production

There are two ways by which an energetic, heavy, charged particle, such as an alpha, produces the ionization which dissipates its energy in its passage through matter. In the primary collision with the electrons in an atom, the most probable of the ionizing collisions are those in which a relatively slow secondary electron is ejected with kinetic energy smaller than the energy necessary to cause ionizationin in subsequent collisions, i.e. the energy required to remove electrons from atoms. These electrons may attach themselves to neutral atoms, forming negative ions. A small fraction of the ionizing collisions, however, produces secondary electrons of relatively high energy (perhaps several keV) called delta rays. The delta rays themselves then go on to produce further ionization in the atoms of the stopping material, leading to secondary ionization and energy loss, just as any electrons of this

energy would. The total ionization is the sum of the primary ionization and this secondary ionization.

An approximate expression for the probability of an electron receiving the energy E is given by

$$P(E) = K \frac{Z}{A} \frac{\rho}{\beta^2} \frac{X}{E^2} ,$$

which corresponds essentially to the first term in the Bethe-Bloch formula. If the reduced thickness $x = X\rho$ is introduced, and given in gcm^{-2}, the probability will be

$$P(E)dE = \frac{K}{\beta^2} \frac{Z}{A} \frac{x}{E^2} dE = W \frac{dE}{E^2} , \qquad (2\text{-}3)$$

where $W=KZx/\beta^2 A$. By integration, we will get the number of δ electrons having an energy E_o or larger:

$$N(E \geq E_o) = \int_{E_o}^{E_m} P(E)dE = W(\frac{1}{E_o} - \frac{1}{E_m}) \sim \frac{W}{E_o} . \qquad (2\text{-}4)$$

the last approximation being valid for $E_o << E_m$.

Now noting that 90% of the gas medium of the proportional counter was argon and its thickness was X = 1.91 cm, we want to calculate the approximate number of electrons emitted with energy above 15 eV (the

ionization potential of argon) at normal conditions by the most and the least energetic alpha particles produced in the reaction $^{13}C(p,\alpha)^{10}B$ (The proportional counter was used for two-dimensional position measurement in this expriment; for details refer to chapter 3 and chapter 4).

From the relation (2-4) we have:

$$N(E \geqslant E_\circ) \sim \frac{W}{E_\circ} \quad , \quad \text{where} \qquad W = \frac{KZx}{\beta^2 A} \; . \tag{2-5}$$

As mentioned before, if the calculated value of K for unit charge projectiles is equal to 0.154 MeV g^{-1} cm^2, then the value of K for alpha particles is

$K = 0.154 \times (2^2) = 0.616$ MeV g^{-1} cm^2

$Z_{(Ar)} = 18$

$x = \rho X = 0.001783 \times 1.91 = 0.0034$ gr cm^{-2} (at NTP)

$A = 39.9$

According to relativistic kinematic calculations, for bombarding energy $E_p = 40.45$ MeV the energy of the most energetic alpha particles is 33.70 MeV and that of low energetic alpha particles is 12.276 MeV. β values corresponding to these energies are $\beta_1 = 0.1336(c)$ and $\beta_2 = 0.081(c)$ respectively.

By replacing the corresponding values in (2-5) above, we get:

$$W_1 = \frac{0.616 \times 18 \times 0.0034}{(0.1336)^2 \times 39.9} = 0.052935 \text{ MeV.}$$

$$W_2 = \frac{0.616 \times 18 \times 0.0034}{(0.081)^2 \times 39.9} = 0.144 \text{ MeV.}$$

From relation (2-5)

$$N_1(E \geqslant 15 \text{ eV}) \sim (0.052935 \times 10^6)/15 = 3529$$

$$N_2(E \geqslant 15 \text{ eV}) \sim (0.144 \times 10^6)/15 = 9600$$

for the most and the least energetic α-particles respectively. It is to be remembered that the maximum energy transfer to emitted electrons can be calculated from expression (2-2). For example for the most energetic alpha particles mentioned above for which $\beta = 0.1336(c)$, the maximum energy transfer is:

$$E_m = (2mc^2\beta^2)/(1-\beta^2)$$

$$= [2 \times 0.511 \times (0.1336)^2]/[1-(0.1336)^2]$$

$$= 0.01857 \text{ MeV} \equiv 18.57 \text{ keV}$$

where $mc^2 = 0.511$ MeV is the rest energy of the electron.

Delta electrons, depending on their energy, will cover a certain distance in the gas, suffering elastic and inelastic scatters from the molecules. The total range R_T for an energy E, along the trajectory, can be calculated integrating the Bethe-Block formula over the range R_T and requiring the integral to equal the total available energy; however, it gives a bad representation of the distance effectively covered by an electron, because of the randomizing effect of the multiple collisions. It is customary to define a practical range R_p that appears to be two or three times smaller than the total range and in general is the result of an absorption measurement. For energies up to a few hundred keV, a rather good approximation for the practical range, in g cm^{-2}, is (Ko 68)

$$R_p = 0.71\ E^{1.72} \qquad \text{(E in MeV)}.$$

2-3 Primary and Total Ionization

A charged particle passing through a gas ionizes it and a discrete number of primary ionizing collisions takes place which liberate electron-ion pairs in the medium. However, only part of the energy goes into ionizing the gas and into imparting kinetic energy to the electrons. The average amount of energy required per ion formed is remarkably independent of the charge, mass, and velocity of the particle producing the ionization, but depends on the gas in which the ions are formed. Table 2-1 gives the average energy spent per ion pair formed in some of the most important gases (Se 77).

Table 2-1. Energy (eV) per ion pair for different gases

He	Ne	Ar	Xe	H_2	O_2	N_2	CO_2	Air	
42.7	36.8	26.4	21.9	36.3	32.5	36.5	34.3	35.0	Polonium α-particle
42.3	36.6	26.4	22.0	36.3	30.9	34.9	32.9	33.8	Tritium β rays

As mentioned in 2-2, the electron ejected can have enough energy (larger than the ionization potential of the medium) to further ionize, producing secondary ion pairs; the sum of the two contributions is called total ionization. The total number of ion pairs can be represented by:

$$n_T = \Delta E / w_i \qquad (2\text{-}6)$$

where ΔE is the total energy loss in the gas volume considered, and w_i is the effective average energy to produce one pair.

Following the above discussion, we want to calculate the number of primary, secondary and total ion pairs produced in the proportional counter by the most and the least energetic α-particles, discussed in section 2-2, as well as those produced by 5.48 MeV α-particles emitted from a ^{241}Am source.

The energy loss of α-particles in passing through the counter were calculated under the same conditions as were explained in section 2-1 for 5.48 MeV α- particles, and the results are shown in Table 2-2.

The values of w_i, the effective average energy to produce one pair in argon and methane are 26 and 28 eV respectively. Then by knowing the energy loss of the α-particles in the gas (from Table 2-2), and using the relation (2-6) we can calculate the total number of ion pairs:

For 5.48 MeV α-particles:

Table 2-2 Energy loss of α-particles in the proportional counter

Medium	Energy loss (MeV)		
	33.70 MeV α-particle	12.27 MeV α-particle	5.48 MeV α-particle
Entrance window (Aluminized mylar)	0.141	0.317	0.538
Gas (P-10 at 0.16 atm)	0.096	0.202	0.371
Exit window (Aluminized mylar)	0.143	0.322	0.592

$$n_T = (0.371 \times 10^6)/(26 \times 0.9 + 28 \times 0.1) = 14160 \text{ pairs.}$$

For 12.27 MeVα-particles:

$$n_T = (0.202 \times 10^6)/(26 \times 0.9 + 28 \times 0.1) = 7710 \text{ pairs.}$$

For 33.70 MeVα-particles:

$$n_T = (0.096 \times 10^6)/(26 \times 0.9 + 28 \times 0.1) = 3664 \text{ pairs.}$$

(It is to be remembered that the above calculations for the energy loss in the gas and consequently for the total ion pairs have been based on the reduced pressure of the gas of 0.16 atm).

According to (Sa 77), the number of primary ion pairs produced per unit length in argon and methane at atmospheric pressure for minimum ionizing particles having energy losses 2.44 keV/cm in argon and 1.48 keV/cm in methane are 29 and 16 respectively. The corresponding number of primary and secondary ion pairs were calculated for the proportional counter described later in this thesis (chapter 3). The results are given in Table 2-3.

Table 2-3 Number of primary, secondary and total ion pairs produced by α-particles at a reduced pressure of P = 0.16 atm.

α-particles	Number of ion pairs			n_s/n_p
	Total (n_T)	Primary (n_p)	Secondary (n_s)	
5.48 MeV	14160	4368	9792	2.24
12.27 MeV	7710	2378	5332	2.24
33.70 MeV	3664	1130	2534	2.24

2-4 Drift and Diffusion of Electrons

The primary act of ionization results in electrons, some of which (delta rays) have sufficient energy to produce secondary ions. The mobility of electrons, except for very low fields, is not constant, and electrons, due to their small mass, can increase their energy between collisions with the gas molecules under the influence of an electric field. The average velocity v in the direction of the field, called the drift velocity, is proportional to the field. The constant of proportionality μ is called the mobility. An electron bouncing between heavy atoms, will not transfer much of its energy to the atoms unless it can excite them by inelastic collision. In the case of noble gases the required energies are of the order of 10 eV. Under the action of the field the electron will acquire a large velocity u, which is randomized in direction by the collisions until an inelastic collision causes a considerable decrease in velocity. If the electric field E lies in the z- direction and the mean free path is denoted by λ, an electron will drift in this direction in time τ between collisions by an amount

$$1/2 \times [(eE)/m] \tau^2 = 1/2 \times [(eE)/m] (\lambda/u)^2,$$

because it is subject to the force eE. The number of collisions per second is u/λ; hence the drift velocity is

$$v = 1/2 \times (eE/m)(\lambda/u) = \mu E.$$

Clearly a low value of the random velocity u increases the mobility μ. For heavy ions the mobility is of the order of 1 cm sec^{-1} per V cm^{-1} at STP; for electrons it is about 1000 times larger. It has been found that the addition of even very small fractions of another gas to a pure gas of the proportional counter can, by slightly modifying the average energy, dramatically change the drift properties. A typical example is given in Fig. 2-1 which gives the measured values of drift velocity in argon, methane-argon mixtures, and methane(Bo 57). In most gases, the drift velocity rises with the value of E/p and approaches a relatively constant value; for E/p greater than about 1 to 10 (volts/cm)$(mm\ Hg)^{-1}$, the electron drift velocity approaches a constant value of about 3×10^5 to 10^7 cm/sec (Pr 64).

Fig. 3-8 represents a two-dimensional (2-D) plot from a calibration run obtained by the use of a 5 X 5 hole configuration collimator. Using the information obtained from the time (vertical) projection of this 2-D plot, it was possible to measure the drift velocity of electrons in the proportional counter which was calculated as 3.87 cm $/\mu$ sec (refer to section 3-7).

2-5 Electric Field Dependence of Proportional Counter

If the electric field across a contained volume of gas is small enough so that the ions and electrons formed do not gain sufficient energy between collisions to produce additional ionization, the apparatus performs as an ionization chamber. The ion pairs formed by each entering ionizing particle should be collected at the electrodes and produce a

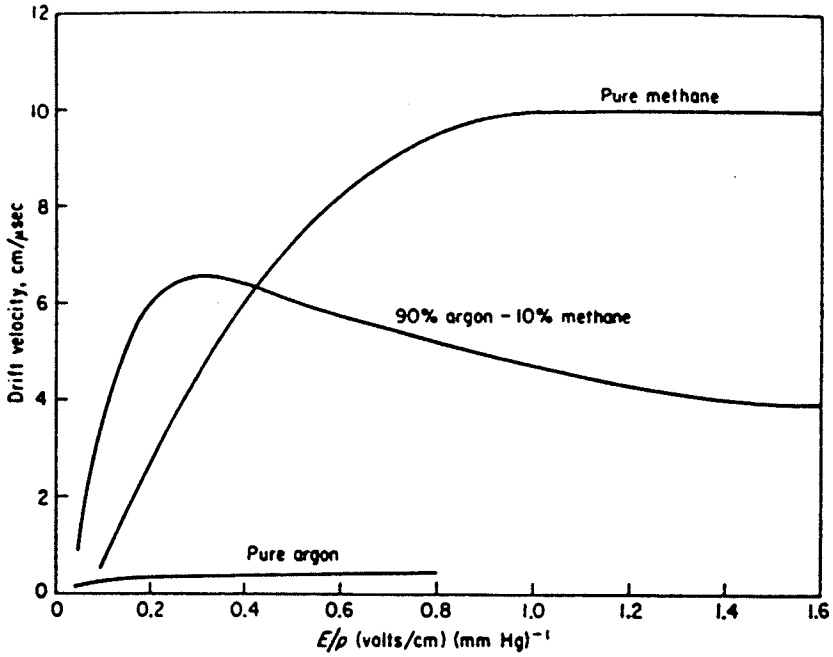

Fig. 2-1 Electron drift velocity as a function of E/p for pure argon, methane, and methane-argon mixture.

pulse of charge which may be counted. The current of the chamber in ionization mode, over a certain voltage interval, is independent of V and the current is said to be saturated; i.e., only the primary ions (including those produced by delta electrons) are being collected.

If the applied voltage is now increased beyond the saturation interval, the primary ions and electrons begin to produce secondaries by collisions with the gas; consequently, the primary ionization is multiplied by a factor that depends on the geometry of the apparatus and on the applied voltage V, and the device functions as a proportional counter.

Increasing the electric field above a few kV/cm, more and more electrons can receive enough energy between two collisions to produce inelastic phenomena, excitation of various kinds, and ionization. Noble gases, being bombarded by the electrons, can only be excited or deexcited through photon absorption or emission, while weakly-bound polyatomic molecules, for example the hydrocarbons used in proportional counters as a quencher, have radiationless transitions of a rotational and vibrational nature. Addition of an organic vapour to noble gases will therefore allow the dissipation of a good fraction of energy in radiationless transition, and this is essential for high gain and stable operation of proportional counters.

When the energy of an electron increases over the first ionization potential of the gas (15.7 eV for argon for example), the result of the impact can be an ion pair, with the scattering of the primary electron.

The probability of ionization rapidly increases above threshold and has a maximum, for most gases, around 100 eV.

Consider now a single electron drifting in a strong electric field; at a given time, it will have an energy $\mathcal{E}$ with a probability given by the appropriate energy distribution function $F(\mathcal{E})$. When, following the statistical fluctuations in the energy increase between collisions, the electron gains an energy in excess of the ionization potential, an ionization encounter may occur. The mean free path for ionization is defined as the average distance an electron has to travel before getting a chance to become involved in an ionizing collision. The inverse of the mean free path for ionization, α, is called the first Townsend coefficient and represents the number of ion pairs produced per unit length of drift. In a limited region one can assume the coefficient to be linearly dependent on the energy of the electrons.

The process of ionization by collision is the basis of the avalanche multiplication in proportional counters. Consider an electron liberated in a region of uniform electric field. After a mean free path α^{-1}, one electron-ion pair will be produced, and two electrons will continue the drift to generate, again after one mean free path, two other ion pairs and so on.

If n is the number of electrons at a given position, after a path dx, the increase in the number will be

$$dn = n\alpha\, dx.$$

and, by integration

$$n = n_o e^{\alpha x}.$$

or
$$M = n/n_o = e^{\alpha x}. \qquad (2\text{-}7)$$

M represents the multiplication factor. In the general case of a non-uniform electric field, $\alpha = \alpha(x)$, equation (2-7) has to be modified in the following way:

$$M = \exp\left[\int_{x_1}^{x_2} \alpha(x)dx\right].$$

The multiplication factor cannot be increased at will. Secondary processes, like photon emission inducing the generation of avalanches spread over the gas volume, and space-charge deformation of the electric field, eventually result in a spark breakdown. A phenomenological limit for multiplication before breakdown is given by the Raether condition

$$\alpha x \sim 20,$$

or $M \sim 10^8$; the statistical distribution of the energy of electrons, and therefore of M, in general does not allow one to operate at average gains above $\sim 10^6$ if one wants to avoid breakdown.

CHAPTER 3

Design, Construction and Testing of Proportional Counter

3-1 Design and Construction

The main design criteria for the position sensitive proportional counter was to produce a counter of simple construction and readout, low cost, and acceptable spatial resolution in two dimensions.

The horizontal position information (position along the anode wire) is extracted using resistive charge division techniques and the vertical position information (distance normal to the wire) is extracted by measuring the time difference between the arrival of the signal from the counter and a surface barrier stopping detector.

A perspective view of the position sensitive proportional counter is shown in Fig. 3-1 and cross-sectional views showing its internal structure are shown in Fig. 3-2. Its over-all dimensions are approximately 87 mm x 67 mm x 38 mm deep. The body of the counter was machined from brass and was mounted on a 3.17 mm thick mounting plate so that the center of the entrance and exit windows were 25.4 mm above the level of the supporting arm, which corresponded to the beam level in the scattering chamber. In the previous design of the counter, the anode wire was 31.7 mm long, 10 μm in diameter with 460Ω resistance. However, it was realized that a shorter anode wire having low resistance did not provide effective charge division and the position computation incurred

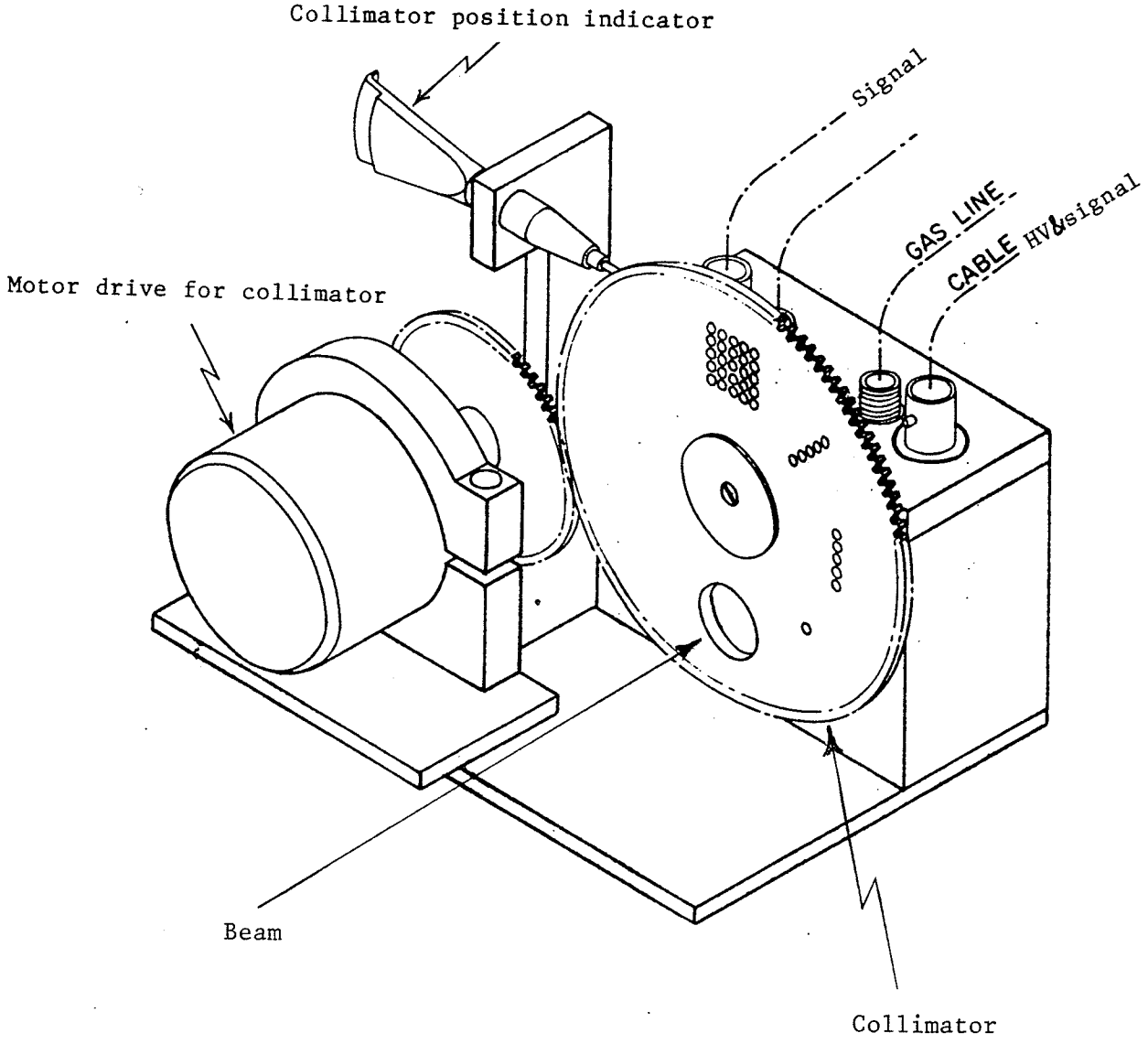

Fig. 3-1 Perspective view of position sensitive proportional counter.

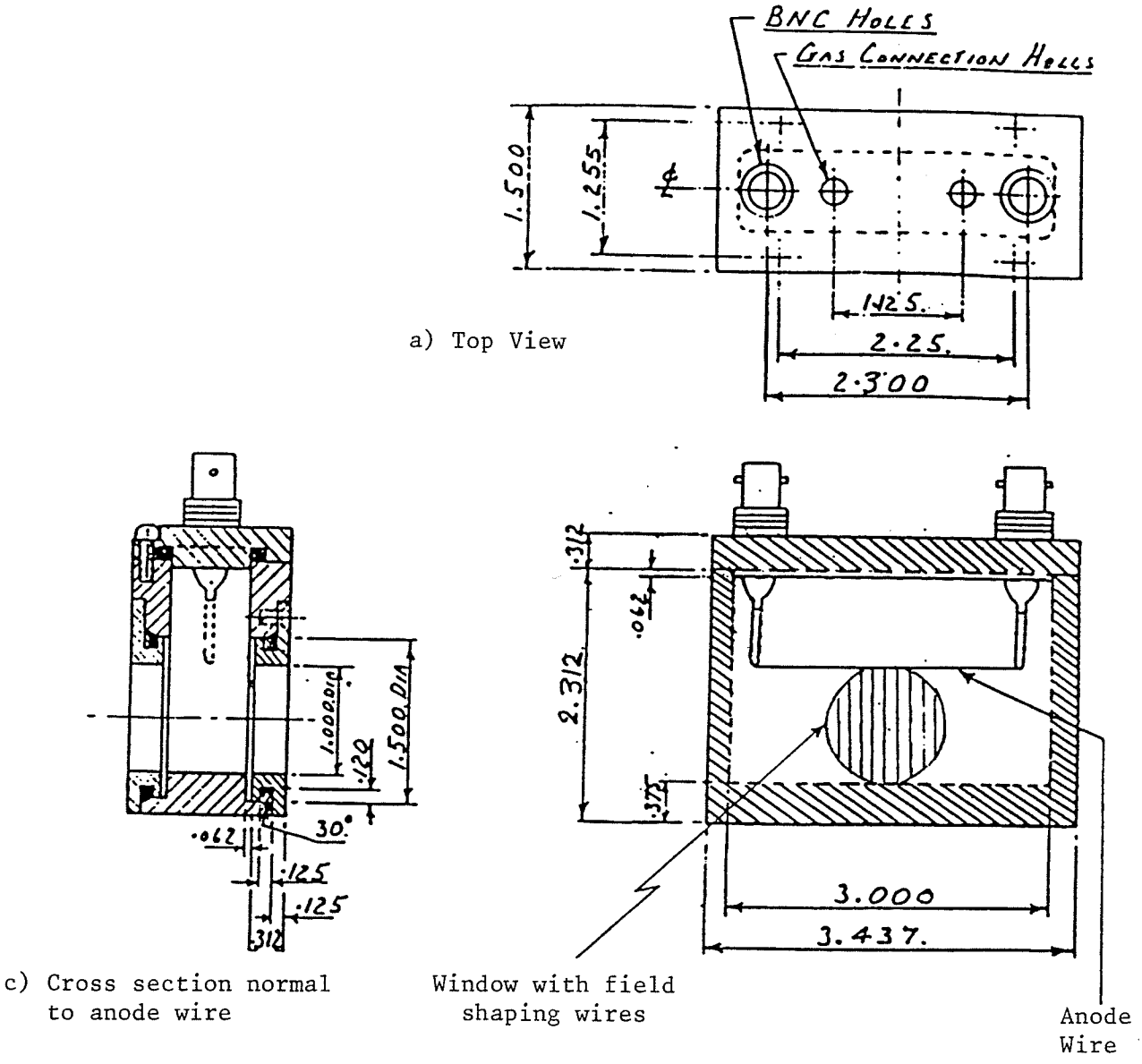

a) Top View

b) Cross section along anode wire

c) Cross section normal to anode wire

Fig. 3-2 Cross sectional views of the counter

(all dimensions are in inches)

loss of accuracy. Therefore, in the modified version of the counter, the anode wire was made 58.4 mm long, with 890Ω resistance and it was placed along a cavity having a rectangular shape. The sensitive area of the counter has a circular cross section 25.4 mm diameter, and the thickness of the gas is nominally 1.9 cm. In order to have good linearity for position coordinates the problem of rapid field change in the drift direction, when deciding the internal dimensions of the counter, had to be considered with some care.

The top portion of the counter was made detachable from the main body in order to facilitate the mounting of the anode wire on the supporting electrodes. These electrodes were wire extensions of standard high voltage vacuum feedthroughs and their lengths were adjusted so that the position of anode wire was just above the top level of the windows. Gas inlet and outlet connections were made through 3.17 mm polyflo tubing connected to polyflo fittings at the top of the counter. Both entrance and exit window frames were made removable and the windows could be easily epoxied in place. Entrance and exit windows on the counter were made from $800 \mu g/cm^2$ aluminized mylar and their openings were 25.4 mm in diameter. A number of windows were carefully mounted in place and tested destructively in order to determine the bursting pressure as well as the bulge of the windows as a function of pressure. The bursting pressure was $\sim$ 1.36 atm. Average bulge of the windows, with the vacuum level in the scattering chamber $\sim 4.0 \times 10^{-6}$ mm Hg and the gas pressure inside the proportional counter 0.16 atm, was $\sim$ 3.0 mm.

For field shaping purposes, wires of 20.0μm in diameter with 3.2 mm spacing between them were soldered onto 1.27 mm thick rings, and these rings were mounted just inside of the entrance and exit windows (Fig. 3-2.b). Without these wires the electric field shape is determined by, among other factors, the aluminized mylar windows. Since these windows bulge considerably under pressure, the field shape is distorted to an unacceptable degree.

A remotely controlled collimator was mounted in front of the proportional counter and different configurations of holes provided the necessary flexibility for testing during the experiment. All holes (except the large one) were 3 mm apart center to center and the diameter of each hole was 3 mm on the front face and 1 mm on the back face. This method provided good collimation and at the same time eliminated to some extent the possibility of excessive beam scattering.

Standard BNC and SHV cable fittings were used for the output signals and high voltage power. The high voltage was applied through one of the preamplifiers connected to the proportional counter.

3-2 Gas Filling

As far as the operation of proportional counters is concerned, a rather large variety of gases can be used in them. However, due to some experimental requirements and restrictions, our choice in selecting a particular gas is limited and it is more or less restricted to several families of compounds. Noble gases are generally preferred as the main

component, and this is because avalanche multiplication occurs in these gases at much lower fields as compared with complex molecules. The next parameter to be considered in selecting a particular gas among noble gases is a high specific ionization which is required at least for the detection of minimum ionizing particles. Xenon or krypton are disregarded due to economic reasons and as a result, argon seems to be most suitable as a main component gas to be used in proportional counters. An argon operated counter, however, does not allow gains in excess of 10^3 - 10^4 without entering into a permanent discharge operation for the following reasons (Sa 77).

During the avalanche process, excited and ionized atoms are formed. The excited noble gases can return to the ground state only through a radiative process, and the minimum energy of the emitted photon (11.6 eV for argon) is well above the ionization potential of any metal constituting the cathode. Photo-electrons can therfore be emitted from the cathode, and initiate a new avalanche. Argon ions, on the other hand, migrate to the cathode and are there neutralized extracting an electron. The energy released in this process is either radiated as a photon, or via secondary emission, i.e. extraction of another electron from the metal surface. Both processes result in a delayed spurious avalanche: even for moderate gains, the probability of the processes discussed is high enough to induce a permanent process of discharge. Polyatomic molecules have a very different behaviour. The large number of non radiative excited states (rotational and vibrational) allows the absorption of photons in a wide energy range: for methane, for example,

absorption is very efficient in the range 7.9 to 14.5 eV, which covers the range of energy of photons emitted by argon. The molecules dissipate the excess energy either by elastic collisions, or by dissociation into simpler radicals. The same behaviour is observed when a polyatomic ionized molecule neutralizes at the cathode; secondary emission is very unlikely. In the neutralization, radicals recombine either into simpler molecules (dissociation) or form larger complexes (polymerization). Even a small amount of a polyatomic quencher added to a noble gas changes completely the operation of a counter, because of the lower ionization potential that results in a very efficient ion exchange. Good photon absorption and suppression of the secondary emission allows gains in excess of 10^6 to be obtained before discharge.

Considering the above discussion, the gas filling of the proportional counter was P-10 (90% argon plus 10% methane) gas mixture. The proportional counter was tested under different conditions of gas pressure, bias voltage and rate of gas flow. The gas pressure proved to be a critical parameter in improving the position resolution. The most suitable pressure was found to be 0.16 atm for P-10 gas mixture. Therefore it was necessary to devise a system to be able to maintain the pressure at the required level without any noticeable fluctuations. After studying and testing different systems, the layout shown in Fig. 3-3 was devised and used during the experiment. Fresh gas continuously flowed through the counter with the pressure accurately maintained at the required level by a manostat. The manostat had a simple construction and its main components were a cylindrical reservoir,

rubber membrane, needle valve and gas inlet and outlet ports as depicted in Fig. 3-4. Pressure control was achieved via the motion of a rubber membrane responding to the differential between the gas pressure in the proportional counter and the reference pressure in the reservoir. In the layout of Fig. 3-3, P_o is the reference pressure in the reservoir which is connected to or separated from the rest of the system by a needle valve and a rubber membrane discussed before. At first, the needle valve is opened while the vacuum pump is operating until the desired level of reduced pressure is attained and indicated by the vacuum gauge. With the pressure of the gas in the system (P) equal to the reference pressure (P_o), the needle valve is closed. As long as $P = P_o$, inlet and outlet of manostat are isolated from each other by the rubber membrane. When $P > P_o$, the excess pressure causes the membrane to be depressed opening the inlet to the pumped outlet tube. Conversely, when $P < P_o$, the membrane closes the inlet and the internal pressure starts to build up until the desired pressure is again established. This system proved to work efficiently throughout the experiment.

3-3 Field Calculations

In order to provide rather good linearity for both position coordinates, the geometry of the proportional counter must be considered with some care. Position measurement with good resolution and particle identification are among the major requirements expected from proportional counters. The realization of these requirements depends to a large extent on properly choosing the geometry of the electric field.

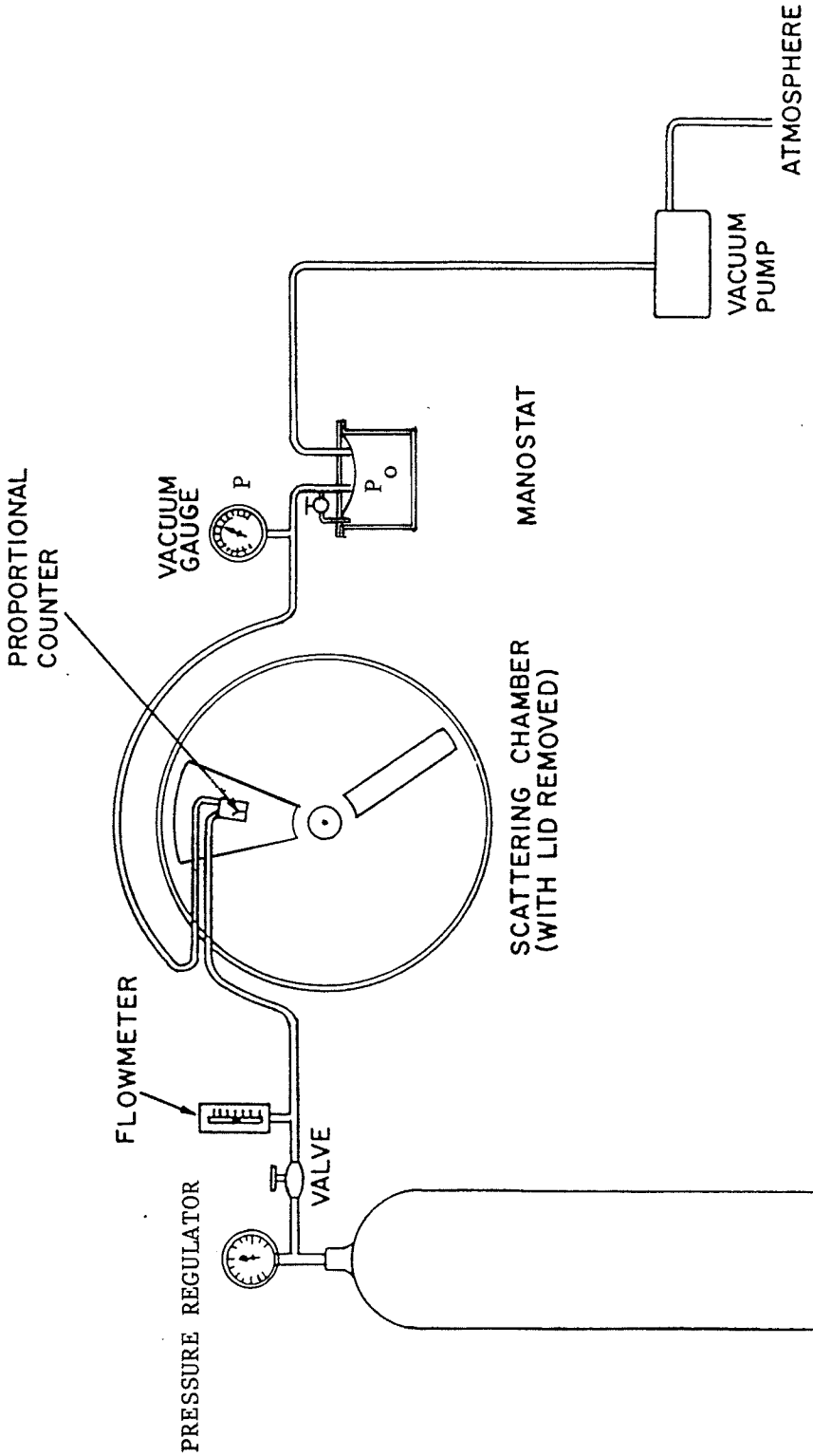

Fig. 3-3 Gas circuit to maintain a constant flow of gas at a required constant pressure.

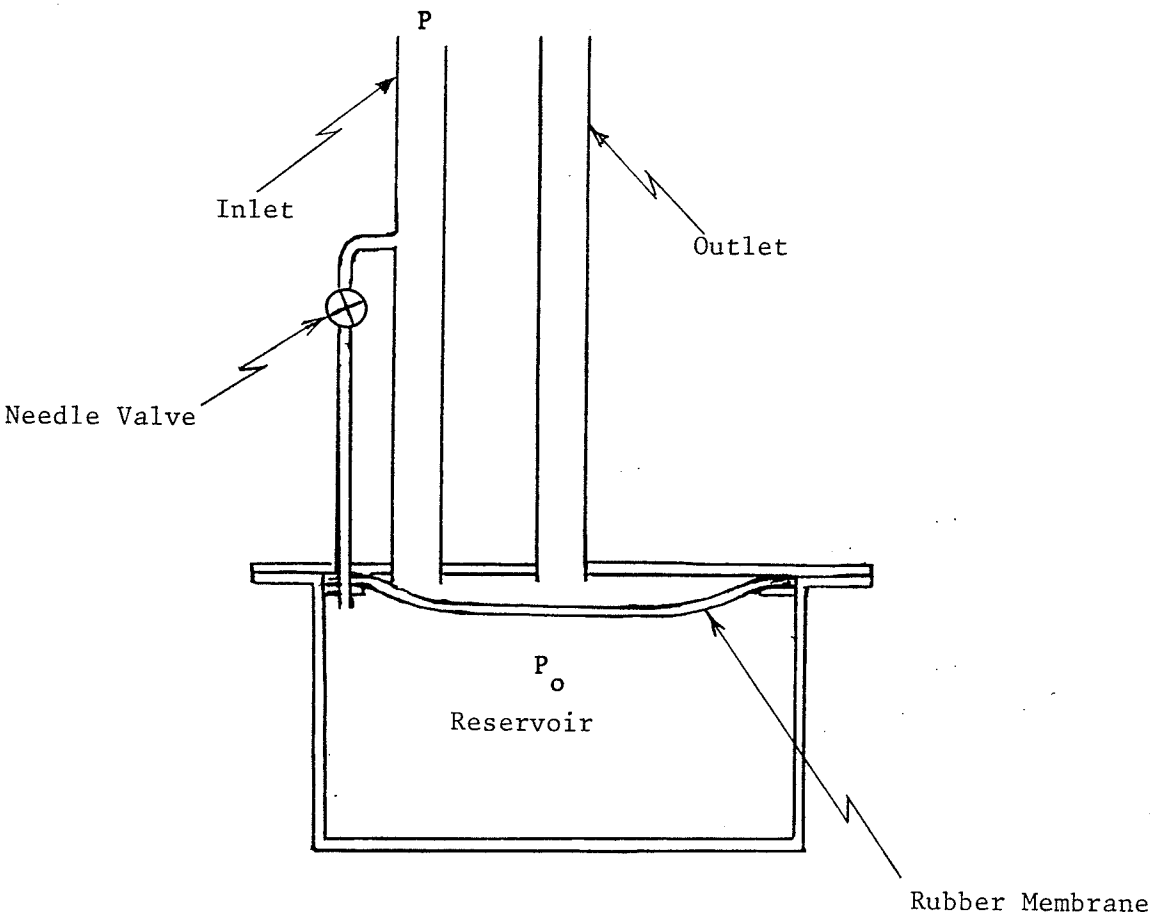

Fig. 3-4 Manostat

The potential distribution in space is entirely defined by the geometry and the potentials of the electrodes. Neglecting space charges, the electrostatic potential distribution can be determined by solution of Laplace ´s differential equation

$$\nabla^2 V = 0.$$

Although the theoretical possibility of obtaining analytical solutions for the field is very interesting in principle, an integration of the above equation under the proper conditions as given by geometry and potentials of the electrodes is generally very complicated. In the majority of practically important cases, analogue or numerical methods have to be used.

Relaxation Methods (Kl 71) (Se 67)

For the three-dimensional case, Laplace ´s equation is

$$\partial^2 V/\partial x^2 + \partial^2 V/\partial y^2 + \partial^2 V/\partial z^2 = 0. \qquad (3\text{-}1)$$

For a numerical method of extrapolating the potentials off the electrodes, let the xy, yz, and xz planes be covered by a net of equidistant lines parallel to the three axes (a two-dimensional representation is shown in Fig. 3-5). The potential V_o at any lattice point should be completely determined by the potentials V_1, V_2, V_3, V_4, V_5, and V_6 of its neighbouring six lattice points. Calling g the distance between the lattice lines, it can be shown that

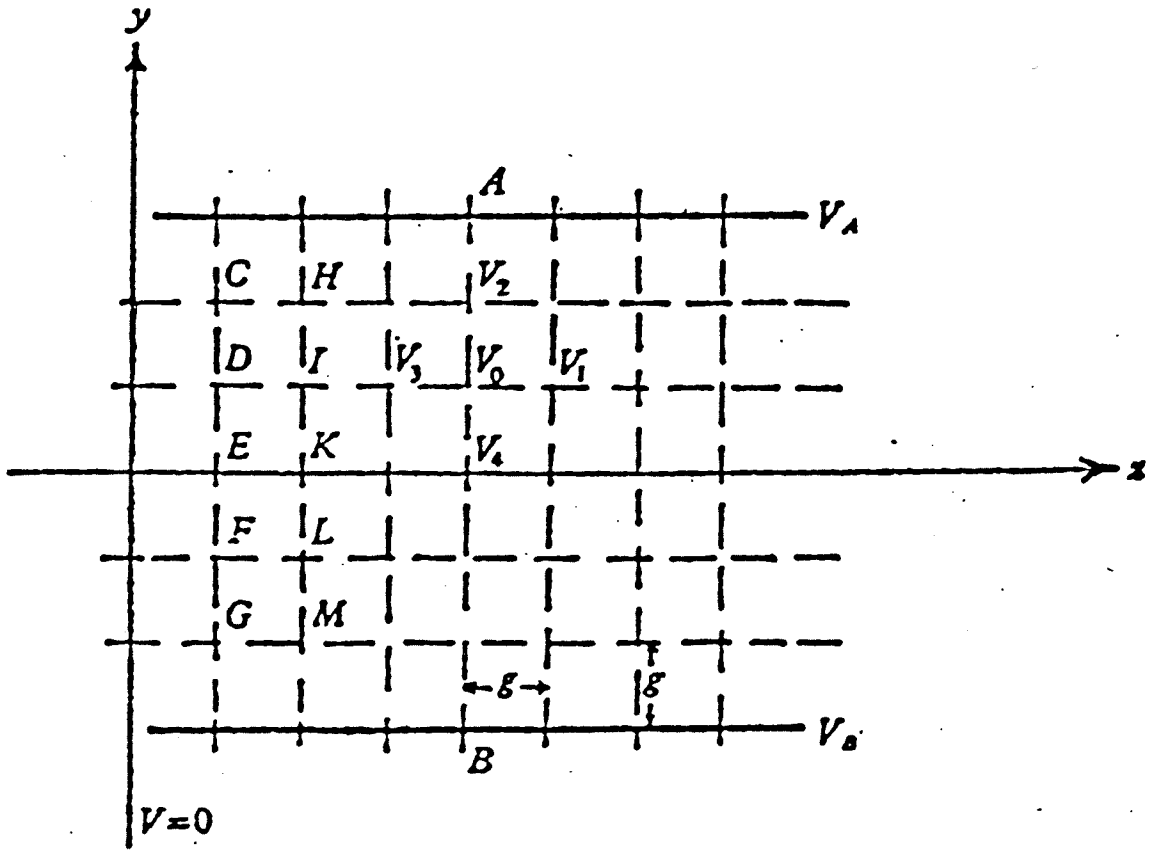

Fig. 3-5 Lattice for computational mapping.

$$(V_2 - V_o)/g - (V_o - V_4)/g \sim (\partial V/\partial y)_{2,0} - (\partial V/\partial y)_{0,4} \sim g(\partial^2 V/\partial y^2)_0 \qquad (3\text{-}2)$$

$$(V_1 - V_o)/g - (V_o - V_3)/g \sim (\partial V/\partial x)_{1,0} - (\partial V/\partial x)_{0,3} \sim g(\partial^2 V/\partial x^2)_0 \qquad (3\text{-}3)$$

$$(V_5 - V_o)/g - (V_o - V_6)/g \sim (\partial V/\partial z)_{5,0} - (\partial V/\partial z)_{0,6} \sim g(\partial^2 V/\partial z^2)_0 \qquad (3\text{-}4)$$

According to Laplace ´s equation (3-1); from the expressions (3-2), (3-3) and (3-4) we get

$$V \sim 1/6 \times (V_1 + V_2 + V_3 + V_4 + V_5 + V_6). \qquad (3\text{-}5)$$

With the help of (3-5) the potential distribution between electrodes of known potential can be extrapolated.

Based on the theory which was discussed above, and in order to get high accuracy in the computation and plotting of the electric field of the proportional counter, the relaxation technique was applied to accurate field determinations by the use of computer. The computer program was the modified version of the program which was initially used to calculate the three-dimensional electric fields by successive

over-relaxation in the central region of the University of Manitoba Cyclotron. A 0.50 mm mesh size was used to study the shape of the field in different layers and a three-dimensional boundary corresponding to the geometry of the proportional counter was specified.

Electrode geometries and the aspects of potential distribution were studied by relaxation calculations in order to find the most appropriate potential shape. A representative potential distribution produced for the geometry shown in Fig. 3-2 with the mesh size of 0.50 mm, and presenting a vertical plane a distance of 1.0 mm. from the anode wire, is shown in Fig. 3-6.

3-4 Leakage Current

The counter was tested under different conditions of gas pressure, bias voltage, and rate of gas flow. The gas pressure proved to be a critical parameter in improving the position resolution. As mentioned in section 3-2, the most suitable pressure was found to be 0.16 atm for the P-10 (90% argon plus 10% methane) gas mixture which was kept constant with constant flow of gas by the use of a manostat. Bias voltage between 680 and 720 volts gave good results at the reduced pressure of 0.16 atm of the gas. The sudden increase of leakage current precluded the use of bias voltage beyond 720 V at the above reduced pressure. Leakage current was due to a discharge which occurred between the electrodes and the body of the counter acting as a cathode, and it was noticeable at higher bias voltages and/or at low pressure of the gas. Some of the results obtained from the leakage current tests are summarized in Table 3-1.

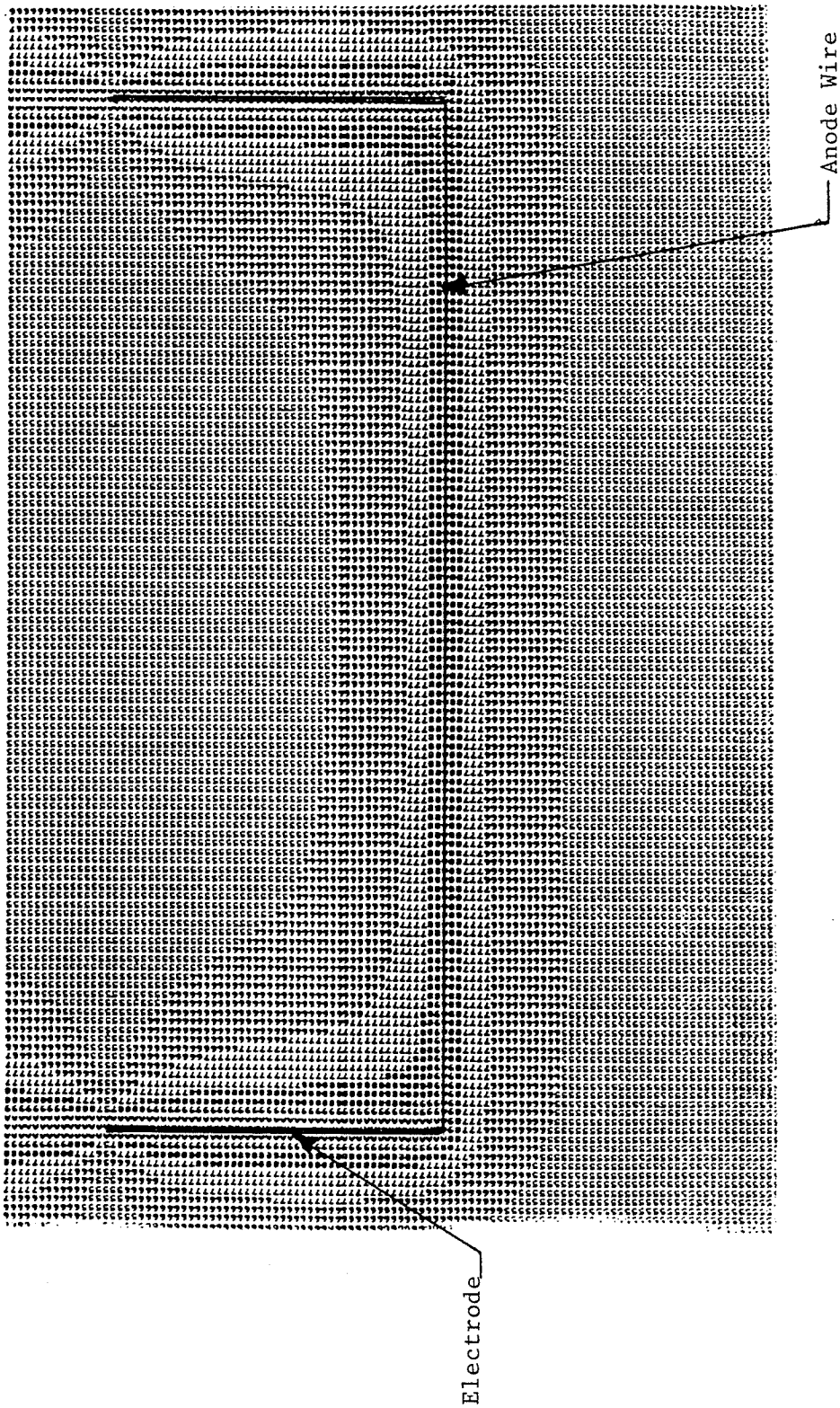

Fig. 3-6 Potential plotting by relaxation calculation.

Table 3-1 Leakage current of proportional counter subject to different conditions of bias voltage and gas pressure.

Bias Voltage (v)	Gas Pressure (atm)					
	1.00	0.50	0.33	0.16	0.12	0.10
660						*
700	0	0	0	0		*
740					0	
750	0	0	0	0	**	*
760					*	
770	0	0	0	0		*
800	0	0	0	0		*
840				*		
900			*			

0 No leakage current

* Sudden rise beyond 1 μA

** Unstable condition

3-5 Electronics

The experimental set-up consisted of two counter telescopes (for detail refer to chapter 4). Telescope # 1 consisted of the X-Y proportional counter, a surface barrier detector (E1) and a veto detector. Telescope # 2 consisted of a surface barrier detector (E2) backed up by a veto detector.

The outputs of the detectors as well as the right and left outputs of the proportional counter were first sent to Ortec pre-amplifiers which in turn were connected to Ortec main amplifiers in the circuit.

In order to observe position sensitivity using charge division, the input impedance to the pre-amplifiers on each end of the anode wire had to be small compared to the 890 Ω resistance of the anode wire. Different types of pre-amplifiers were tested and Ortec pre-amplifiers (model 109A) proved to give good results. It is to be noted that the fraction of the total charge induced on the wire that is collected at one end is linearly related to the position when low impedance pre-amplifiers are used on each end of the wire. For the purpose of obtaining the optimum signal to noise ratio, the pre-amplifiers gain switches were put in the x 10 position.

The signals from the main amplifiers were transmitted to analog-to-digital converters (ADC), which in conjunction with a data accumulation program, BTEN, produced spectra. The energy per channel for alpha spectra was pre-set to be approximately 34 keV using a ^{241}Am alpha source mounted in front of the detectors, in conjunction with a

charge terminator.

The output from the E1 detector provided the common start pulse to a time-to-digital converter (TDC). The stop pulses came from the right and left outputs of the proportional counter as well as from the E2 detector. The outputs from ADC and TDC were fed to the interface of an on-line VAX computer.

A block diagram of the electronics reflecting the complete singles experiments and simultaneous coincidence experiments is shown in Fig. 3-7. The coincidence portion (bottom part, involving telescope E2) of the circuit will be explained later in detail in chapter 4.

Legend to Electronic Circuit in Fig. 3-7

A	Anticoincidence
ADC	Analog-to-digital converter
C	Coincidence
DA	Delay amplifier
DGG	Dual gate generator
G & D	Gate & delay generator
IR	Input register
PA	Pre-amplifier
PU	Pile-up
RA	Reject amplifier
SCA	Single channel analyzer
TDC	Time-to-digital converter
V	Veto input

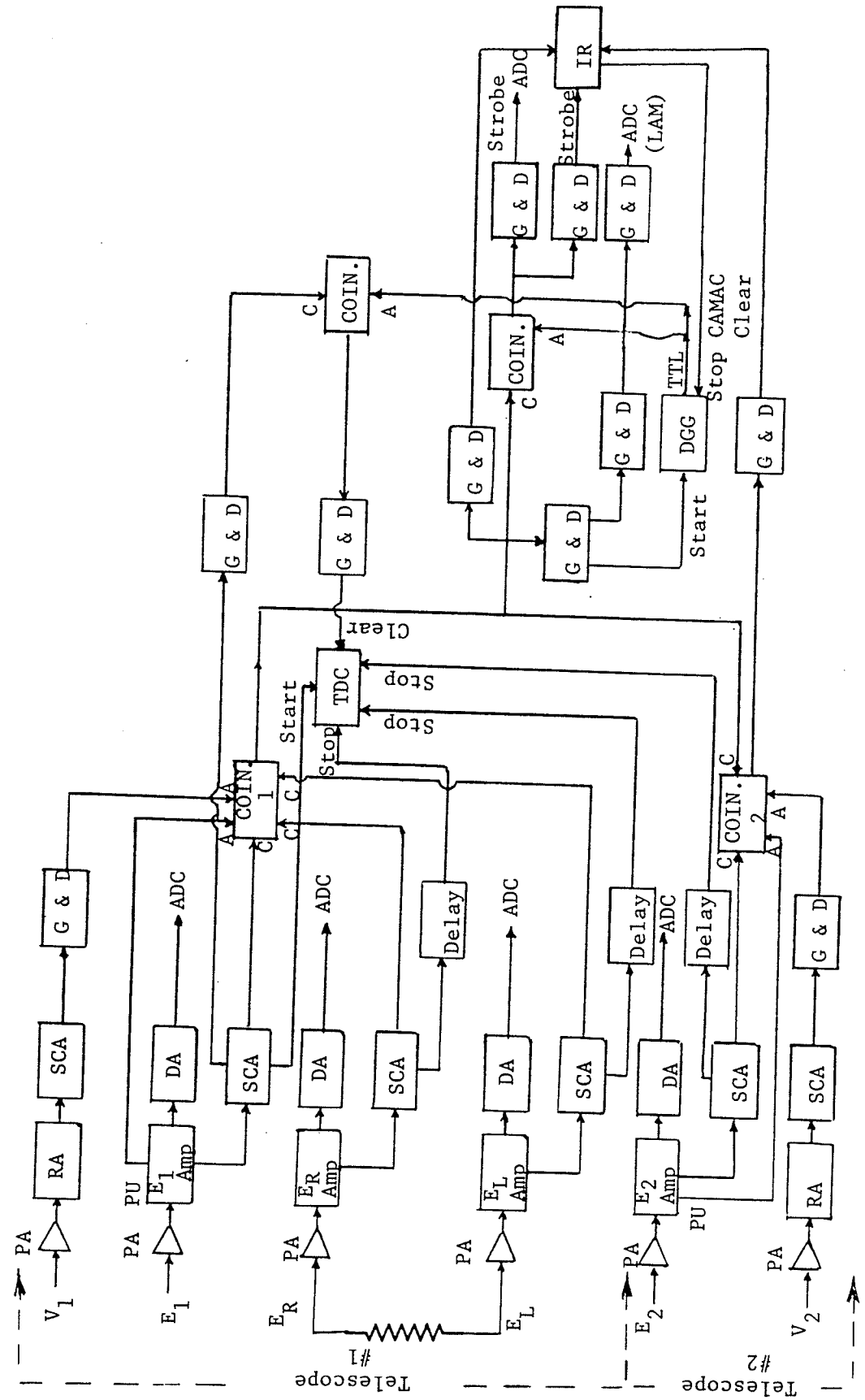

Fig. 3-7 Block Diagram of Electronics

3-6 Calibration of Position and Time

After some preliminary tests of the proportional counter using 5.48 MeV alpha particles from a ^{241}Am source, it was used as an X-Y counter in a study of the $^{13}C(p,\alpha)^{10}B$ reaction investigating the decay properties of ^{10}B (refer to Chapter 4). The proton beam was provided by the University of Manitoba Cyclotron at an energy of 40.45 MeV on a ^{13}C target.

Fig. 3-8 represents a two-dimensional plot from a calibration run obtained by the use of a 5 x 5 hole configuration collimator. The holes were 1 mm in diameter and 3 mm apart center to center. The surface barrier detector used in conjunction with the proportional counter was not large enough to cover completely the array of holes in the collimator and this accounts for the absence of some of the corresponding peaks in Fig. 3-8.

Fig. 3-9 and Fig. 3-10 represent respectively the time and position one-dimensional projections obtained from the two-dimensional plot. Noting that the holes of the collimator corresponding to the peaks obtained from these projections were 3 mm apart, it was possible to deduce calibration information both for time and position. Fig. 3-11 and Fig. 3-12 show the time and position calibration curves together with the corresponding equations which were used in the computer program for the right output of the counter, and Fig 3-13, and Fig. 3-14 represent the same information for the left output of the counter.

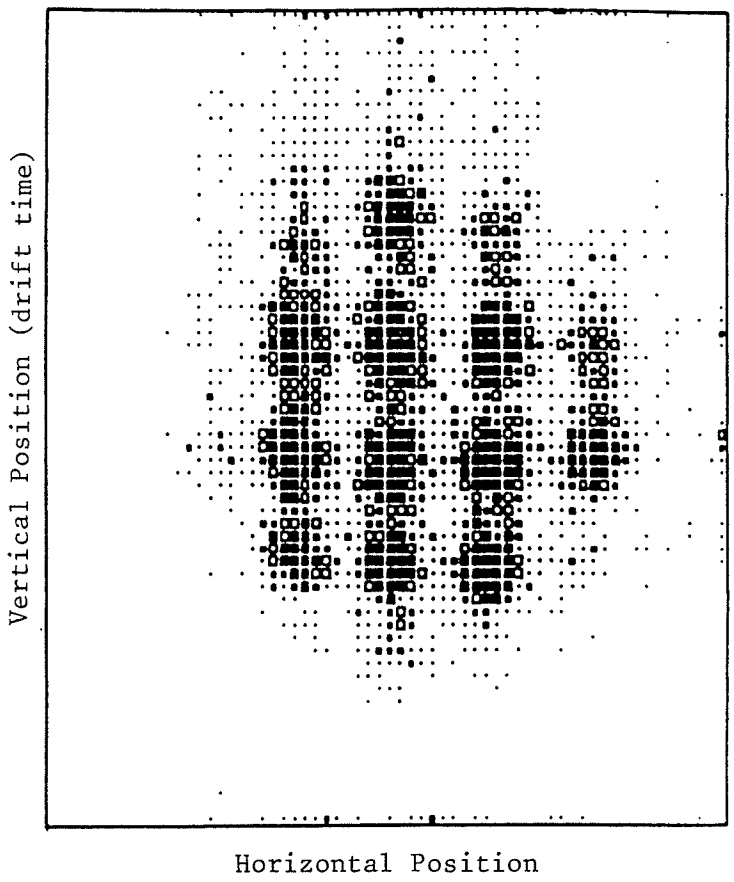

Fig. 3-8 Two-dimensional Plot

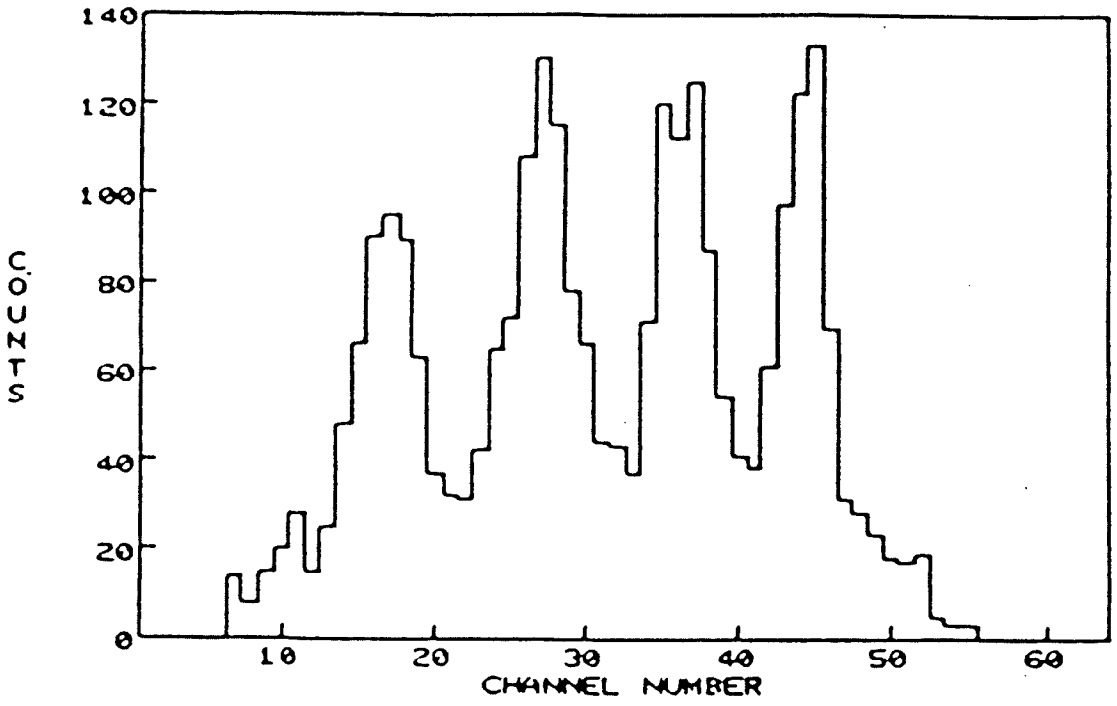

Fig. 3-9 Vertical time distribution (right)

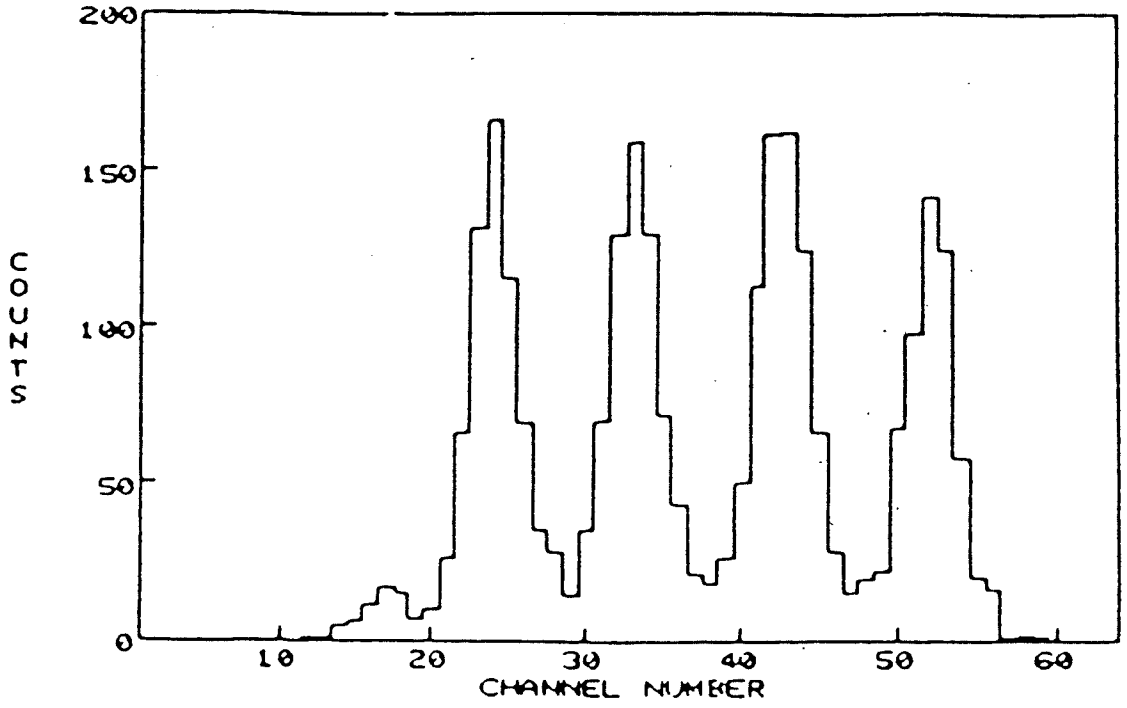

Fig. 3-10 Horizontal position distribution (left)

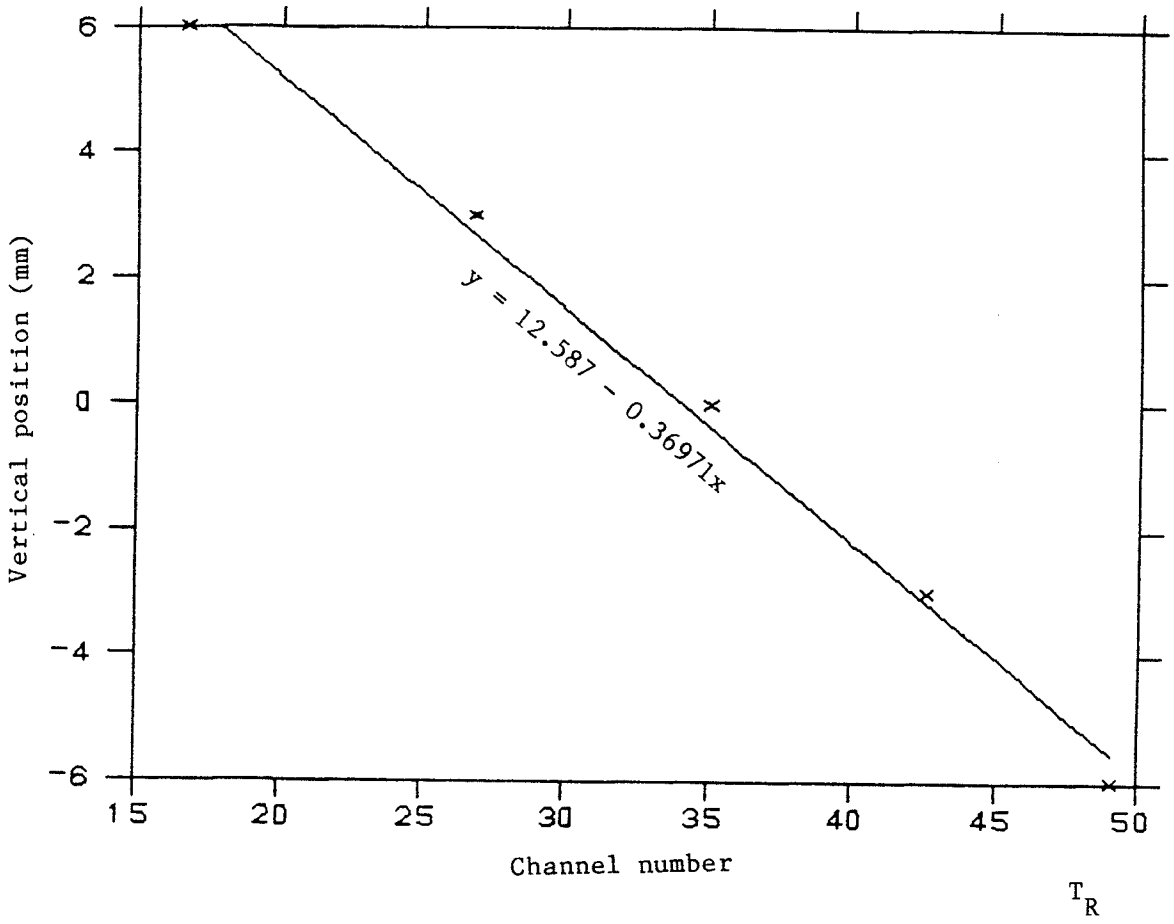

Fig. 3-11 Time (right) calibration curve.

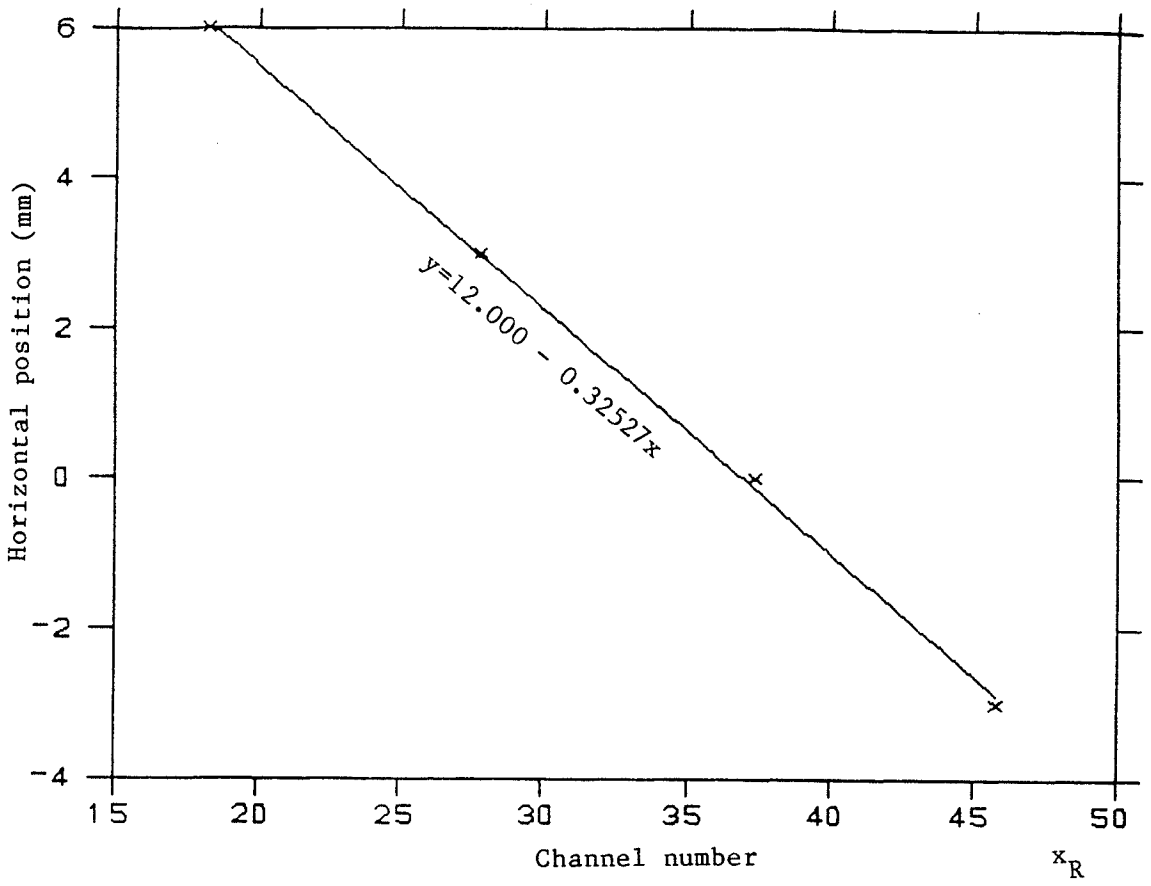

Fig. 3-12 Position (right) calibration curve.

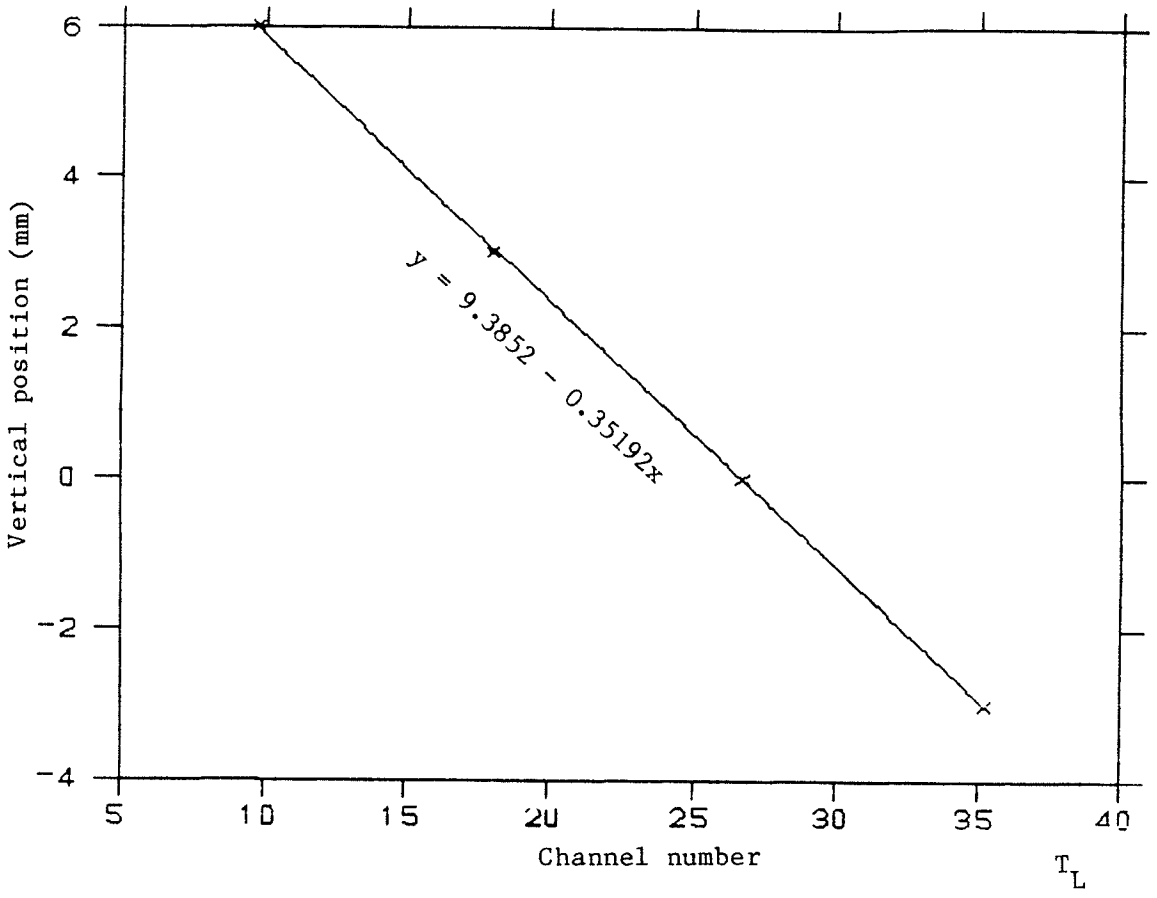

Fig. 3-13 Time (left) calibration curve.

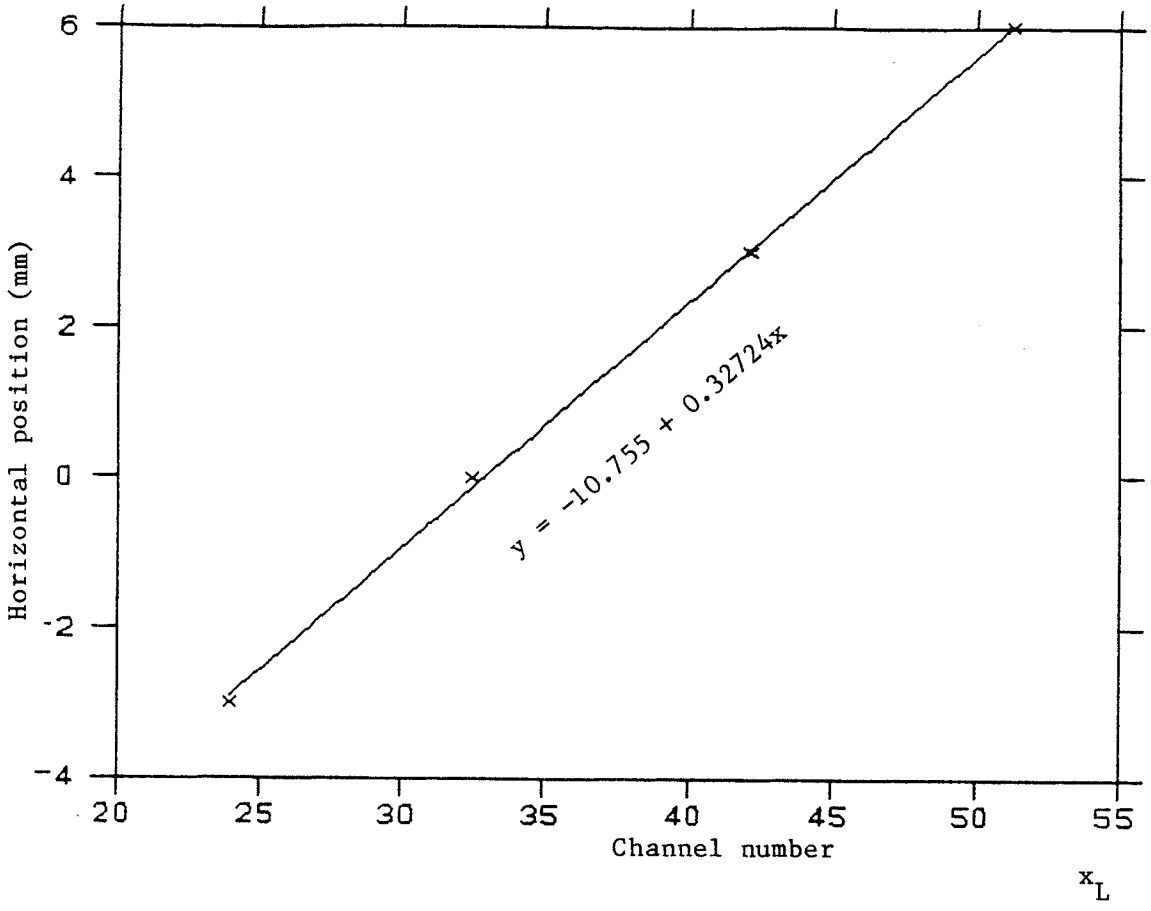

Fig. 3-14 Position (left) calibration curve.

3-7 Position Resolution

As explained before, the horizontal position information (position along the anode wire) was extracted using resistive charge division techniques and the vertical position information (distance normal to the wire) was extracted by measuring the time difference between the arrival of the signal from the proportional counter and a surface barrier detector. Now we want to calculate the position resolutions in both vertical and horizontal directions.

a) Vertical Position Resolution

By referring to Fig. 3-9 (vertical time, right), the average FWHM was calculated as $\overline{FWHM} = 4.96 \pm 0.14$ and the average spacing between the centroids of the peaks was 9.9 ± 0.1 channels. Remembering that the holes of the collimator were 3 mm apart center to center, the experimental position resolution in the vertical direction (Γ_{exp}) was calculated as

$$\Gamma_{exp} = [(4.96) \pm 0.14)/(9.9 \pm 0.1)] \times (3 \text{ mm})$$
$$= 1.50 \pm 0.05 \text{ mm}.$$

Taking the finite size of the holes of the collimator (1 mm in diameter) into consideration, the intrinsic position resolution was calculated as follows

For a Gaussian probability distribution we have (Be 69)

$$\Gamma = 2.345\,\sigma,$$

where Γ represents the FWHM and σ is the standard deviation.

We have

$$\Gamma_{exp} = 1.50 \pm 0.05 \text{ mm.}$$

$$\therefore\ \sigma_{exp} = (1.50 \pm 0.05)/2.345$$

$$= 0.64 \pm 0.02 \text{ mm.}$$

If the variance due to the finite size of the holes is denoted by σ_ϕ^2, the experimental variance, i.e., $(\sigma_{exp})^2$ will be approximately given by

$$(\sigma_{exp})^2 = (\sigma_{int})^2 + \sigma_\phi^2. \qquad (3\text{-}6)$$

By referring to Fig. 3-15, we will have

$$\sigma_\phi^2 = [2 \times \int_{-a}^{+a} (y\,dx)x^2]/A,$$

where the numerator represents the second moment of the area with respect to y-axis and A is the total area.

We have

$$x^2 + y^2 = a^2$$

$$y = (a^2 - x^2)^{1/2}$$

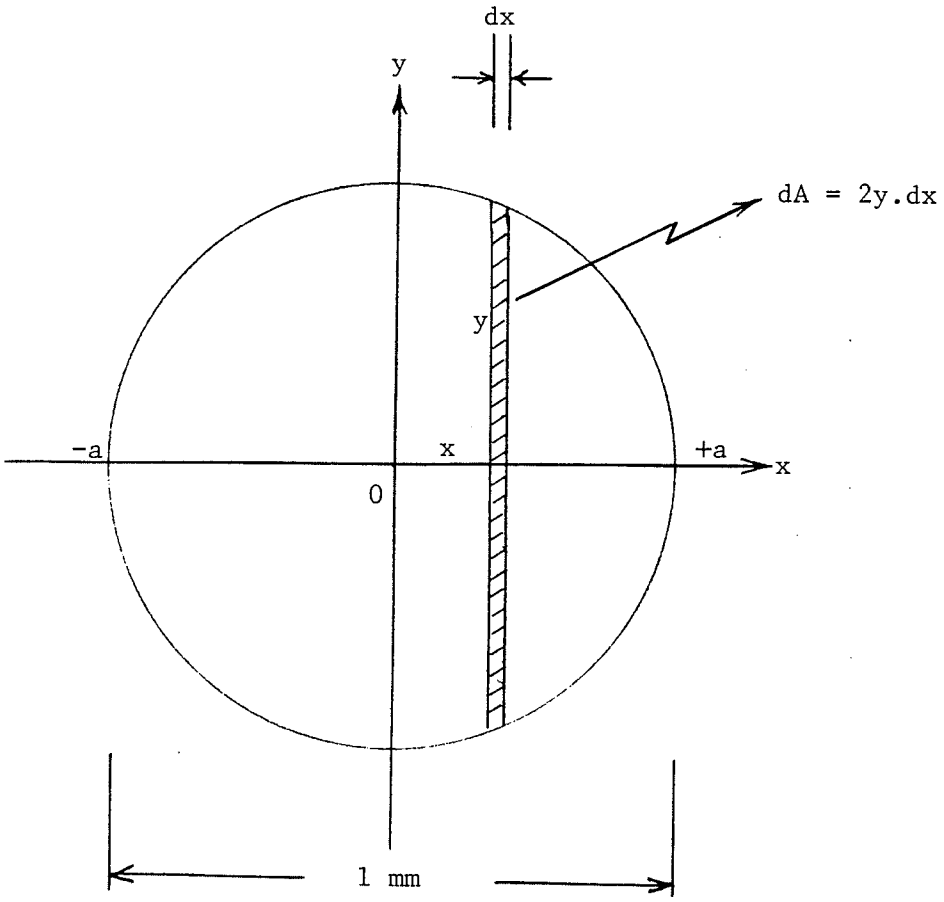

Fig. 3-15

$$\therefore \sigma_\phi^2 = [2 \times \int_{-a}^{+a} (a^2 - x^2)^{1/2} \cdot x^2 \, dx] / \pi a^2$$

$$= 4/\pi a^2 \int_0^a (a^2 - x^2)^{1/2} \cdot x^2 \, dx.$$

By using the expression:

$$\int_0^a x^m (a^n - x^n)^p \, dx$$

$$= \{a^{(m + 1 + np)} \Gamma[(m + 1)/n] \Gamma(p + 1)\} /$$

$$\{n \Gamma[(m + 1)/n + p + 1]\},$$

where m = 2, n = 2, and p = 1/2.

We get

$$\sigma_\phi^2 = a^2/4.$$

But a = 1/2 mm.

$$\therefore \sigma_\phi^2 = 1/16 \text{ mm}^2.$$

From (3-6)

$$(\sigma_{int})^2 = (\sigma_{exp})^2 - \sigma_\phi^2$$

$$= (0.64 \pm 0.02)^2 - 1/16$$

$$\therefore \sigma_{int} = 0.59 \pm 0.02 \text{ mm}$$

Finally, the intrinsic resolution is

$$\Gamma_{int} = 2.345\ \sigma_{int}$$

$$= 2.345 \times (0.59 \pm 0.02)$$

$$= 1.38 \pm 0.05 \text{ mm.}$$

As was shown above, the contribution of the finite size of the holes of the collimator is quite small.

b) Calculation of Drift Velocity

In the vertical time (right) distribution shown in Fig. 3-9, the axis of 64 channels corresponds to 502 nsec. As mentioned in a) above, the spacing in channel number between the centroids of the peaks was 9.9 ± 0.1 channels which corresponds to 3 mm distance between the holes of the collimator. Therefore, the drift time for 1 cm is

$$[9.9/64 \times (502 \times 10^{-9})] \times 10/3 = 0.258 \times 10^{-6} \text{ sec.}$$

The drift velocity is

$$v_d = 3.87 \pm 0.04 \text{ cm}/\mu\text{sec.}$$

c) Horizontal Position Resolution

By referring to Fig. 3-10 (horizontal position, left), $\overline{FWHM}$ = 4.47 ± 0.13 and the average spacing between the centroids of the peaks is 9.2 ± 0.1 channels.

Following the same procedure as discussed in a) above, the experimental and intrinsic position resolutions in the horizontal direction were calculated as

$$\Gamma_{exp} = 1.46 \pm 0.04 \text{ mm}$$

$$\Gamma_{int} = 1.31 \pm 0.05 \text{ mm}.$$

The position resolution of proportional counters can get worse in situations where some conditions, for example normal incident particles, are not present. The explanation for this effect probably is that energy loss fluctuations can lead to position fluctuations for non-normal particles. The energy-loss fluctuation effects can be calculated by integration of the Vavilov distributions for energy loss in the halves of the counter (Va 75).

According to the calculations made by R.G. Markham and R.G.H. Robertson, for moderate and low ionizing particles incident at 45° to the normal, the resolution of resistive anode counters is dominated by energy-loss fluctuation effects (Ma 75a), (Ma 75b), (Sa 75).

Some other factors responsible for position resolution deterioration are as follows:

- Multiple scattering in the entrance window and counter gas can be a serious problem, especially for more heavily ionizing particles.
- Limitations imposed by beam geometry and target.
- The energy resolution of the counter is restricted by the energy straggling of the ions in the entrance window of the chamber.

As far as the above calculated values of the position resolution for the proportional counter are concerned, the deteriorating effect of the beam geometry could be ignored. But the energy-loss fluctuations as well as multiple scattering in the entrance window and counter gas could deteriorate the resolution by up to ~ 0.7 mm. This value is added in quadrature to the resolution calculated for normal incident particles.

3-8 Kinematic Correction

Fig. 3-16 shows a spectrum from the $^{13}C(p,\alpha)^{10}B$ reaction at $E_p = 40.45$ MeV taken at a laboratory scattering angle of $\theta_3 = 40^\circ$. Due to the finite size of the acceptance angle of the α-particle detector $\sim \pm 2^\circ$ (refer to chapter 4), kinematic broadening, which is a feature of all two-body reactions, was large, accounting for the poor energy resolution expected and observed. Some states like the g.s. and the 0.718 MeV state or 1.74 and 2.15 MeV states were not resolved and the FWHM of the states were large. However, by calculating the scattering angle (refer to chapter 4) and applying the kinematic correction, which was made possible by the use of the X-Y position information obtained

from the 2-D proportional counter, the resolution was greatly improved, as shown for the same data of Fig. 3-16 in Fig. 3-17. The computer "XSYS" program, BTEN, and the subroutine "EVLSUB1" used during the experiment and susequently improved for data analysis are attached as Appendix 1.

The FWHM of the g.s. which was 10 channels in Fig. 3-16 (corresponding to 0.356 MeV), was improved to 6 channels (corresponding to 0.215 MeV) in Fig. 3-17.

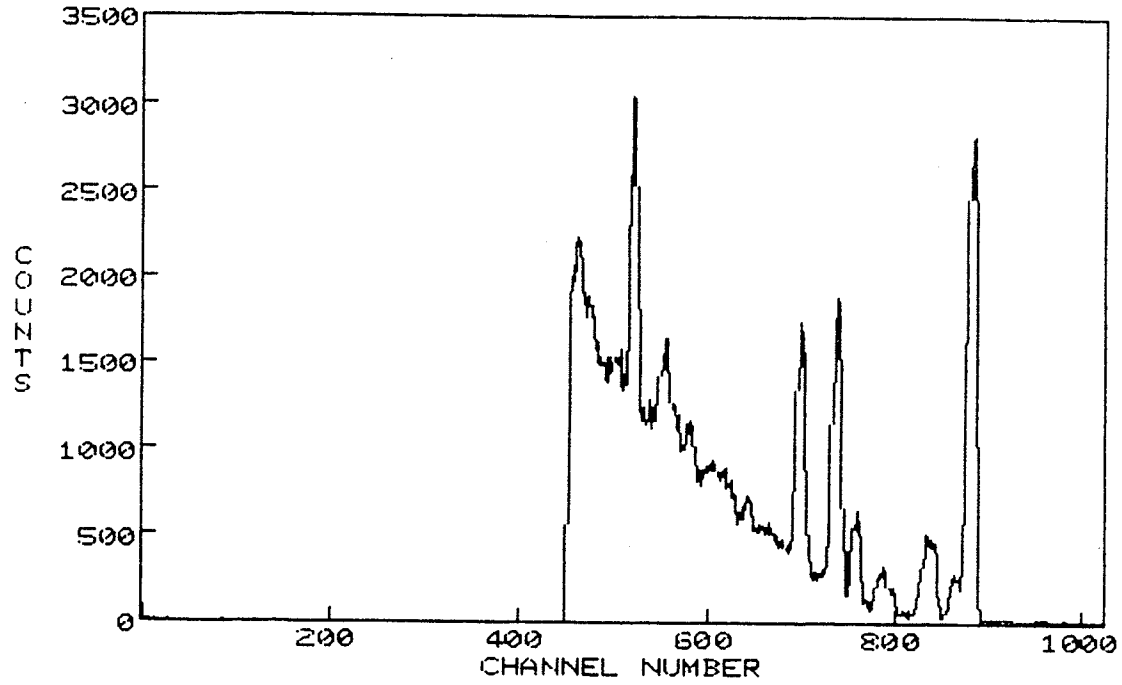

a) Full scale

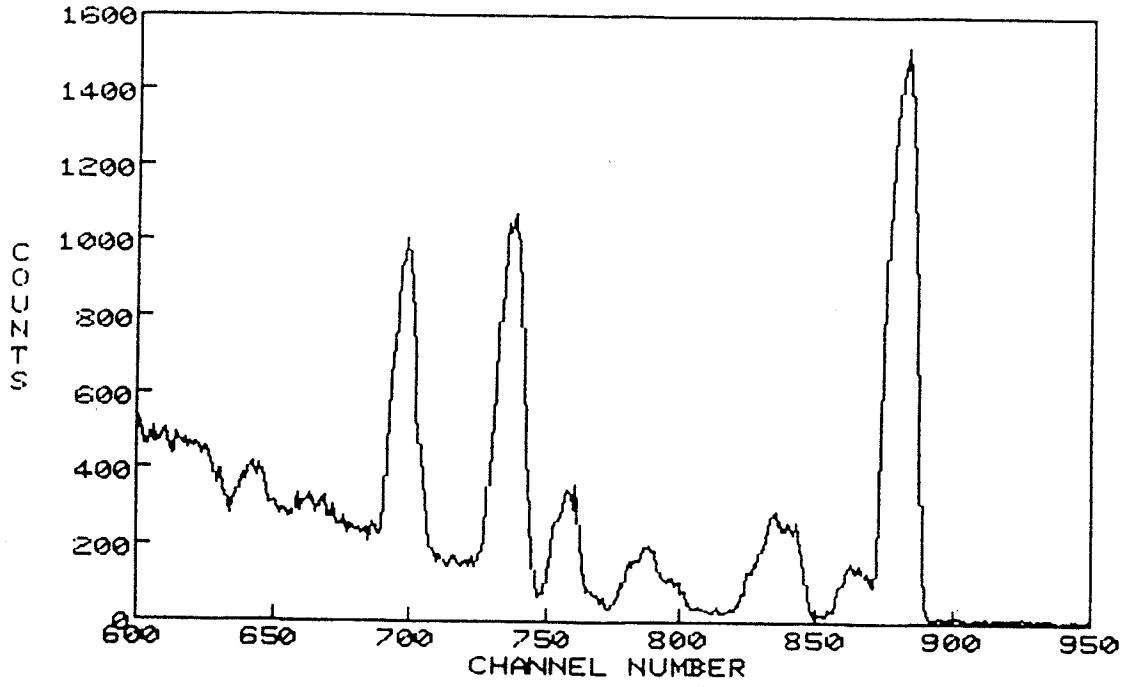

b) Expanded scale

Fig. 3-16 Energy spectrum (raw) of the $^{13}C(p,\alpha)^{10}B$ reaction at an incident proton energy of 40.45 MeV, at a lab. angle of 40°.

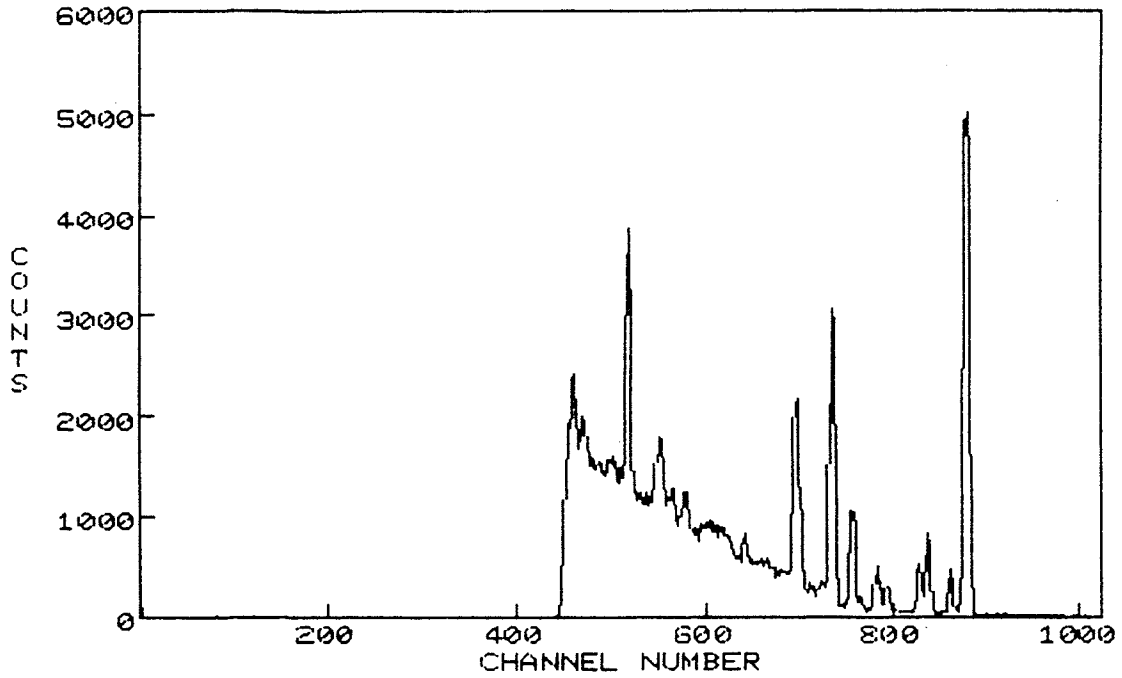

a) Full scale

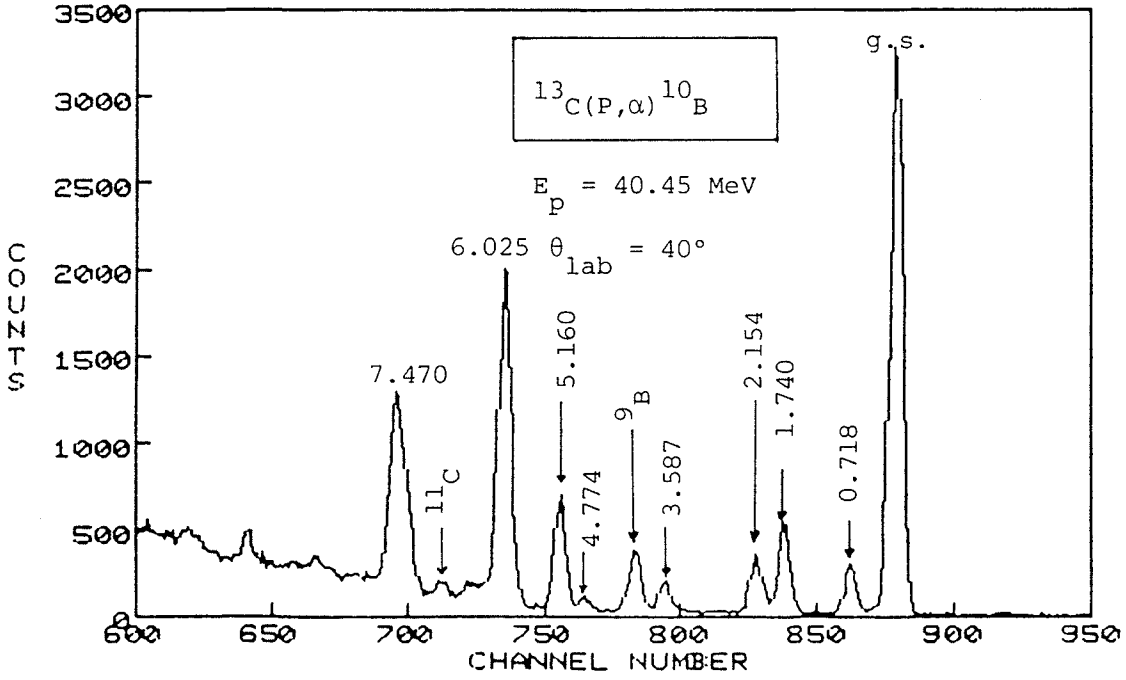

b) Expanded scale

Fig. 3-17 Energy spectrum (improved) of the $^{13}C(p,\alpha)^{10}B$ reaction at an incident proton energy of 40.45 MeV, at a lab. angle of 40°.

CHAPTER 4

Experimental Considerations and Data Analysis on Excitation and Decay of States in ^{10}B from the $^{13}C(p,\alpha)^{10}B$ Reaction

4-1 Introduction

The $^{13}C(p,\alpha)^{10}B$ reaction was investigated with the proton beam of the University of Manitoba Cyclotron laboratory at an energy of 40.45 MeV on a ^{13}C target using the 71 cm scattering chamber on the R-45 beam line. The products of interest were detected and identified using surface barrier detectors and the two-dimensional proportional counter discussed in the previous chapters. The beam was collected in a Faraday cup at the exit from the chamber and the beam current was integrated by scaling the output of a voltage-to-frequency converter. Fig. 4-1 shows a floor plan of the laboratory.

The experiment, reflecting the complete singles experiments and the simultaneous coincidence experiments, used a kinematic coincidence technique to measure the production of ^{10}B residual nuclei to various states and to study their decay properties. It was possible to largely separate the gamma decaying states from those states that decayed by particle emission.

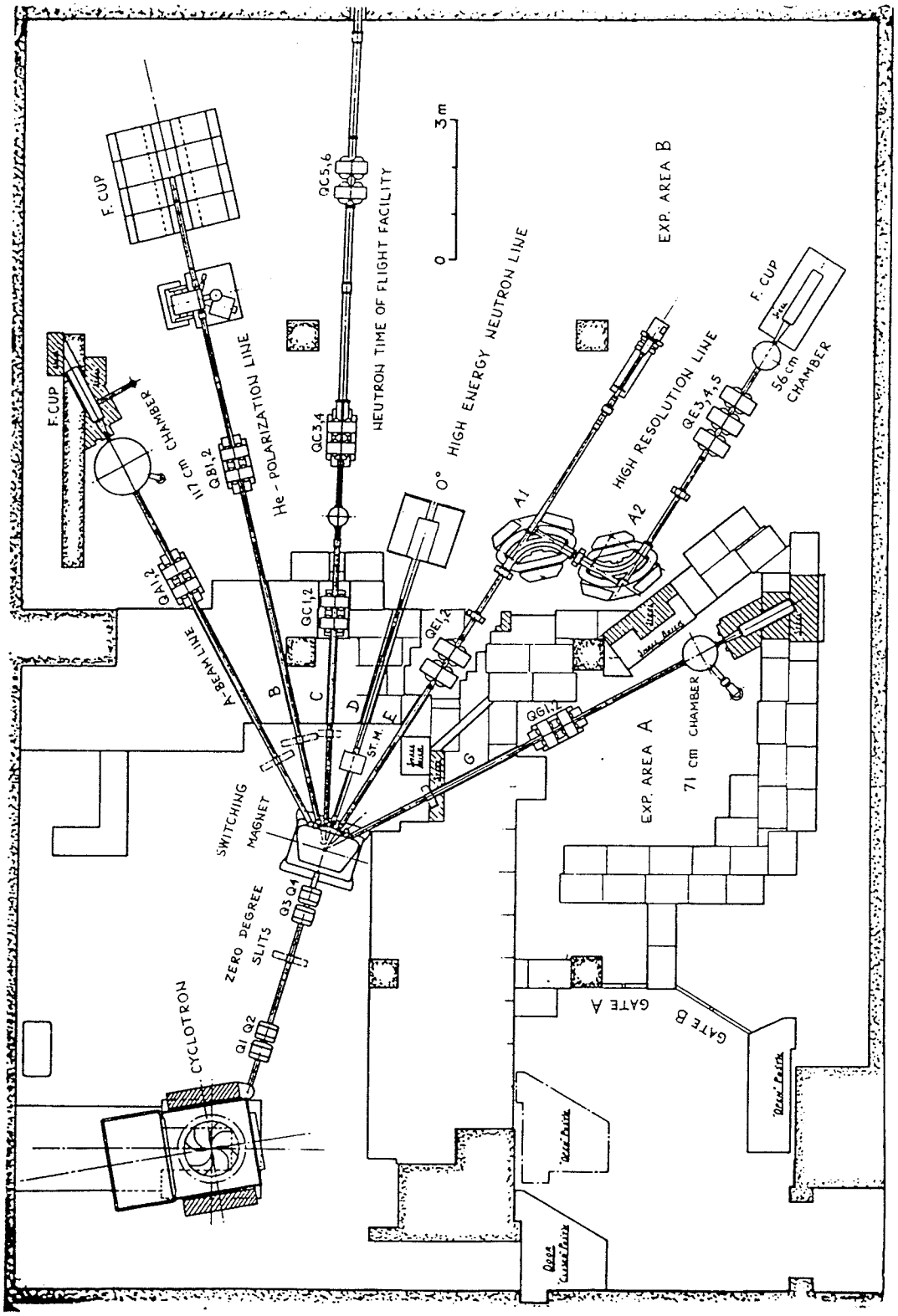

Fig. 4-1 University of Manitoba Cyclotron Laboratory.

By referring to the diagram of the electronics shown in Fig. 3-7 (chapter 3), it is noticed that two coincidence circuits were used. The inputs to the first coincidence circuit were provided from the outputs of single channel analyzers (SCA's) connected to the main amplifiers of the E1 detector and the proportional counter, which were in coincidence, and the output of the SCA connected to the main amplifier of the veto detector of telescope #1, which was in anticoincidence. In addition, an anticoincidence pile-up gate from amplifier E1 was also connected. This coincidence circuit defined the logic conditions for recording of single events. The second coincidence circuit, defining the logic conditions for recording of coincidence events, had two coincidence and two anticoincidence inputs. The coincidence inputs were supplied from the output of the first coincidence circuit and the output of the SCA connected to the main amplifier of the E2 detector. The anticoincidence signals were from the veto detector of telescope #2 and the pile-up output of the main amplifier of E2. The coincidence events were registered by connecting the outputs from this coincidence circuit to the input register.

4-2 Target and Detectors

The ^{13}C target in the form of a thin foil of areal density of about 100 $\mu g/cm^2$ was mounted at the center of the scattering chamber (for target angles refer to Table 4-1). The experimental set-up (refer to Fig. 4-7) consisted of two counter telescopes separated by an angle determined by kinematics to detect the reaction products. Telescope #1

consisting of an X-Y proportional counter, a 1000 μm (E1) stopping surface barrier detector and a 1000 μm veto detector, was used for detecting and measuring the energy of the outgoing alpha particles. The proportional counter, the design and construction of which was discussed in the previous chapters, provided position information in two dimensions. The stopping detector (E1) was thick enough to stop the alpha particles of interest and the veto detector was used to reject, by anticoincidence, events from long range particles, primarily elastically scattered protons. The solid angle was defined by the 15 mm diameter aperture of the E1 detector. Telescope #2 consisting of a 100 μm (E2) surface barrier detector, backed by a 1000 μm veto detector, was used for detecting coincidence ^{10}B recoils or ^{10}B breakup fragments mainly ^{6}Li and alpha particles or ^{9}Be and protons.

The front planes of the proportional counter and stopping surface barrier detector (E1) of telescope #1 were mounted 172.4 ± 0.5 mm and 216.6 ± 0.5 mm respectively from the target, and the E2 detector of telescope #2 was mounted 152.9 ± 0.5mm from the target(refer to Fig. 4-7). Considering the 15 mm diameter apertures of E1 and E2 detectors, the acceptance angles of these detectors were as follows:

- Acceptance angle of E1 detector:

$$\Delta\theta_3 = 1/2\ [15/(216.6 \pm 0.5)] \times 57.29 = 1.98^{\circ}$$

- Acceptance angle of E2 detector:

Table 4-1 Detector and target angles

Target angle (θ_t) (deg)	Detector angle (deg)	
	α-particle detector (θ_3)	Recoil detector (θ_4)
30	40	102
30	40	104
30	40	106
45	70	71

$$\Delta\theta_{\psi} = 1/2\ [15/(152.9 \pm 0.5)] \times 57.29 = 2.81^{\circ}$$

For detector and target angles refer to Table 4-1.

4-3 Energy Calibration

a) Scattered α-particles

After the kinematic correction, which was required in order to improve the spectrum resolution, and which was explained in chapter 3, the peaks in the alpha spectrum were identified and an energy calibration established. The centroids of these peaks were calculated and a least-squares straight line was fitted to these points, giving the energy as a function of the channel number. Fig. 3-17b), discussed in chapter 3, represents the expanded view of the alpha spectrum from which the centroids of the peaks were calculated and Fig. 4-2 shows the energy calibration curve for the scattered alpha particles. Table 4-2 contains the information obtained from the experimental peaks, kinematics and least-squares fitting.

Noting that the rate of change of alpha energy with respect to angle, $(dT/d\theta)$, depends on the particular reaction taking place, the calibration was carried out for two different angles of $\theta_3 = 40^{\circ}$ and $\theta_3 = 70^{\circ}$. The values of excitation energies at the two angles were compared and used to identify clearly those states excited via the $^{13}C(p,\alpha)\ ^{10}B$ reaction. As far as resolution is concerned, the FWHM

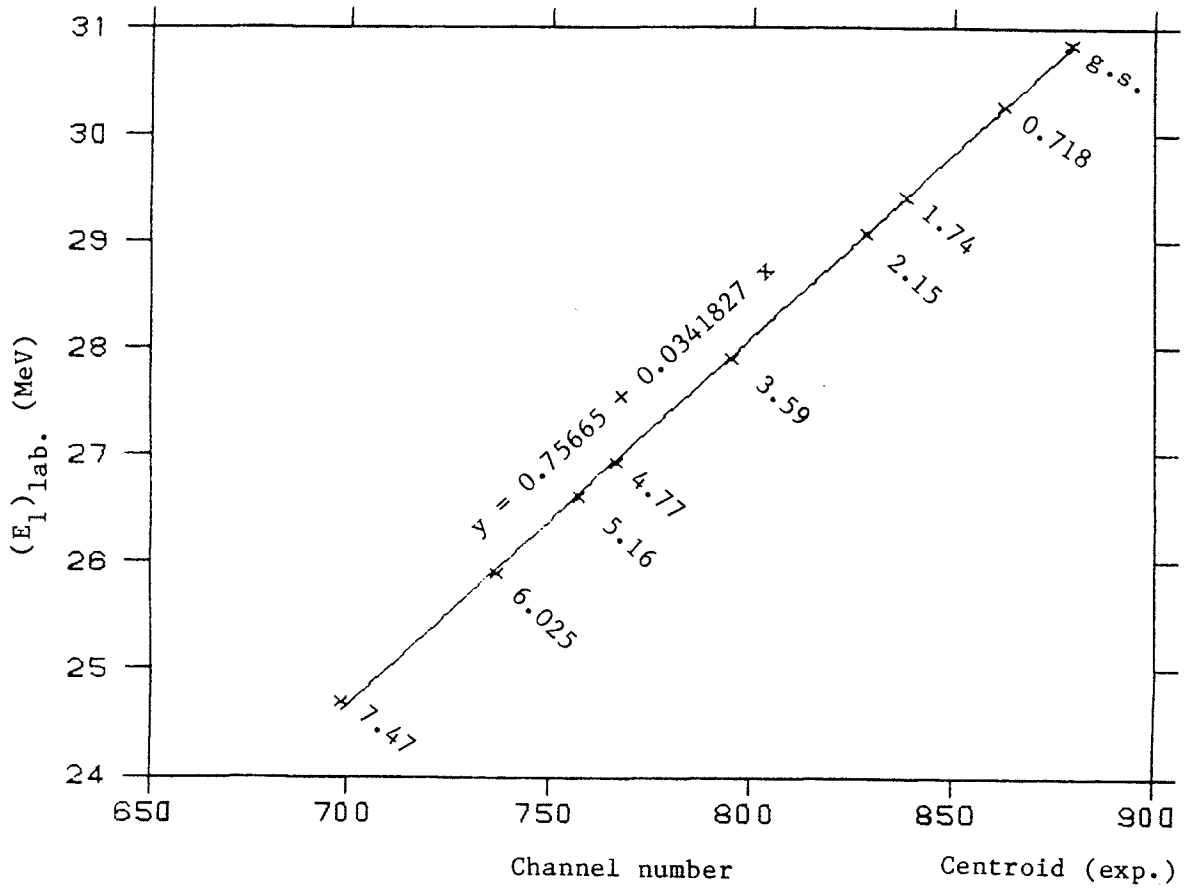

Fig. 4-2 Energy calibration curve for α-particles.

Table 4-2 Information obtained from the kinematics and the experimental peaks for the α-particles.

State	Centroid ($\bar{\chi}$) Channel	$(E_1)_{Kin}$ (MeV)	$(E_1)_{Fit}$ (MeV)	$\Delta E = (E_1)_{Kin} - (E_1)_{Fit}$ (MeV)
g.s	879.4	30.843	30.817	0.026
0.718	862.5	30.256	30.240	0.016
1.74	838.4	29.419	29.415	0.004
2.15	828.7	29.080	29.084	- 0.004
3.59	794.7	27.903	27.929	- 0.026
4.77	766.5	26.925	26.959	- 0.034
5.16	756.9	26.606	26.629	- 0.023
6.025	736.4	25.890	25.930	- 0.040
7.47	698.0	24.692	24.615	0.077

of the g.s. peak (Fig. 3-17b) is 6 channels corresponding to 0.215 MeV.

b) Recoil Nuclei

A two-dimensional energy spectrum, E_2 vs. E_1, of particles detected in coincidence with the scattered α-particles in telescope 1, is shown in Fig. 4-3. γ-decaying states are expected to result in a very high coincidence detection efficiency between the ^{10}B recoil nuclei and the scattered α-particles. Windows were set on identified peaks in the 1-D alpha spectrum and the resulting 2-D spectra corresponding to the gated peaks were projected on the vertical, E2, axis. The centroids of these projected spectra were calculated and used to obtain the energy calibration curve for recoil nuclei. The low-lying states of ^{10}B, which can only decay by γ-emission to form a clearly identifiable major group, were used to calibrate the coincidence detection efficiencies. These states are shown enclosed by dashed lines in Fig. 4-3 and the particle-decaying states are largely located outside of these bonds. Fig. 4-4 shows the energy calibration curve and Table 4-3 contains the information obtained from the experimental peaks, kinematics and least squares fitting.

The energy calibration was established without the energy loss corrections in the target. The intercept noticed in the energy calibration curve is mostly attributable to neglect of this energy loss.

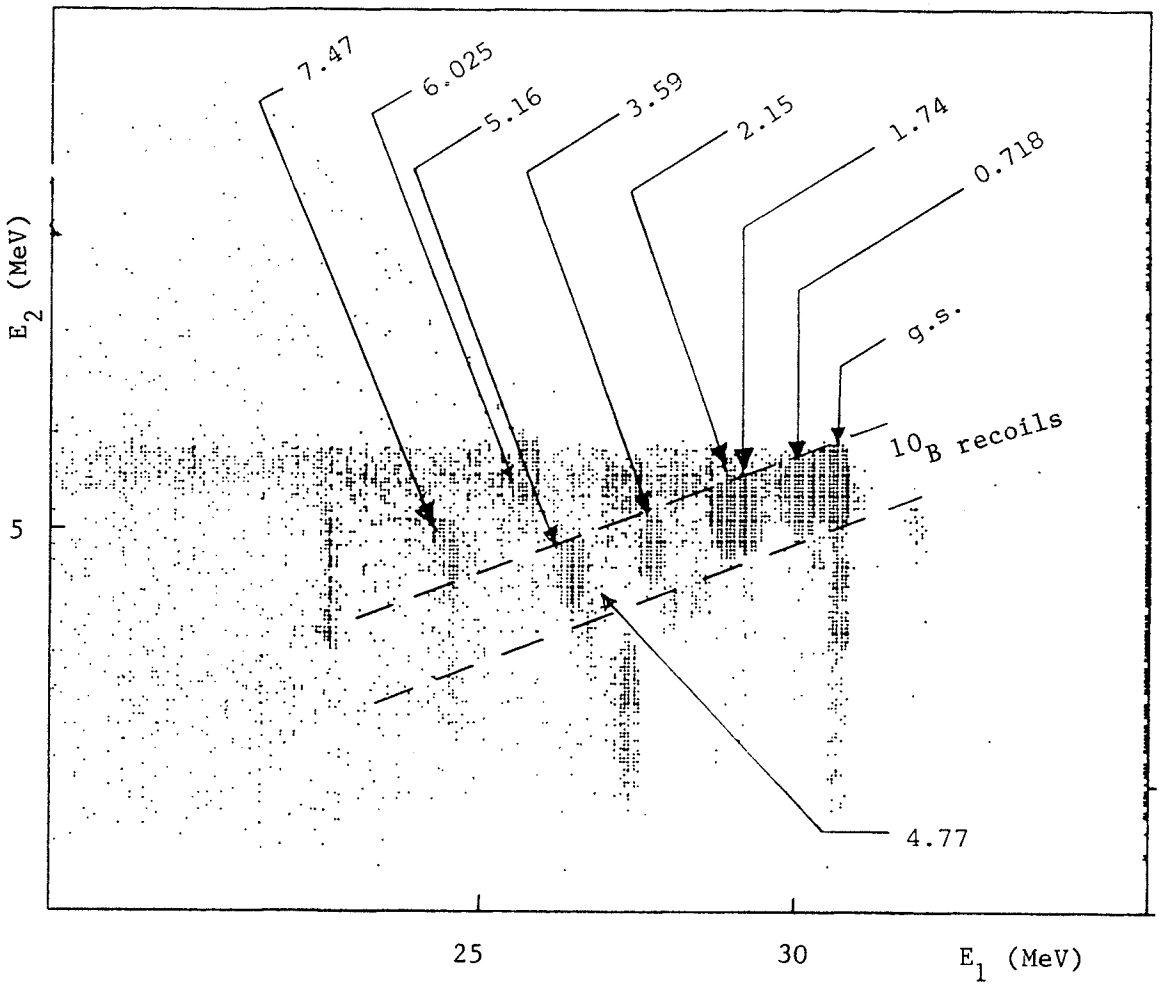

Fig. 4-3 Two-dimensional spectrum of recoil nuclei energy vs. scattered α-particles energy at a lab. angle of 40° and recoil detector angle of 106°.

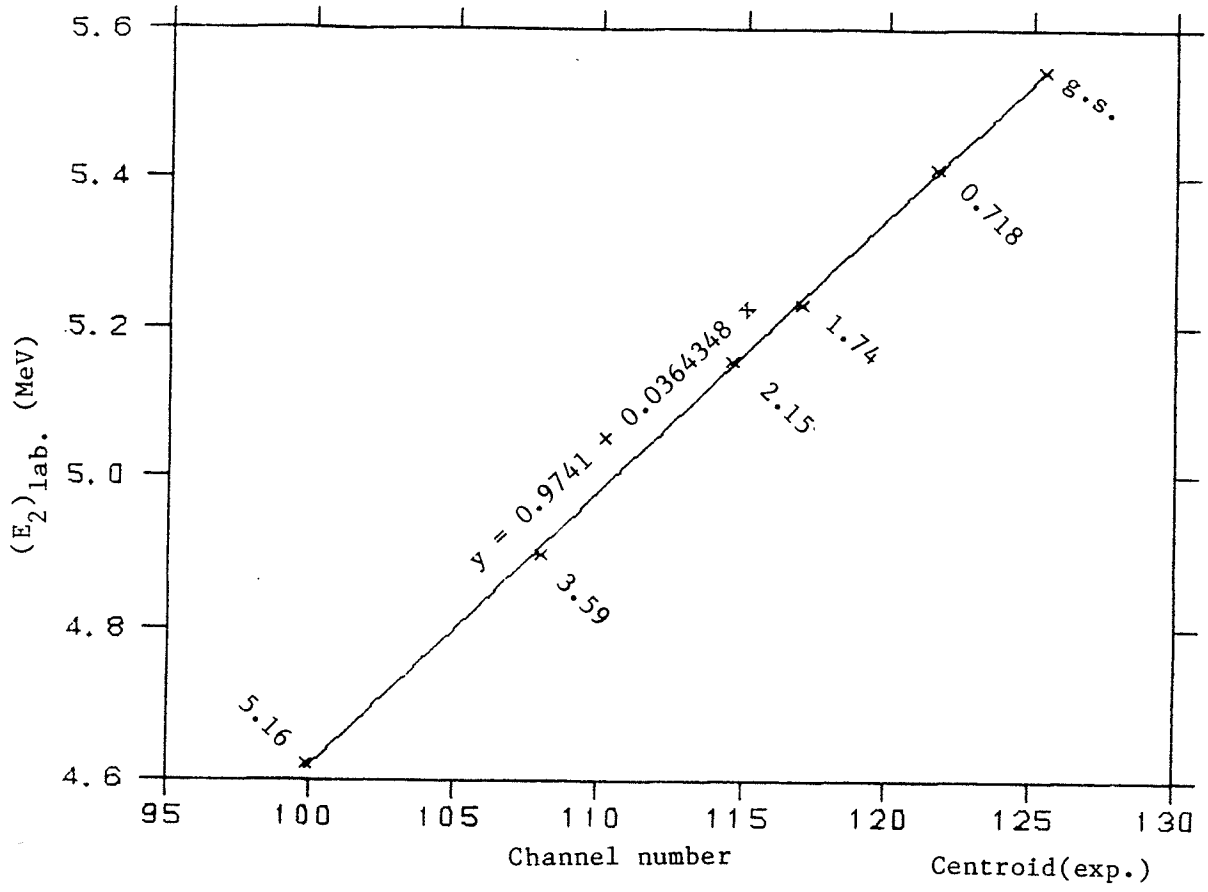

Fig. 4-4 Energy calibration curve for recoil nuclei.

Table 4-3 Information obtained from the kinematics and the experimental peaks for the ^{10}B recoil nuclei.

State	Centroid ($\bar{\chi}$) (Channel)	$(E_2)_{Kin}$ (MeV)	$(E_2)_{Fit}$ (MeV)	$\Delta E = (E_2)_{Kin} - (E_2)_{Fit}$ (MeV)
g.s.	125.4	5.544	5.544	0.000
0.718	121.7	5.413	5.407	0.006
1.74	117.0	5.228	5.236	- 0.008
2.15	114.5	5.153	5.146	0.007
3.59	108.0	4.897	4.909	- 0.012
5.16	99.9	4.621	4.614	0.007

4-4 Calculation of Scattering Angle

For kinematic correction of the spectrum it was necessary to calculate the scattering angle and use it in the following relation

$$T_3(\theta_3)_{corrected} = T_3(\theta_{3scatt})_{measured} - (dT_3/d\theta_3)\Delta\theta ,$$

where

T_3 is the energy (in MeV) of the scattered particle,

θ_3 is the angle of the corresponding detector (in radians) with respect to beam,

$dT_3/d\theta_3$ is the scattered particle energy change as a function of angle (in MeV/rad),

and

$$\Delta\theta = \theta_3 - \theta_{scattered}.$$

One of the main features of a two-dimension position sensitive proportional counter is the ability to calculate the scattering angle on an event by event basis. By referring to Fig. 4-5, the calculation of the scattering angle proceeds as follows. In this calculation, s,z denote the coordinates of a detector element in horizontal and vertical directions respectively on the plane of the proportional counter. The x-y coordinate system is defined by the beam which is in the x-direction and its origin located at the center of the target. The y-axis is in the scattering plane and the z-axis perpendicular to this plane. The

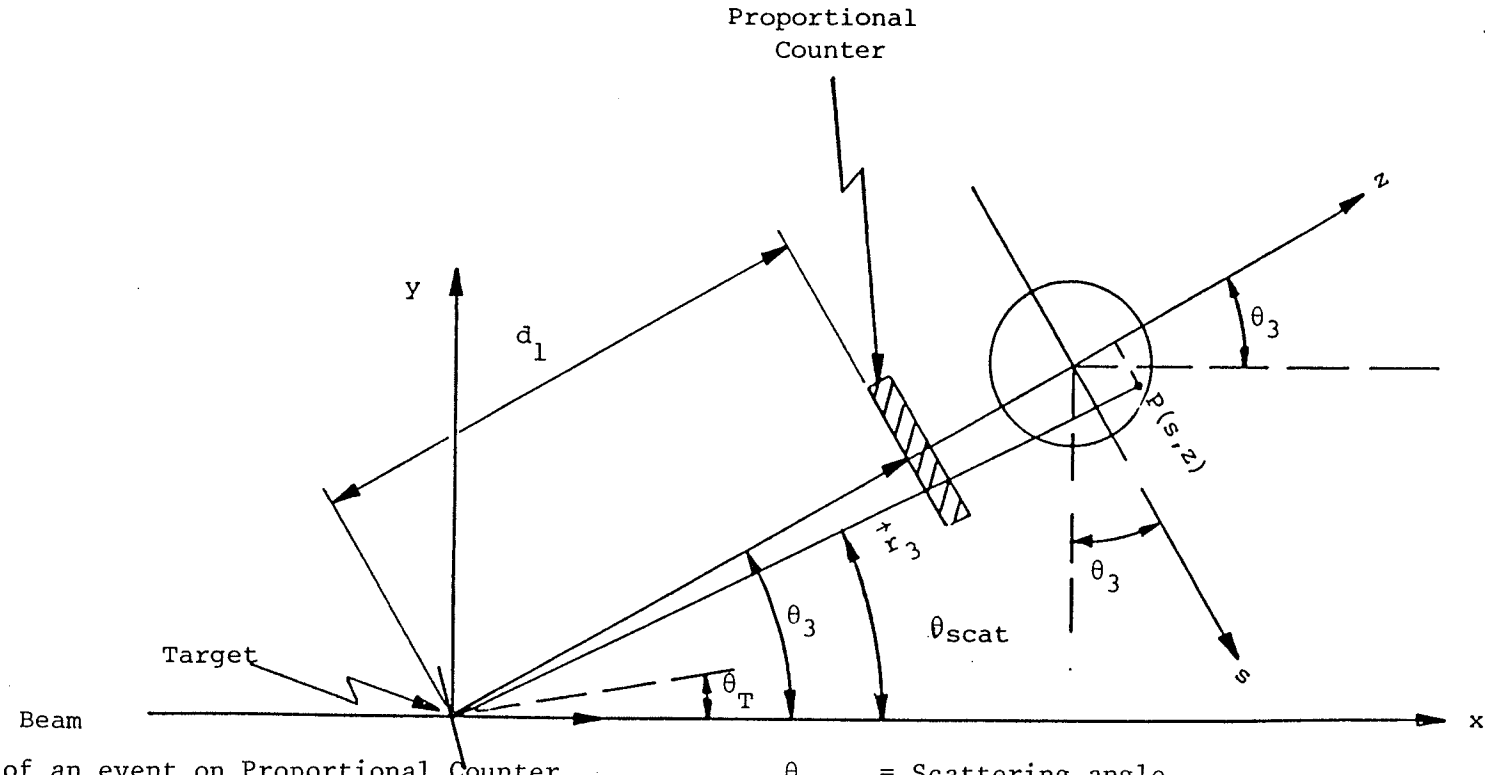

P= Position of an event on Proportional Counter

θ_3= Angle of detector with respect to beam

d_1= Distance from target to Proportional Counter

$\theta_{scat.}$ = Scattering angle

θ_T = Target angle

$\vec{r}_3$ = Position vector of scattered particle

Fig. 4-5 Scattering angle

definition of the other elements are explained in Fig. 4-5.

$$x_P = d_1 \cos\theta_3 + s \sin\theta_3.$$

$$y_P = d_1 \sin\theta_3 - s \cos\theta_3.$$

$$z_P = z.$$

Then, the position vector, $\vec{r}_3$, of the scattered particle can be written as follows

$$\vec{r}_3 = x_P \hat{i} + y_P \hat{j} + z_P \hat{k}.$$

$$\vec{r}_3 . \hat{i} = r_3 \cos(\theta_{scatt}).$$

From Fig. 4-5

$$\cos(\theta_{scatt}) = (\vec{r}_3 . \hat{i})/r_3 = x_P/r_3,$$

where

$$r_3 = [(x_P)^2 + (y_P)^2 + (z_P)^2]^{1/2}.$$

$$\therefore \quad \theta_{scatt} = \cos^{-1}\{(d_1 \cos\theta_3 + s \sin\theta_3)/[(x_P)^2 + (y_P)^2 + (z_P)^2]^{1/2}\}.$$

4-5 Theoretical considerations

Many nuclear reactions at low energy are of the type

$$A + a \text{ ----------> } B + b + Q, \quad (4\text{-}1)$$

with $b = a + x$.

where A is a target nucleus, a is the impinging particle, and B and b are the products; b is usually a light nucleus or a gamma ray with x referring to the transferred particle(s). The reaction represented in eq.(4-1) is often described in a very convenient notation

$$A(a,b)B.$$

The Q of the reaction is the rest mass difference multiplied by c^2 of the left side minus that of the right side of the equation. For endothermic reactions, $|Q|$ is the minimum center-of-mass kinetic energy required for the reaction to take place.

We may consider the target nucleus, as seen from an incoming particle, as a region with a potential and an absorption coefficient. When the incoming particle hits the target it may be diffracted by the potential without losing any energy (elastic scattering).

If the incoming particle enters the nucleus, it may hit one nucleon and lift it to a higher energy state or even to an unbound state and still preserve enough energy to leave the nucleus. This process is called inelastic scattering.

The incident particle may lose so much energy that it cannot escape the struck nucleus. If this energy is transferred to a nucleon leaving it bound, however, we have the case of formation of a compound nucleus. The energy is distributed among the nucleons and no nucleon can leave the nucleus until, by further collisions, the energy reconcentrates in one nucleon. The compound nucleus gives rise to a typical energy spectrum for the emitted particles, having a nearly Maxwell distribution of velocities and a practically isotropic angular distribution. In contrast, the direct-interaction mechanism gives strong angular dependences, and characteristic maxima of the cross section as a function of energy. Between these two extreme cases there is also "preequilibrium emission", in which a nucleon is emitted after some collisions, but before thermalization. The preequilibrium emission is recognizable from its energy and angular distribution; (p,α) and (n,α) reactions exhibit characteristics of preequilibrium reactions.

Diffraction scattering and direct interactions are expected to occur in periods of the order of 10^{-22} sec., the time a nucleon takes to travel the nuclear diameter. The compound nucleus, on the other hand, reaches thermal equilibrium in times very much greater than this period.

Excited levels have lives strongly dependent on the excitation energy. Their level widths,

$$\Delta E = \Gamma = h/\tau.$$

go from a small fraction of an eV to several MeV.

The probability that the reaction will take place rapidly and involve fewer target nucleons increases at higher energies (Ma 71).

The results of some (p,α) reactions have been interpreted on the basis of the presence of both compound nuclear and direct reaction transitions (Bl 63), or alternatively with a pre-compound decay model (Gu 71).

At energies comparable to our experiment the primary interaction occurs in times roughly equivalent to the transit time across the nucleus of the incident particles ($\sim 10^{-22}$ sec.). Assuming the reaction to involve only a few target nucleons, and if there is a good overlap between the initial and final state wave functions, the (p,α) reaction of our interest is considered to be direct. For details about direct reaction formalism, refer to (Ma 71), (Hi 67), (Au 69), (Gl 71) and (Sat 64).

4-6 Data Analysis

Energy levels of ^{10}B are shown diagrammatically in Fig. 4-6a) and in tabulated form in Table 4-4 (Aj 79) and (Aj 84). Each nuclear energy level is specified by excitation energy E, nuclear spin (total angular momentum) J, parity π, lifetime τ, and isospin T. Because of the small momentum carried by γ-rays, γ-decaying states (low lying states) result in nearly 100% coincidence detection efficiency between the ^{10}B recoil nuclei and alpha particles passing through the central region of the X-Y counter. Particle decaying states, on the other hand, result in lower

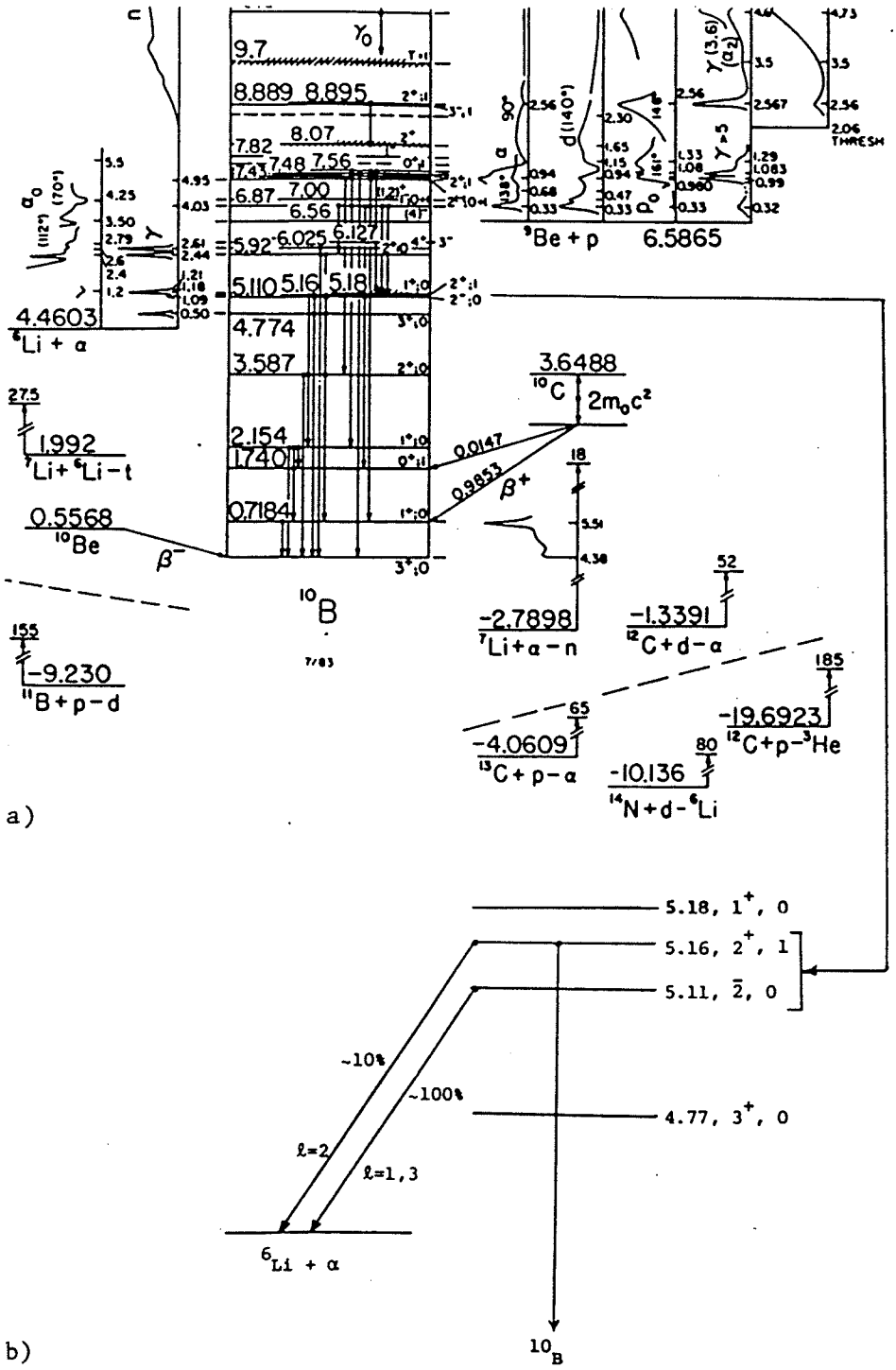

Fig. 4-6 Energy levels of ^{10}B.

E_x (MeV±keV)	$J^\pi; T$	τ_m or $\Gamma_{c.m.}$ (keV)	Decay
g.s.	$3^+;0$	stable	
0.71835±0.04	$1^+;0$	$\tau_m = 1.020 \pm 0.005$ nsec $g = +0.63 \pm 0.12$	γ
1.74015±0.17	$0^+;1$	7±3 fsec	γ
2.1543±0.5	$1^+;0$	2.13±0.20 psec	γ
3.5871±0.5	$2^+;0$	153±12 fsec	γ
4.7740±0.5	$3^+;0$	$\Gamma = 8.7 \pm 2.2$ eV	γ, α
5.1103±0.6	$2^-;0$	0.93±0.07 keV	γ, α
5.1639±0.6	$2^+;1$	$\tau_m < 6$ fsec	γ, α
5.180±10	$1^+;0$	$\Gamma = 110 \pm 10$	γ, α
5.9195±0.6	$2^+;0$	6±1	γ, α
6.0250±0.6	4^+	0.05±0.03	γ, α
6.1272±0.7	3^-	2.36±0.03	α
6.561±1.9	$(4)^-$	25.1±1.1	α
6.873±5	$1^-;0+1$	120±5	γ, p, d, α
7.002±6	$(1,2)^+;(0)$	100±10	p, d, α
7.430±10	$2^{(-)};0+1$	100±10	γ, p, d, α
7.467±10	1^+	65±10	p
7.479±2	$2^+;1$	74±4	γ, p
7.5607±0.9	$0^+;1$	2.65±0.18	γ, p
(7.67±30)	$(1^+;0)$	250±20	p, d
7.819±20	1^-	260±30	p
8.07	2^+	800±200	γ, p, d
(8.7)	$(1^+, 2^+)$	(~200)	p
8.889±6	$3^-;1$	84±7	γ, n, p, α
8.895±2	$2^+;1$	40±1	γ, p, α
(9.7)	$(T=1)$	(~700)	n, p, α
10.84±10	$(2^+, 3^+, 4^+)$	300±100	γ, n, p
11.52±35		500±100	(γ)
12.56±30	$(0^+, 1^+, 2^+)$	100±30	γ, p
13.49±5	$(0^+, 1^+, 2^+)$	300±50	γ, p

Table 4-4 Energy levels of ^{10}B.

coincidence detection rates because of the much larger solid angle into which the breakup fragments are emitted. Fig. 4-7 represents a schematic view of the experimental set-up and the detection system. The breakup cones correspond to the 5.16 MeV excited state of ^{10}B producing α and ^{6}Li fragments. In this experiment, in addition to the coincidence study of the breakup of states in ^{10}B to measure the branching ratios for gamma and particle decay, particular emphasis was placed on investigating the excitation region of the doublet consisting of the 5.11 MeV, 2^-, T=0 and 5.16 MeV, 2^+, T=1 states, Fig. 4-6b). These states are of interest from the point of view of parity mixing.

4-6-1 Resolution Improvement in the α-particle Singles Spectrum

As discussed in section 3-8; due to the finite size of the acceptance angle of the α-particle detector ($\sim \pm 2$), kinematic broadening was large, accounting for the poor energy resolution expected and observed in the α-particle spectra. Some states like the g.s. and the 0.718 MeV state or 1.74 and 2.15 MeV states were not resolved (Fig. 3-16). However, by applying the kinematic correction, the resolution was greatly improved as shown in Fig. 4-8 (Fig. 3-17 repeated) at lab angle of 40° and in Fig. 4-9 at lab angle of 70°. The width (FWHM) for the g.s. which was 0.356 MeV in Fig. 3-16 was improved to 0.215 MeV in Fig. 4-8.

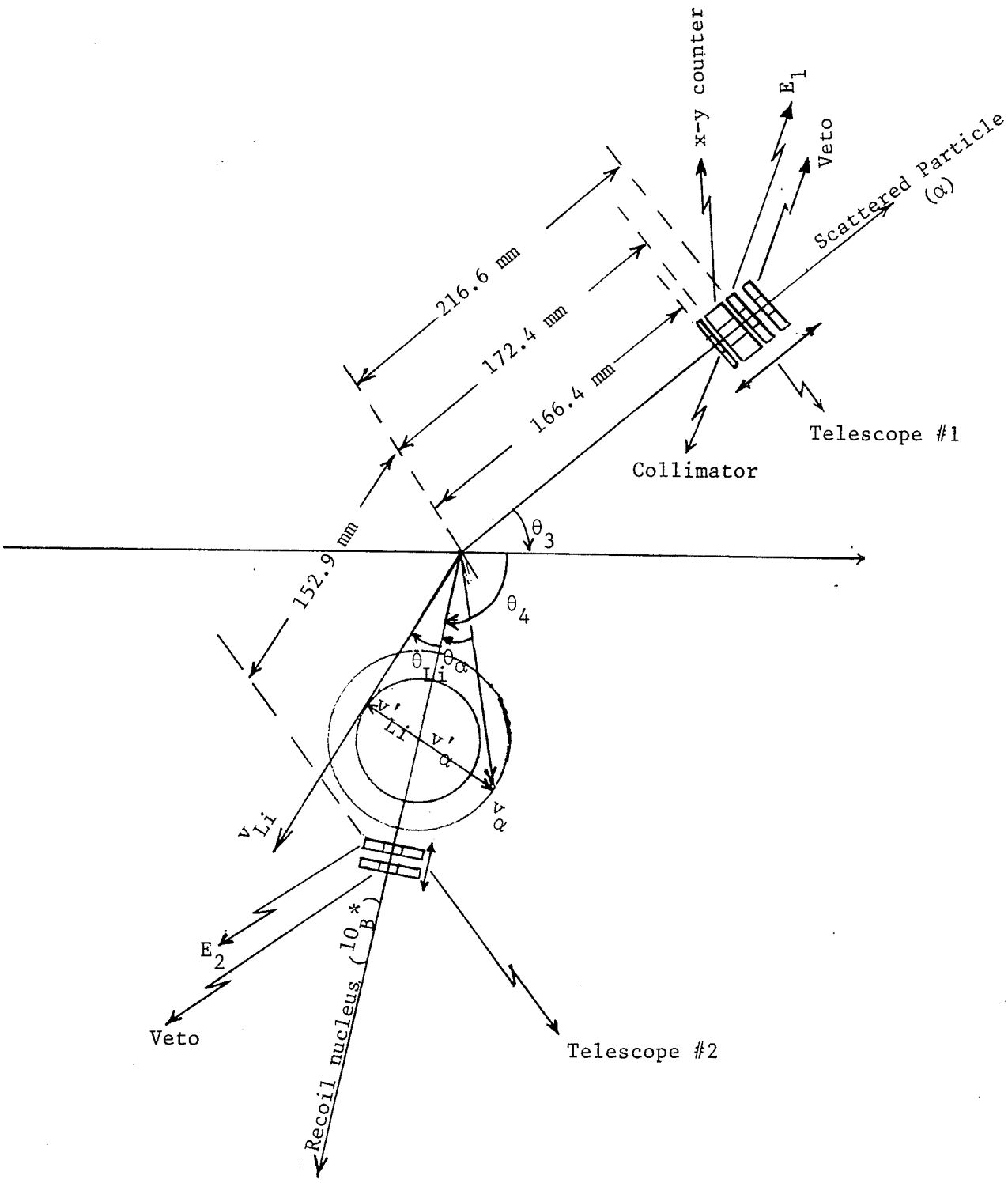

Fig. 4-7 Schematic view of the experimental set-up.

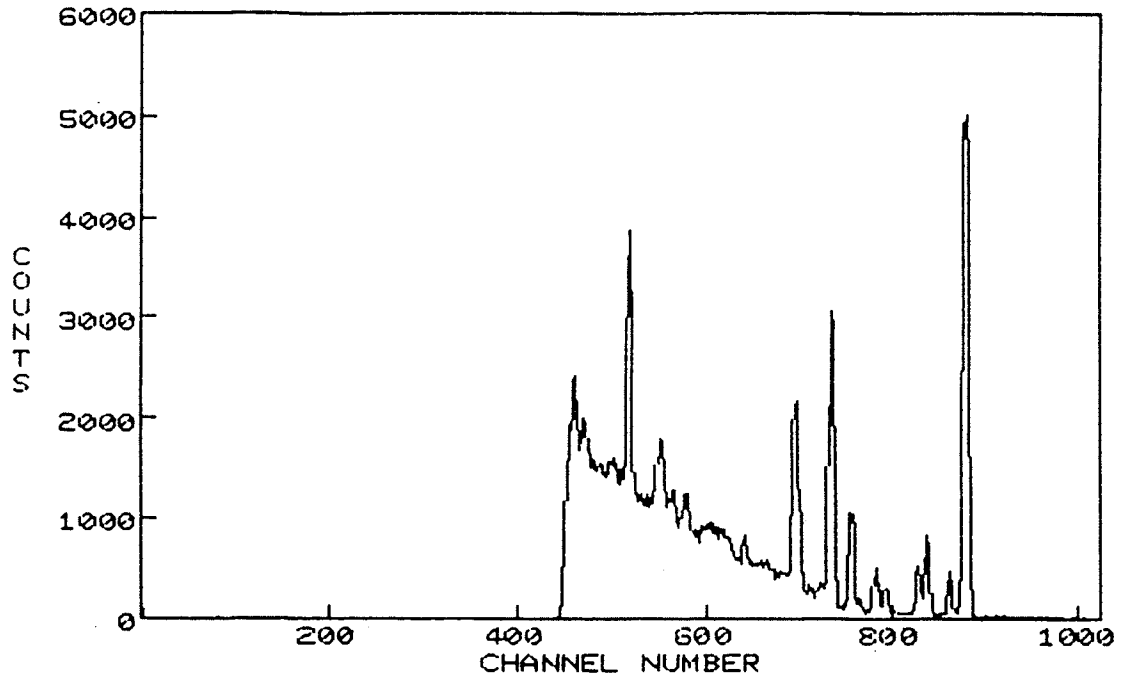

a) Full scale

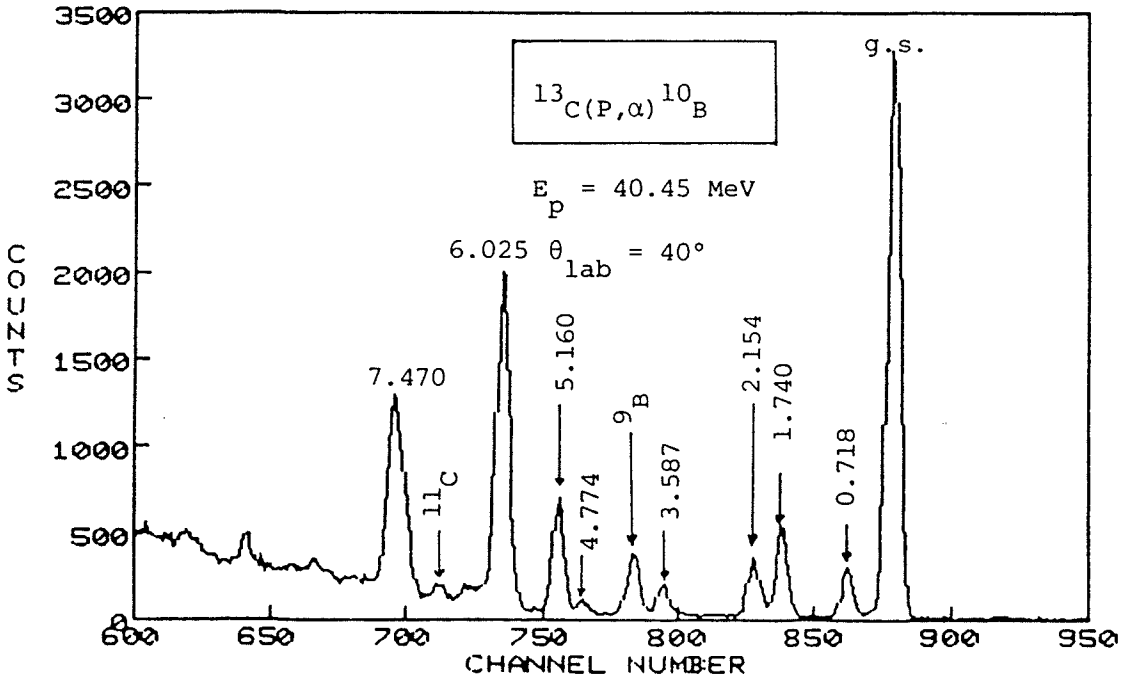

b) Expanded scale

Fig. 4-8 Improved energy spectrum of the $^{13}C(p,\alpha)$ ^{10}B reaction at an incident proton energy of 40.45 MeV and at a lab. angle of 40°.

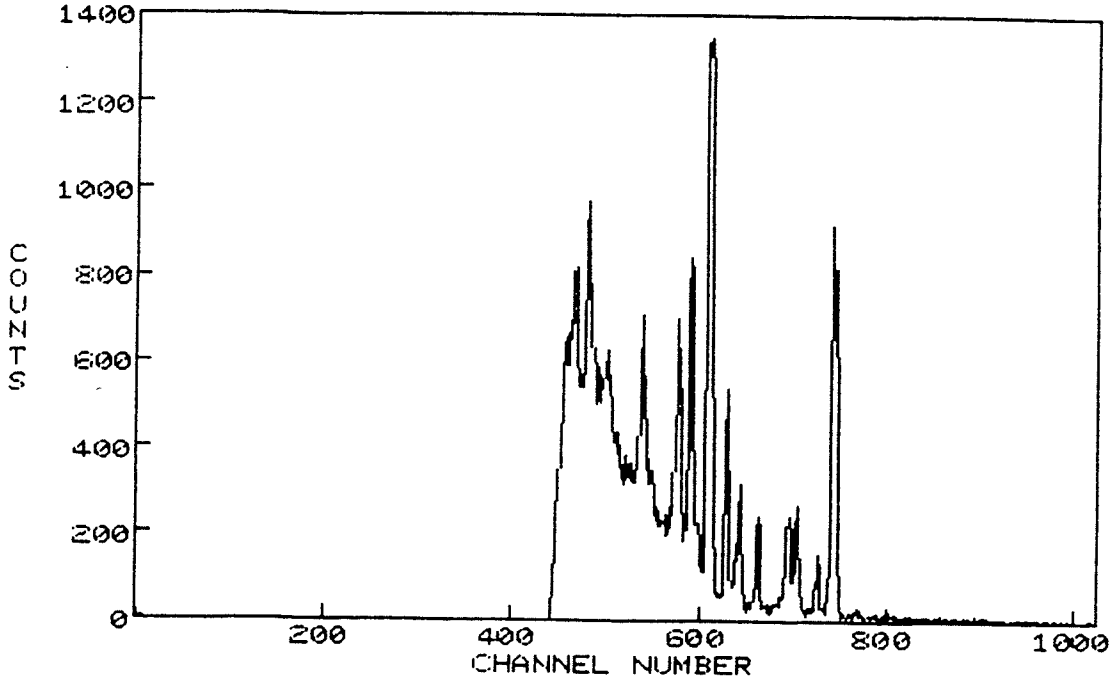

a) Full scale

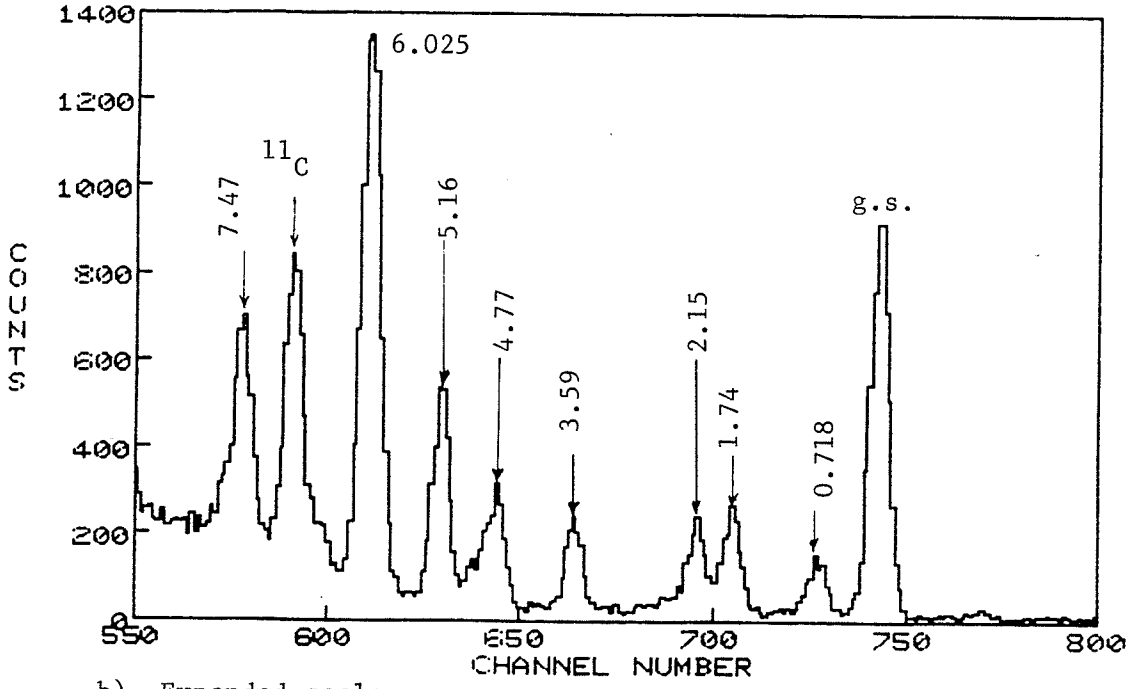

b) Expanded scale

Fig. 4-9 Improved energy spectrum of the $^{13}C(P,\alpha)^{10}B$ reaction at an incident proton energy of 40.45 MeV at a lab. angle of 70°.

4-6-2 Investigation of Energy Levels in ^{10}B

Levels were examined in the recoil nucleus (^{10}B) up to 7.47 MeV in excitation. The two-dimensional spectra of recoil nucleus (or breakup fragment) energy vs. scattered α-particle energy at a lab angle of 40° are shown in Fig. 4-10 and that at a lab angle of 70° is shown in Fig. 4-11. The corresponding angles for detector 2 were 106°, 104°, and 102° for Fig. 4-10 and 71° for Fig. 4-11 (refer to Table 4-1).

a) Gamma Decaying States

Because of the small momentum carried by γ-rays, γ-decaying states rapidly lead to ^{10}B recoil nuclei in their ground states, whose direction deviates only by a small amount (for example, max. deviation for 1.74 MeV state is 0.47°) from the initial direction of emission of the ^{10}B nuclei. The result is that the coincidence detection efficiency between the α-particle and the detected ^{10}B recoil is very high, if the two detectors are set at corresponding kinematic angles (refer to Fig. 4-7). The low lying states in the recoil nucleus, up to and including the 3.59 MeV state, can decay by γ-emission only, and these states were used to calibrate the coincidence detection efficiency. For the purpose of examining these states, gates were set on the corresponding peaks in the improved one-dimensional α-spectrum and the resulting 2-D spectrum for each state was projected vertically (on E_2-axis) to calculate and verify the corresponding energies for recoil nuclei. As an example, and in order to clarify the procedure, Fig. 4-12 represents a 1-D alpha spectrum with a gate set on the 1.74 MeV state.

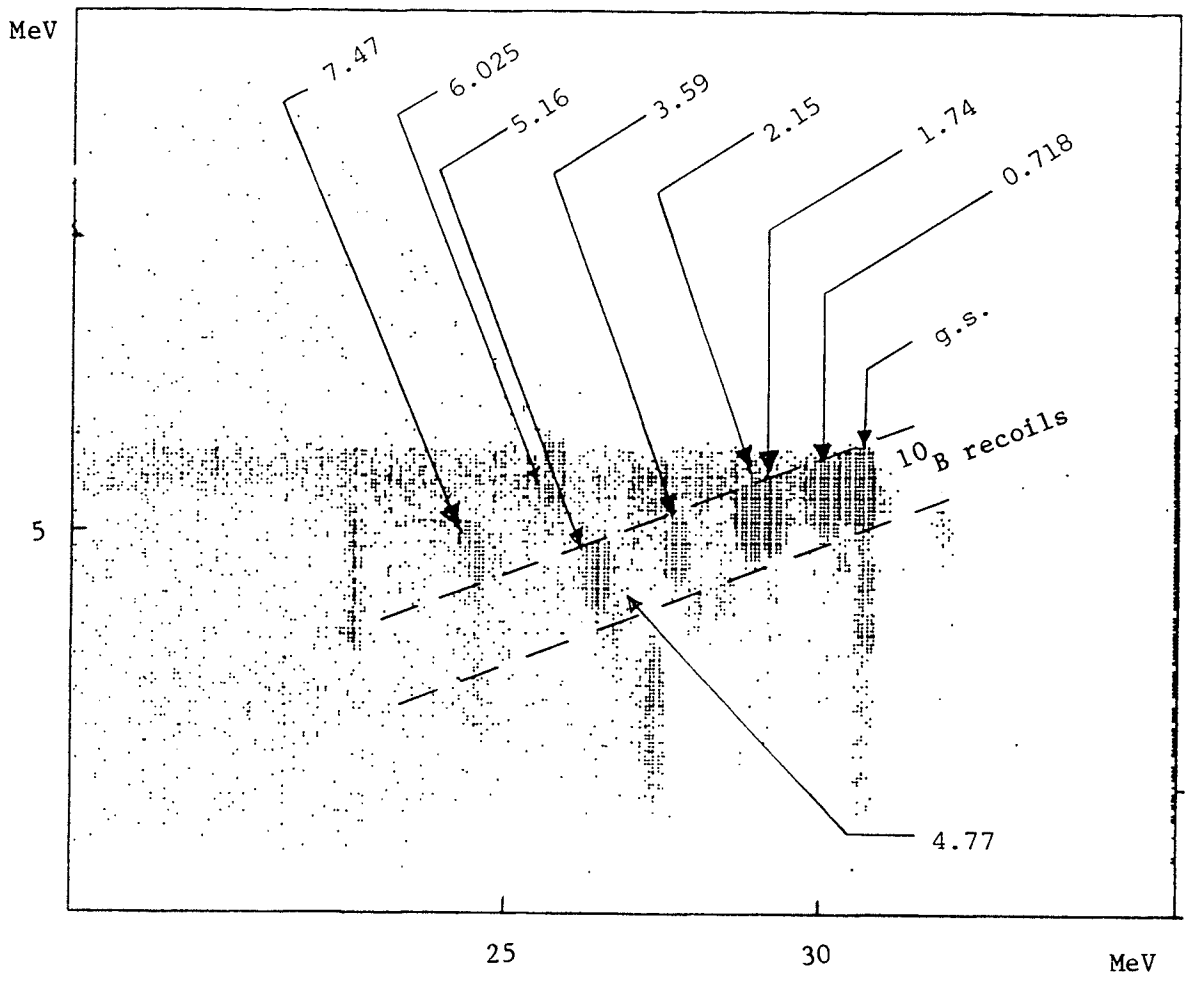

Fig. 4-10a) A two-dimensional spectrum of recoil nucleus (or breakup fragments) energy vs. scattered α-particle energy at a lab. angle of 40° (telescope E_1) and recoil detector angle of 106°.

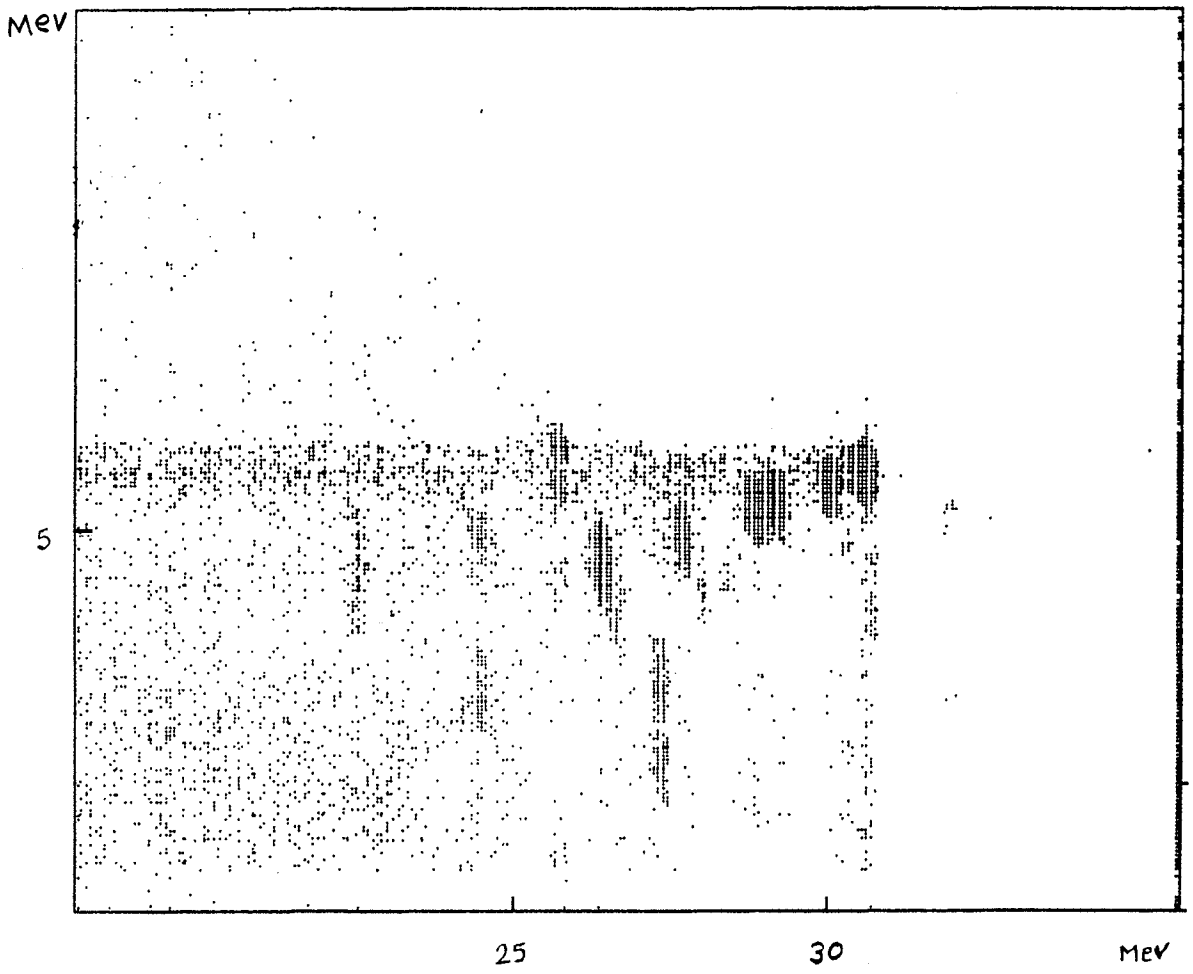

Fig. 4-10b) A two-dimensional spectrum of recoil nucleus (or breakup fragments) energy vs. scattered α-particle energy at a lab. angle of 40° (telescope E_1) and recoil detector angle of 104°.

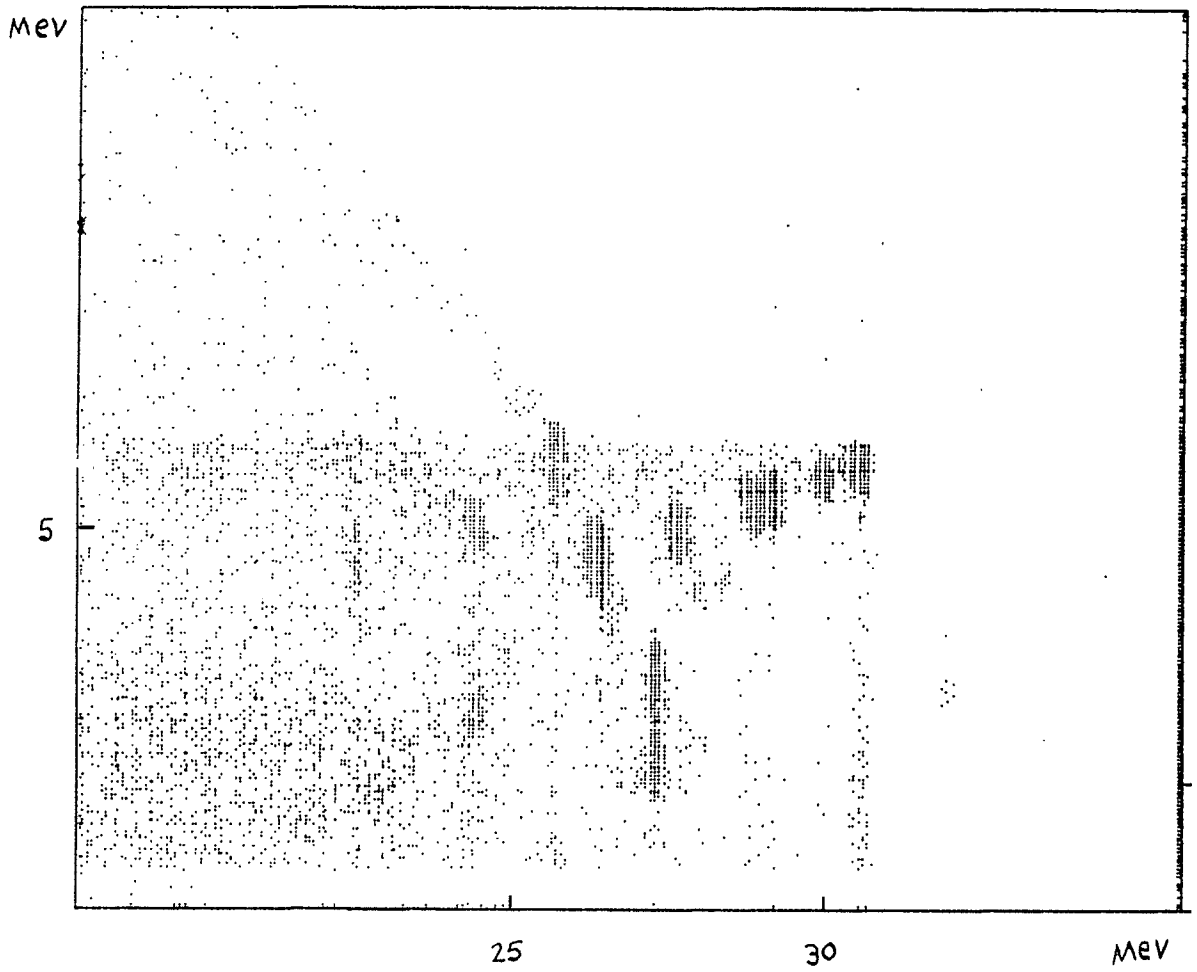

Fig. 4-10c) A two-dimensional spectrum of recoil nucleus (or breakup fragments) energy vs. scattered α-particle energy at a lab. angle of 40° (telescope E_1) and recoil detector angle of 102°.

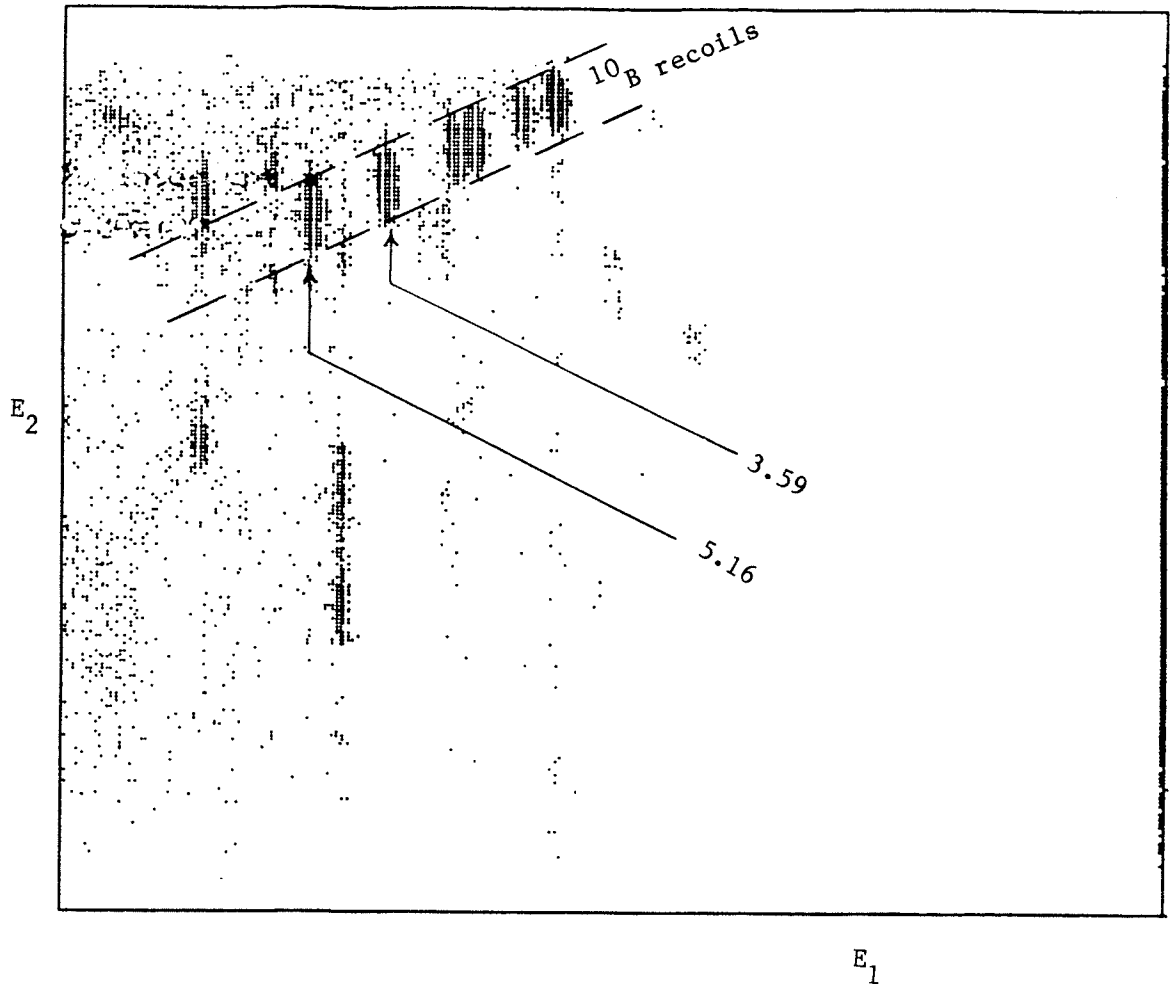

Fig. 4-11 A two-dimensional spectrum of recoil nucleus (or breakup fragments) energy vs. scattered α-particle energy at a lab. angle of 70° (telescope E_1) and recoil detector angle of 71°.

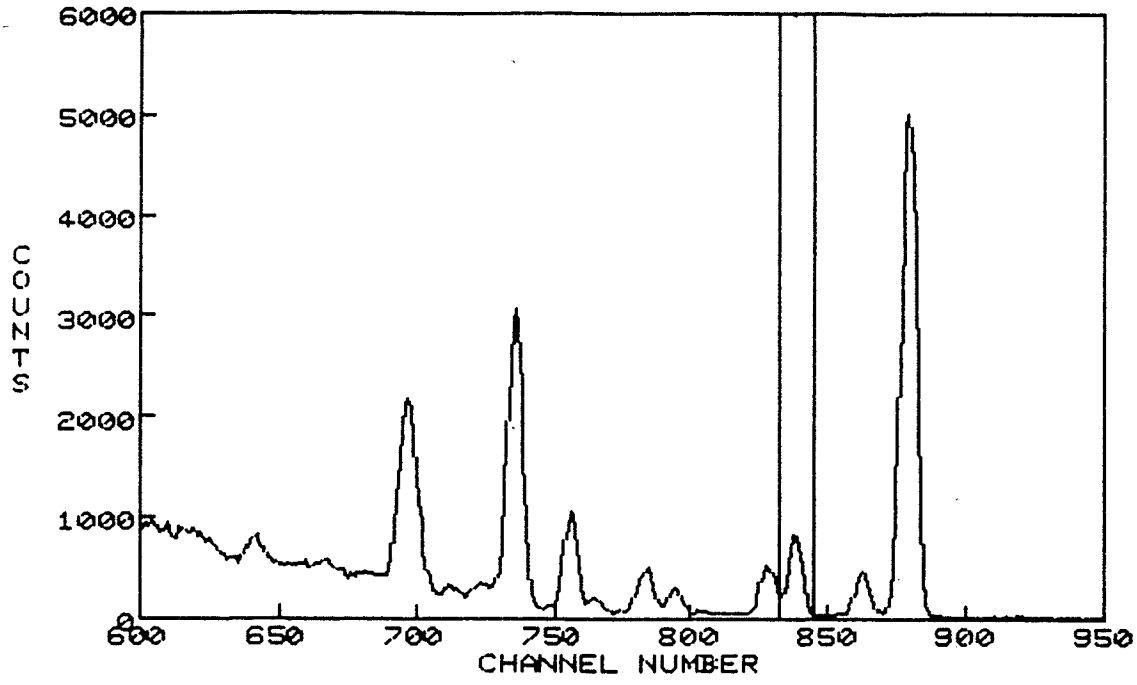

Fig. 4-12 α-spectrum with a gate set on the 1.74 MeV state.

Fig. 4-13 shows the resulting 2-D spectrum for this state picked out from the 2-D plot shown in Fig. 4-10a. By projecting the spectrum in Fig. 4-13 onto the vertical axis, Fig. 4-14 was obtained. The energy corresponding to the centroid of this peak was calculated and compared with that obtained from kinematics. The same procedure was repeated for the other states.

By referring to the 2-D plot shown in Fig. 4-10, it is concluded that the 0.718, 1.74, 2.15, and 3.59 MeV states are γ-decaying(as they must be, since this is the only channel allowed energetically), the 5.16 MeV state is primarily γ-decaying, but the other states of interest are particle-decaying. γ-decaying states, forming a major group, are shown within dashed lines in Fig. 4-10.

b) Particle decaying states

Particle decaying states result in low coincidence detection efficiencies because of the rather large solid angle into which the breakup fragments are emitted. On the basis of the detailed E_2 vs. E_1 2-D energy plots and the coincidence detection efficiency, it was possible to separate particle-decaying states from gamma decaying ones. The following states are primarily particle decaying states:

- 4.77 MeV state, mainly alpha decaying.
- 6.025 MeV state, mainly alpha decaying.
- 7.47 MeV state, mainly proton and alpha decaying.

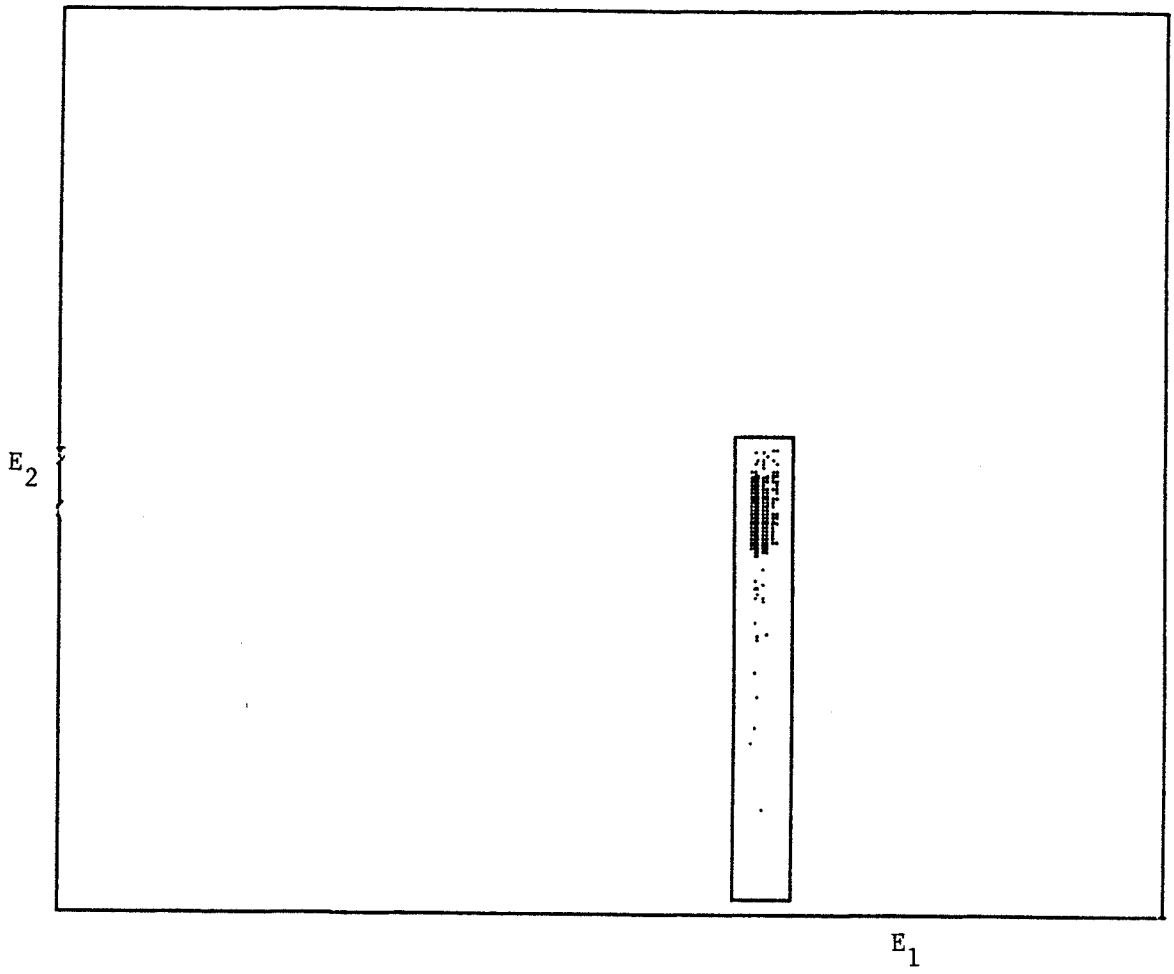

Fig. 4-13 2-D plot of E_2 vs. E_1 for the 1.74 MeV state.

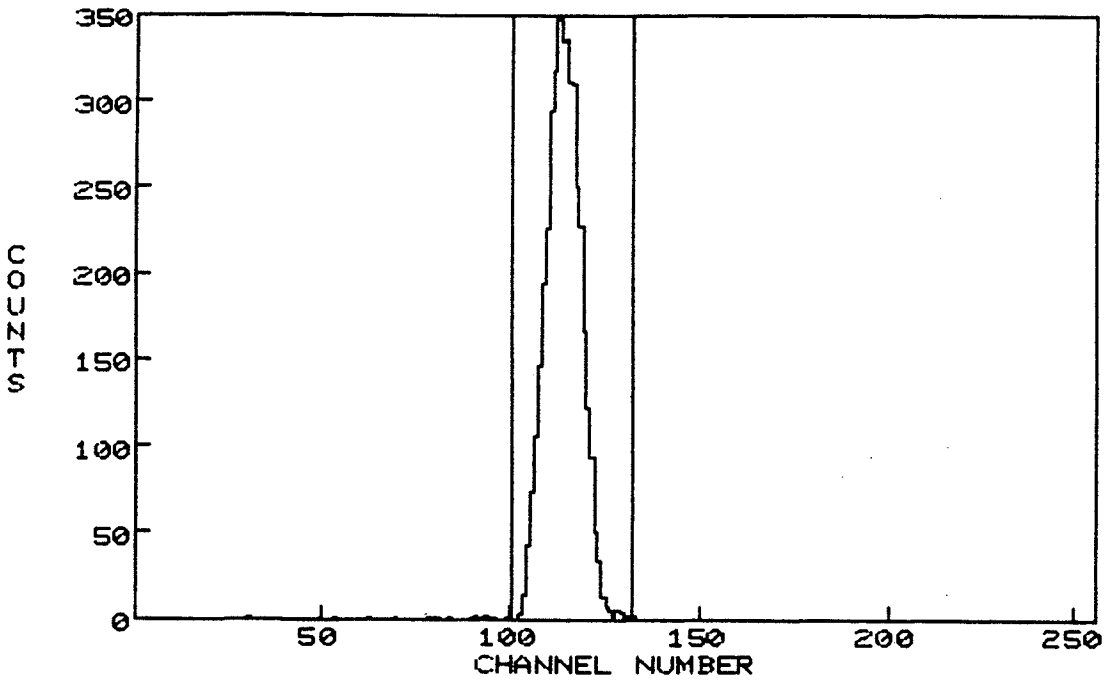

Fig. 4-14 Projection on the vertical axis of 1.74 MeV state.

In order to be able to present a good description of the above states and to study their branching ratios, it was necessary to calculate their detection efficiencies by using the efficiencies of the known γ-decaying states as a calibration. This subject is explained in detail in the following sections.

4-6-3 Efficiency Calculation

For the efficiency calculation it was necessary to separate random coincidence events from true events, to make background corrections, and then to verify the calculated values of efficiency by comparing these values with those obtained from a Monte Carlo simulation.

a) Effect of Setting Gate on the E2-TAC

The first attempt to remove a considerable fraction of random coincidence events was to set a gate on the time spectrum of the recoil nucleus, E_2-TAC. Fig. 4-15 shows a two-dimensional spectrum of recoil nucleus energy vs. alpha particle energy (kinematically corrected) while Fig. 4-16 represents the same spectrum with a gate set on E_2-TAC. A comparison of these two spectra immediately indicates the removal of a considerable portion of the random events in Fig. 4-16.

In addition to improving the two-dimensional spectrum, E_2 vs. E_1, as previously noted additional timing improvements could be made in the E_2-TAC spectrum by setting a gate on the respective peak in the alpha spectrum. As an example Fig. 4-17 and Fig. 4-18 show the energy and time spectra for E_2 and E_2-TAC respectively for all coincidence

events, and Fig. 4-19 and Fig. 4-20 represent the same spectra with an additional constraint of a gate set on the g.s. alpha peak. In addition setting a prompt coincidence gate on the E_2-TAC for each state under consideration, results in still further improvement. Fig. 4-21 shows a spectrum of E_2 for the g.s. when a gate was set on the E_2-TAC spectrum in Fig. 4-20. A comparison of the E_2 spectrum in Fig. 4-21 with that in Fig. 4-19 indicates the removal of some random events, especially in the region below channel 200.

Referring to Fig. 4-20, E_2-TAC (g.s.), the FWHM of the peak was 8 channels. Noting that a full scale of 1024 channels corresponds to 502 nsec, the timing resolution calculated is then 3.9 ± 0.1 nsec.

The frequency of the RF of the cyclotron producing the proton beam was 28 MHz, which corresponds to a period of T = 35 nsec. With a 1024 channel time scale of 502 nsec, one RF period thus corresponds to 71 channels. The spectrum of E_2-TAC, shown in Fig. 4-18 was expanded vertically by a factor of 200 with the intention that the peaks corresponding to random events for each beam burst be revealed (Fig. 4-22). Although the random coincidence background was too low to reveal this structure a timing gate of the same width as the prompt gate, but displaced by 71 nsec, was set on the E_2-TAC spectrum in order to display purely random events. Fig. 4-23 shows the resulting plot; it was found that the number of random events was negligible.

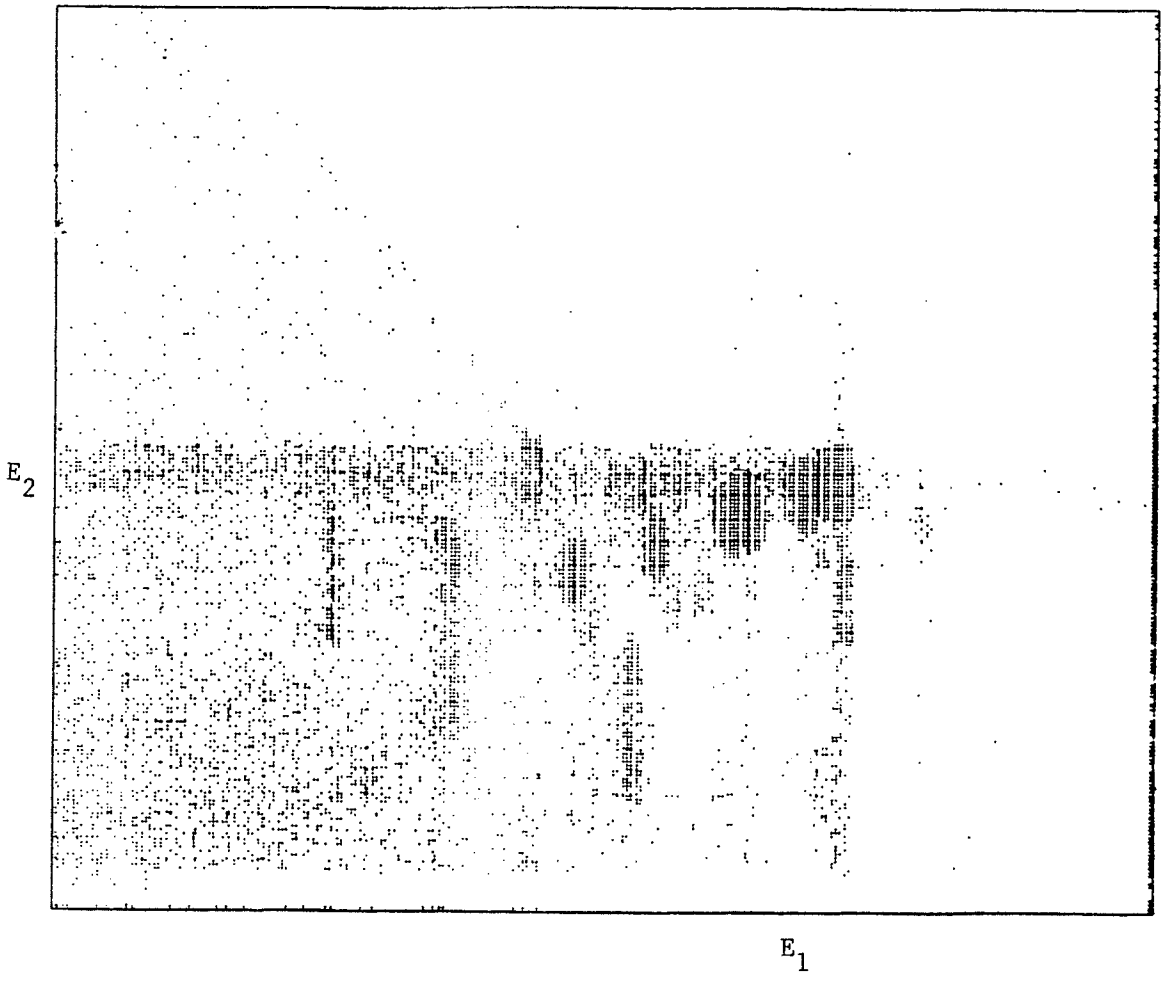

Fig. 4-15 E_2 vs. E_1 without setting a gate on the E_2-TAC.

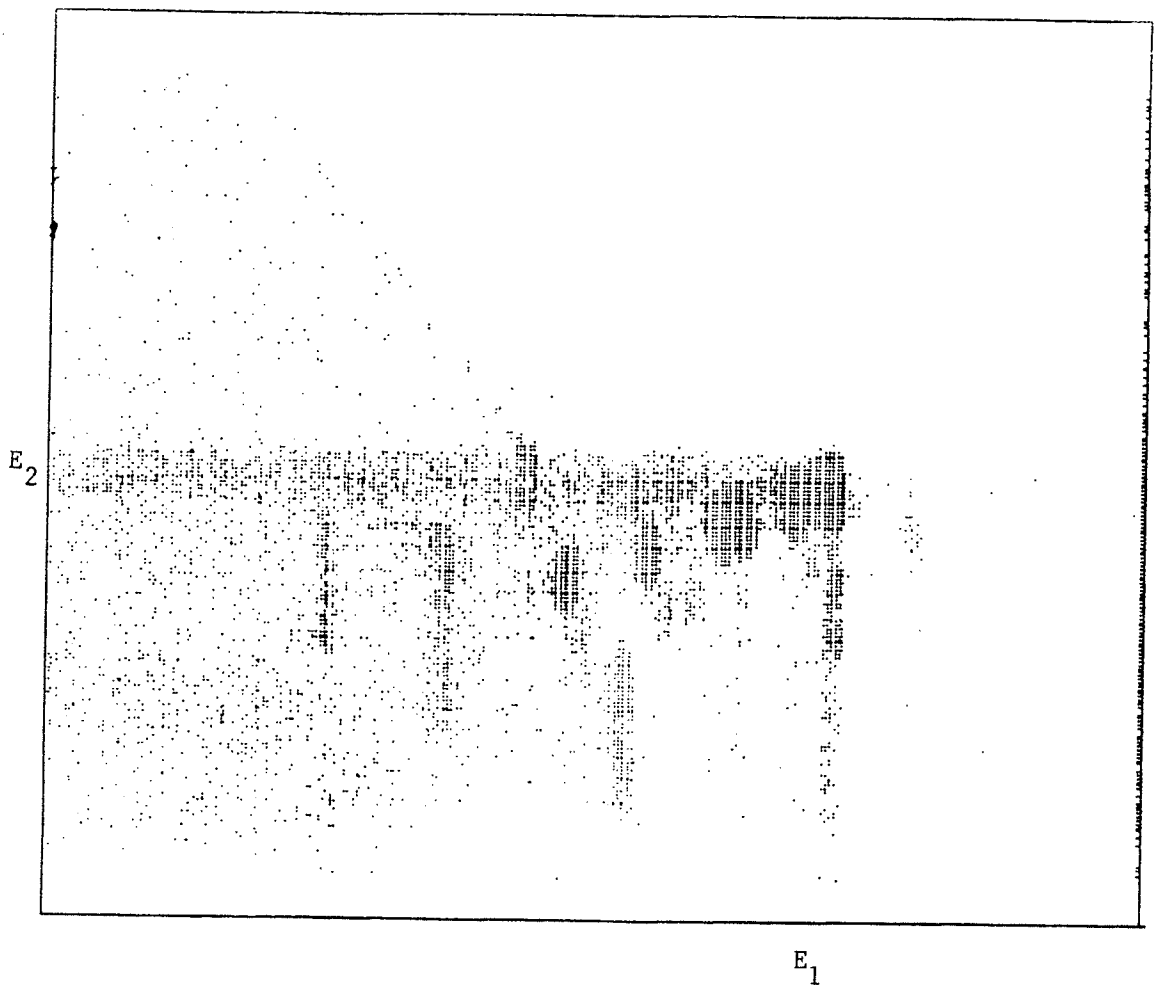

Fig. 4-16 E_2 vs. E_1 with a gate on the E_2-TAC.

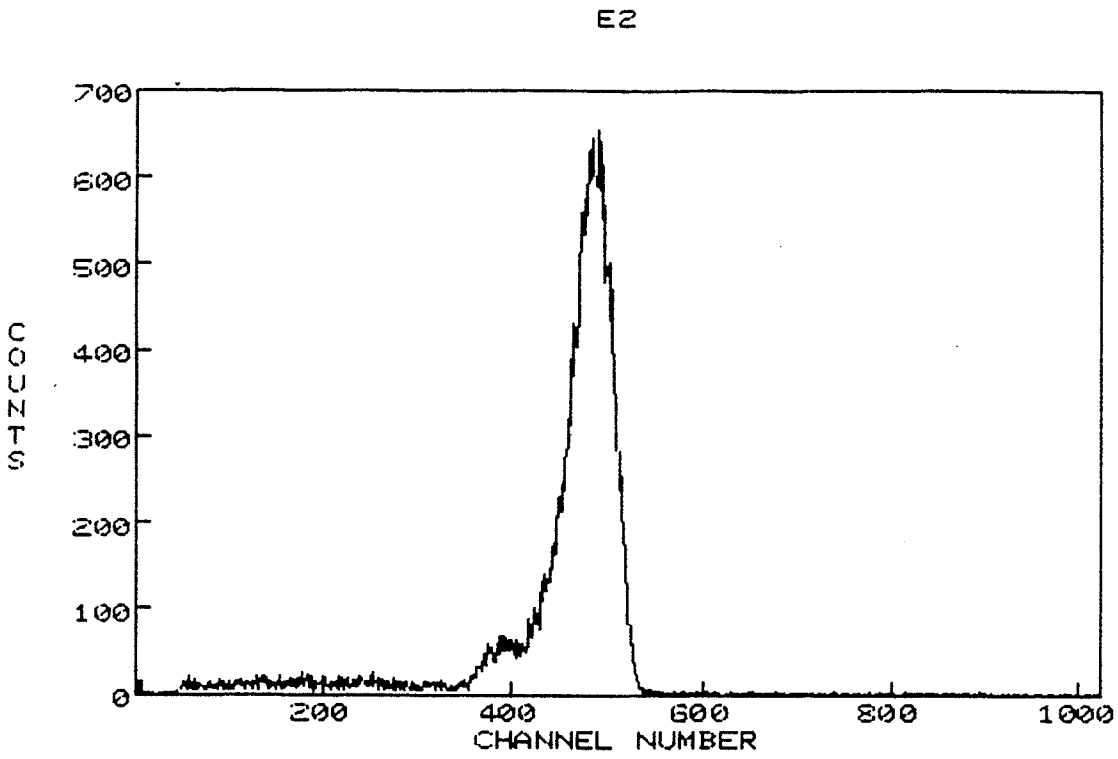

Fig. 4-17 E_2 (all coincidence events).

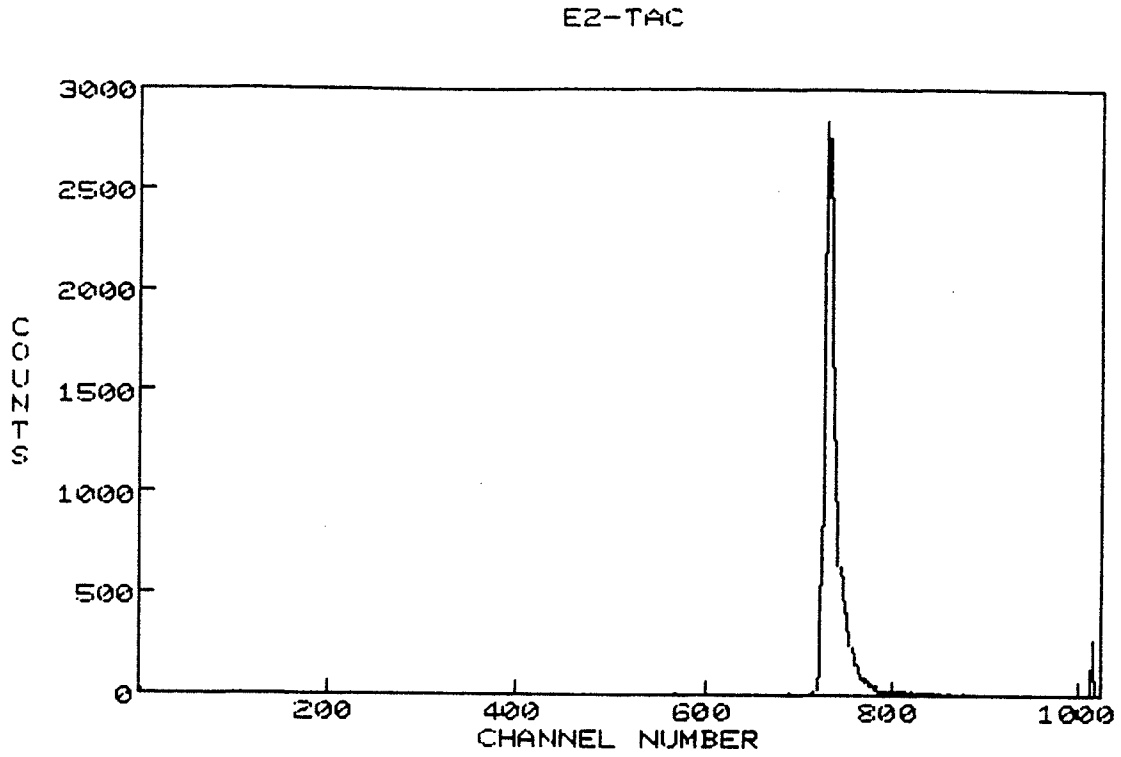

Fig. 4-18 E_2-TAC (all coincidence events).

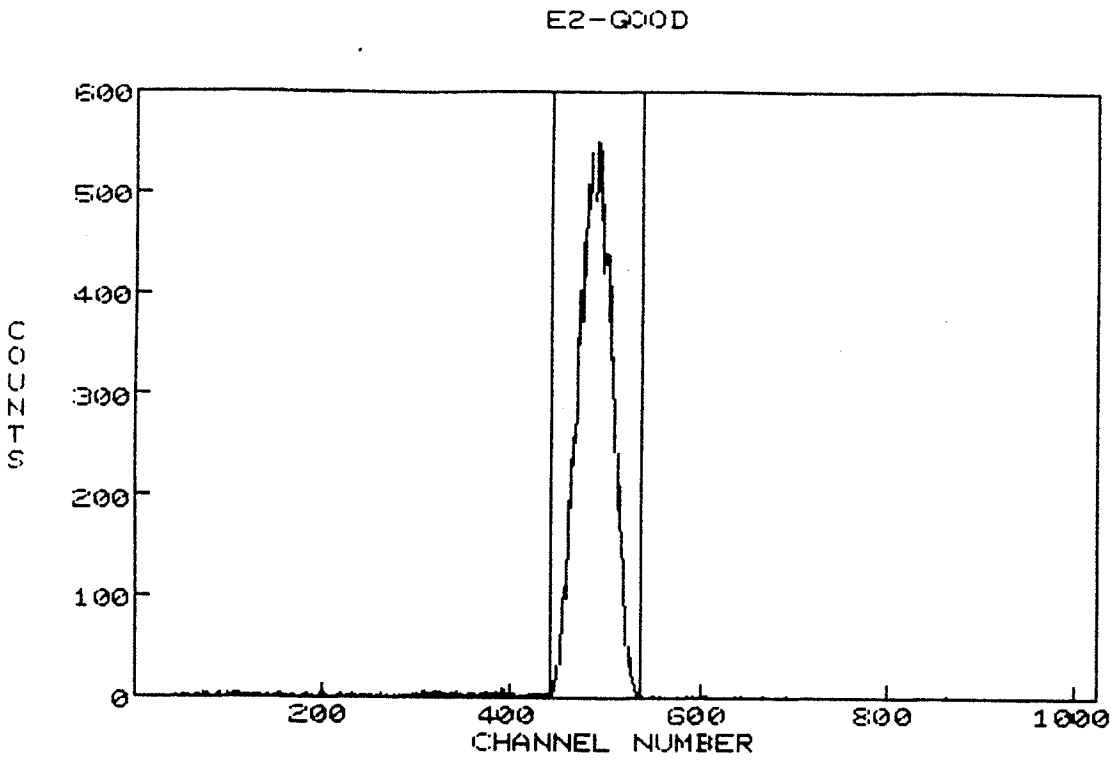

Fig. 4-19 The spectrum of Fig. 4-17 with a gate set on the g.s.

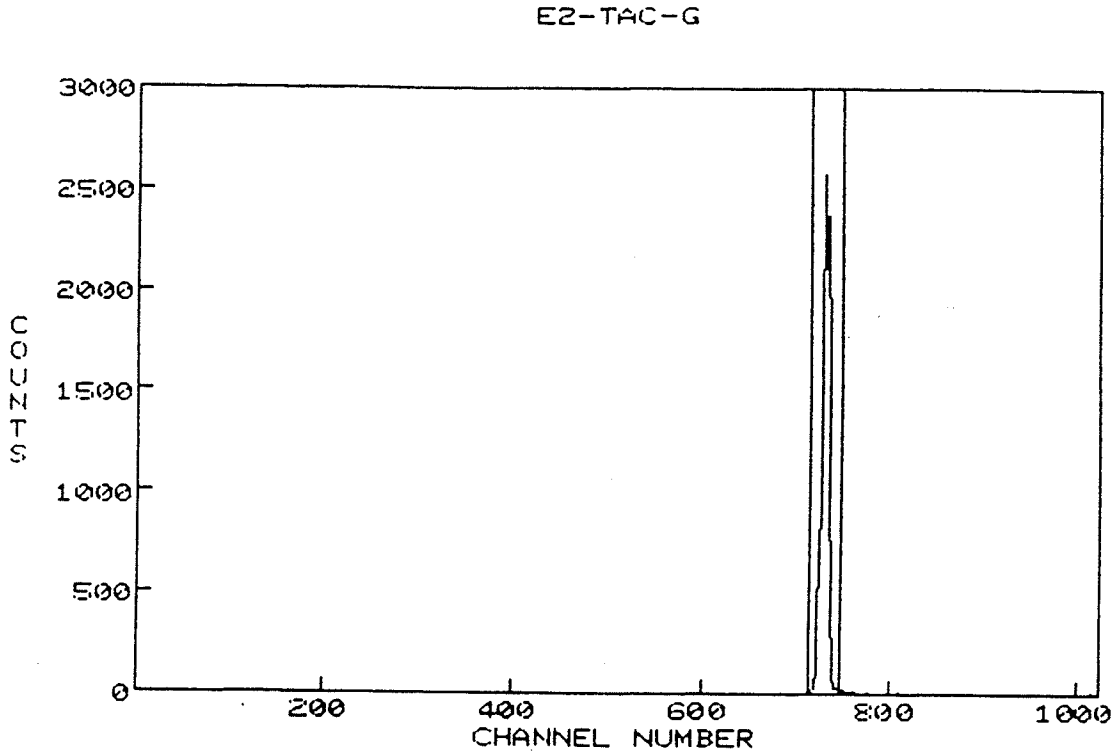

Fig. 4-20 The spectrum of Fig. 4-18 with a gate set on the g.s.

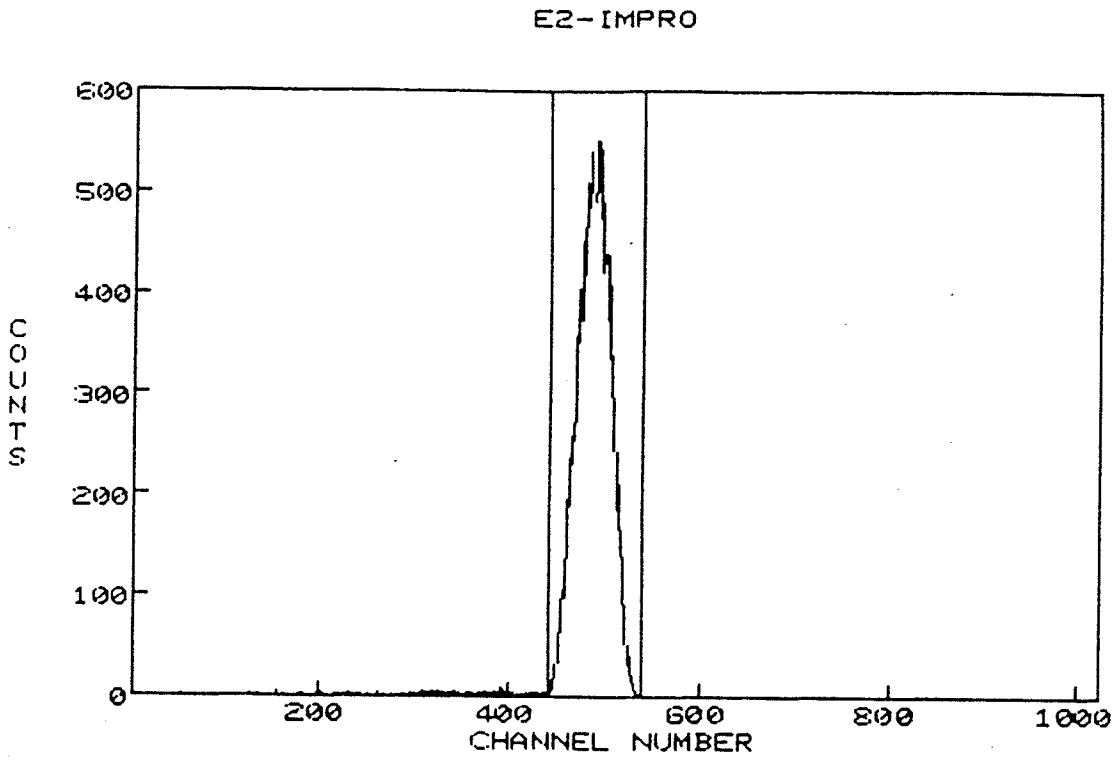

Fig. 4-21 E_2 (g.s.) with an additional gate on E_2-TAC in Fig. 4-20.

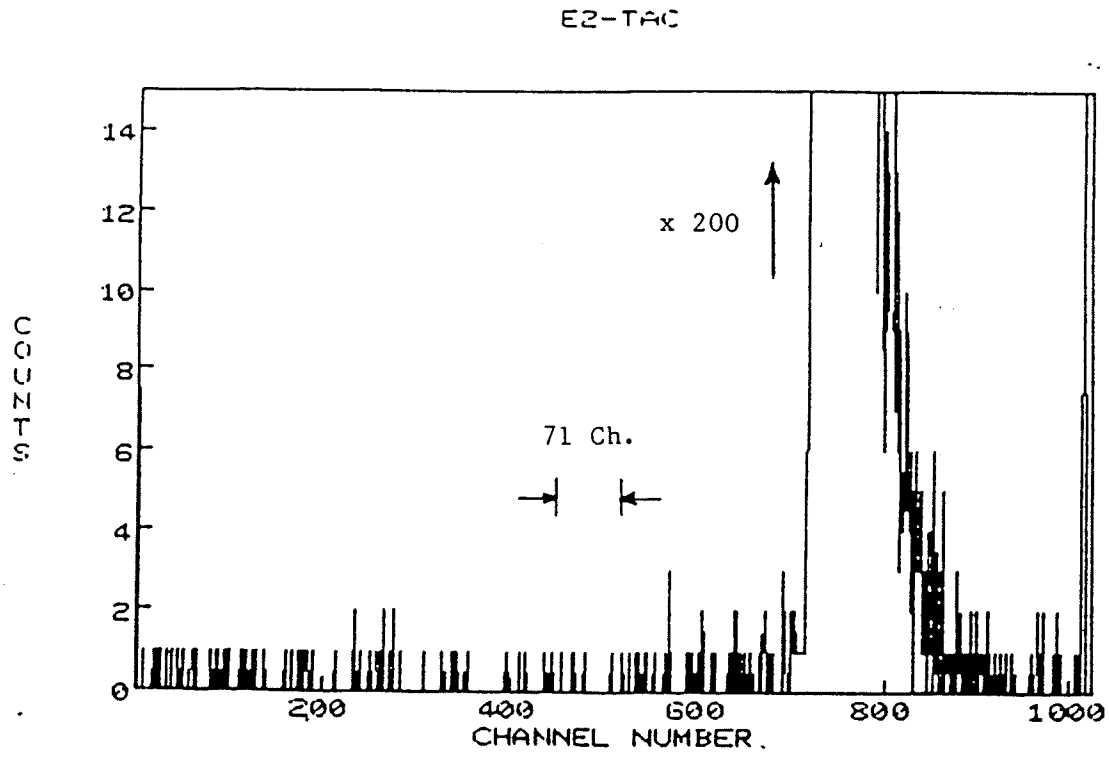

Fig. 4-22 E_2-TAC expanded vertically by a factor of 200.

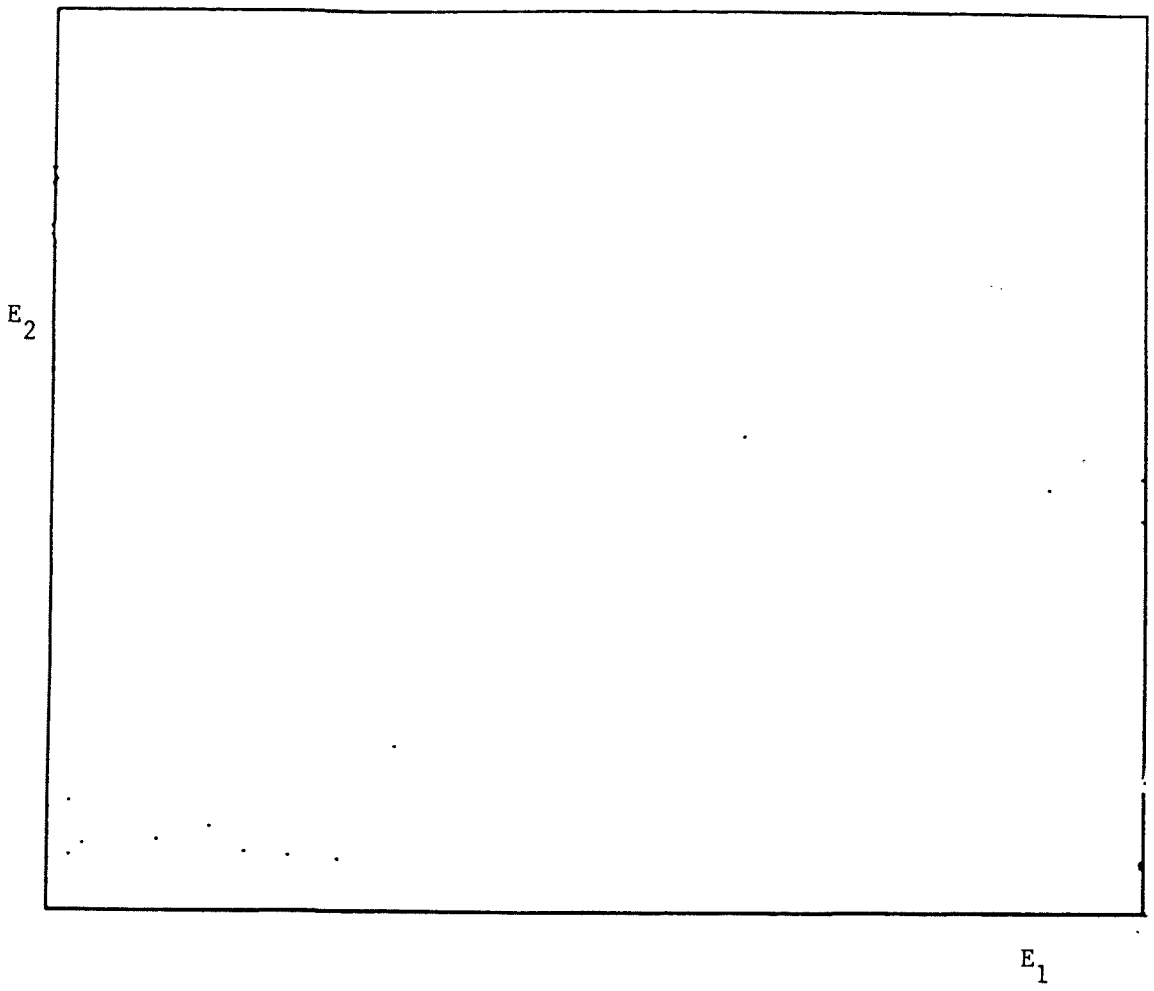

Fig. 4-23 Random events in a time window displaced by an RF period from the prompt coincidence window.

b) Background Correction

Figures. 4-24 through 4-27 represent the spectra of α-particles for single and coincidence events for the various scattered α-particle detector angle (θ_3) and recoil detector angle (θ_4) pairs of ($\theta_3 = 40^\circ$, $\theta_4 = 104^\circ$), ($\theta_3 = 40^\circ$, $\theta_4 = 106^\circ$), ($\theta_3 = 40^\circ$, $\theta_4 = 102^\circ$) and ($\theta_3 = 70^\circ$, $\theta_4 = 71^\circ$). The channel by channel information from these spectra is given in Appendix 2 in which the subscripts 1,2,3 and 4 refer to $\theta_4 = 104^\circ$, 106°, 102° and 71° respectively, and R = (no. of coincidence events)/(no. of single events), the ΔR values represent the uncertainties in the R values.

Using the information obtained from the spectra in Figs. 4-24 through 4-27 and Appendix 2; Tables 4-5 through 4-8 were developed. In these tables, the corrected efficiency, f', is calculated by taking the effect of background into consideration. The background in this calculation is assumed to be smooth and continuous. Some specific cases for reactions will be discussed later. The above tables are of special importance for our future study in measuring the branching ratios of the different states of ^{10}B. The definitions of the terms used in these tables are as follows.

N_s	total single events under peak
$(\bar{N}_s)_b$	average background for singles per channel
N_2	= (no. of channels under peak) x $(\bar{N}_s)_b$
N_1	= $N_s - N_2$.
N_c	total coincidence events under peak

$(\bar{N}_c)_b$ average background for coincidences per channel

$(N_c)_b$ = (no. of channels under peak) x $(\bar{N}_c)_b$

N'_c = $N_c - (N_c)_b$.

$(f)_{exp.}$ experimental efficiency(= N_c/N_s)

(f') corrected efficiency(= N'_c/N_1)

$\Delta f'$ uncertainty in (f'),

$$\Delta f' = [(\Delta N'_c/N'_c)^2 + (\Delta N_1/N_1)^2]^{1/2} \times f'$$

where $\Delta N'_c$ and ΔN_1 are the statistical errors in N'_c and N_1 respectively (see for example (Be 69).).

4-6-4 Monte Carlo Simulation

A Monte Carlo simulation, assuming isotropic c.m. breakup for γ- and particle-decay, was carried out which took into account beam spot size, beam energy resolution and geometric acceptance of detectors. This was used to calculate the theoretical coincidence efficiency. In this effort, special emphasis was laid upon determining optimum values for beam parameters etc. by comparing the calculated efficiencies for gamma decaying states with the experimental ones. After numerous trials, the following values were assigned to respective parameters in the Monte Carlo program. The Monte Carlo program used was a modified version of the program which was used in the experiment "Measurement of the Recoil Polarization of $^6Li^*$ (2.186 MeV, 3^+) Following the $^9Be(p,\alpha)^6Li$ Reaction" (Ar 86).

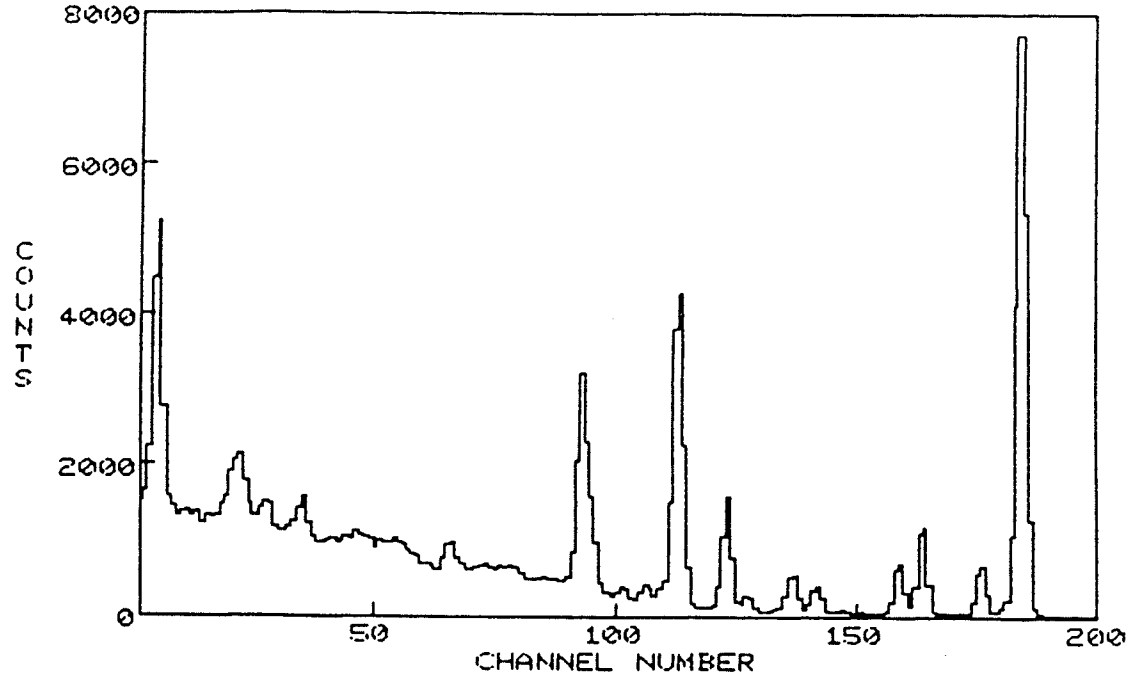

a) Single events

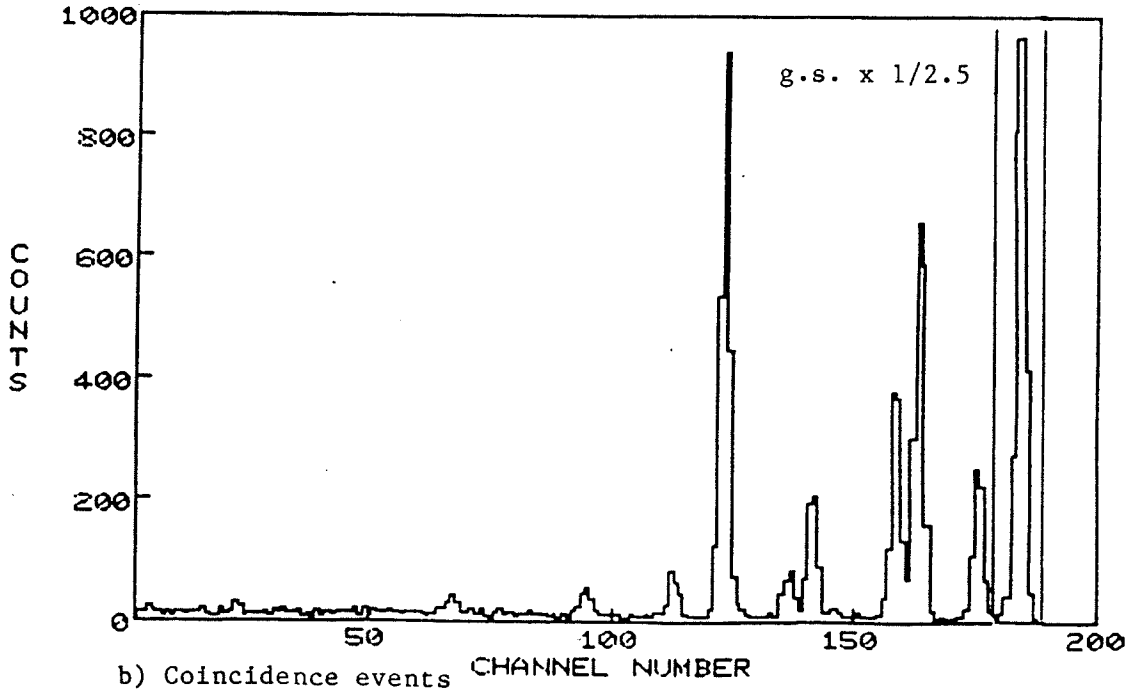

b) Coincidence events

Fig. 4-24 Single and coincidence events for $\theta_3 = 40^\circ$ and $\theta_4 = 104^\circ$.

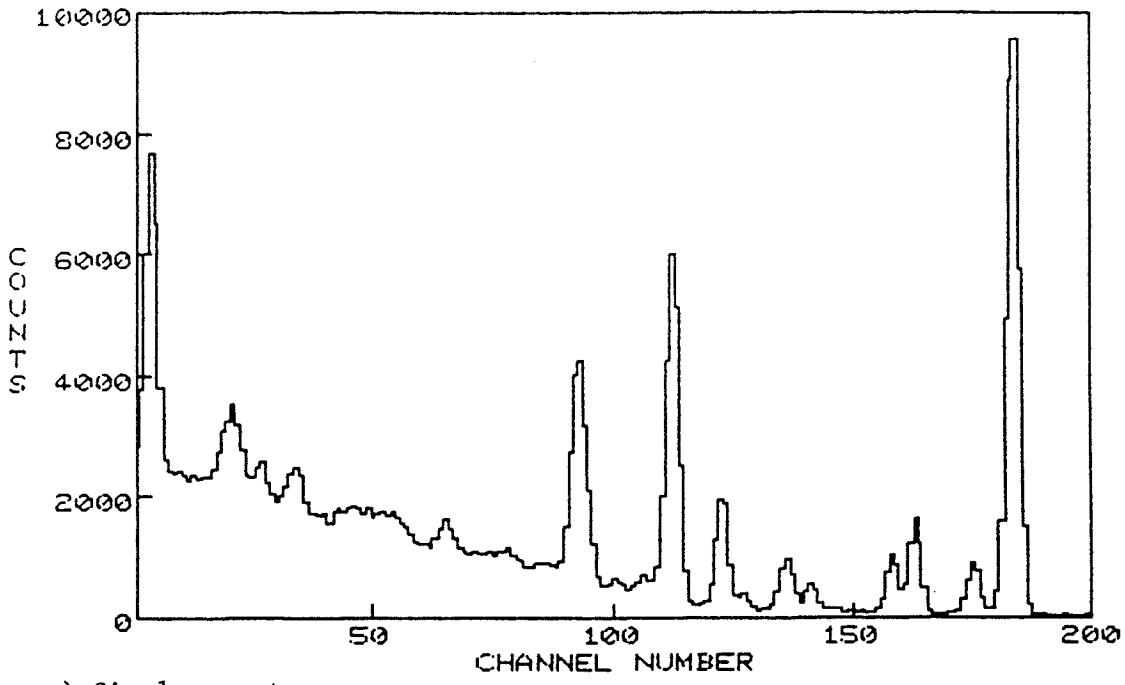

a) Single events

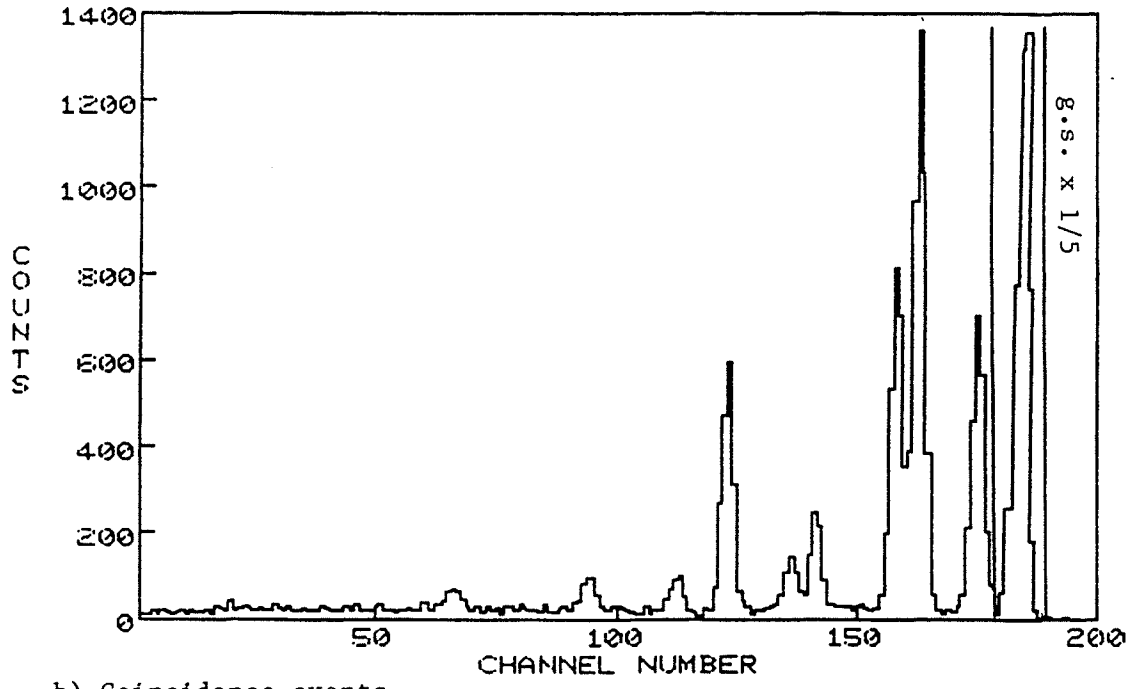

b) Coincidence events

Fig. 4-25 Single and coincidence events for $\theta_3 = 40^\circ$ and $\theta_4 = 106^\circ$.

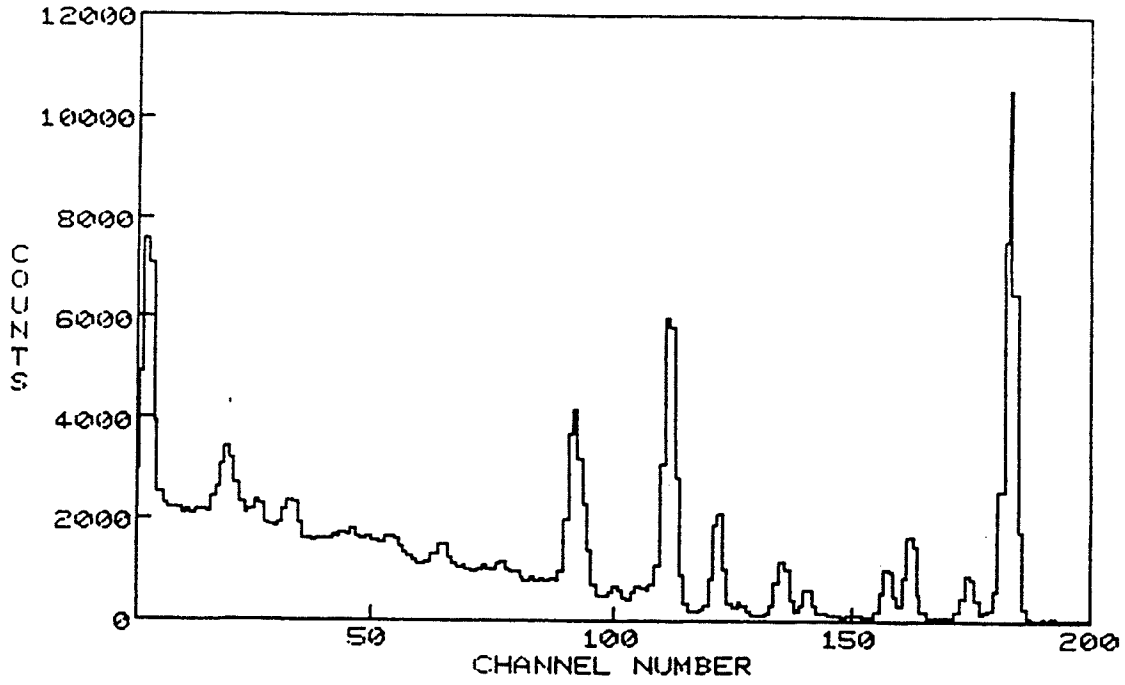

a) Single events

b) coincidence events

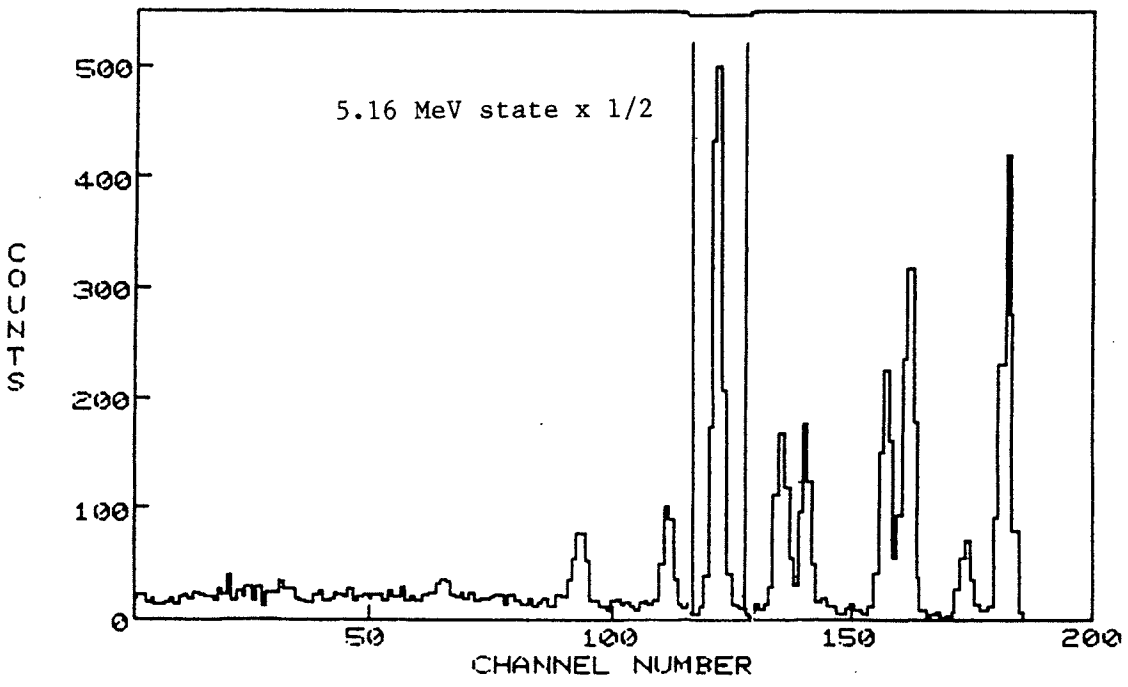

Fig. 4-26 Single and coincidence events for $\theta_3 = 40^\circ$ and $\theta_4 = 102^\circ$.

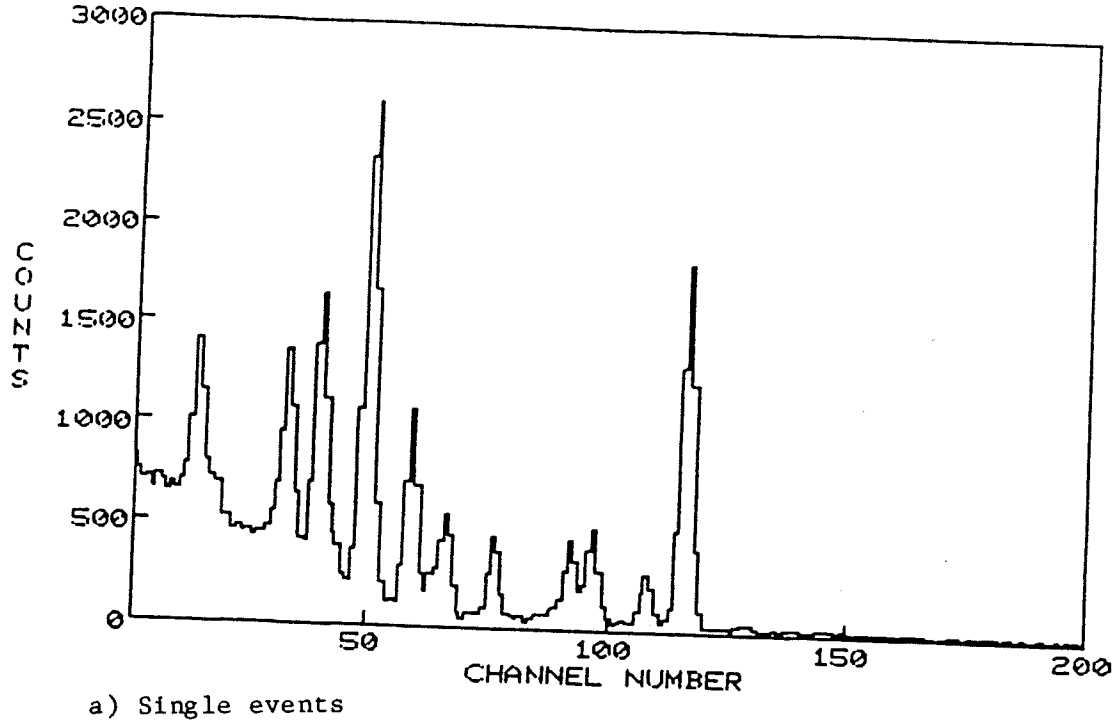

a) Single events

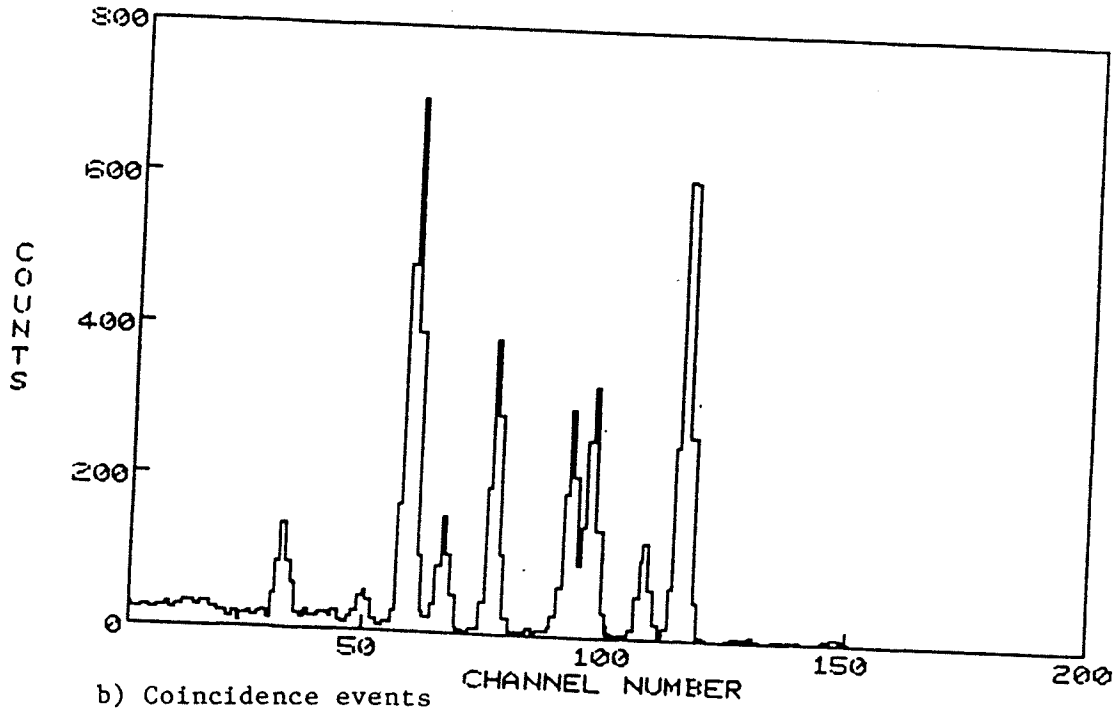

b) Coincidence events

Fig. 4-27 Single and coincidence events for $\theta_3 = 70^{\circ}$ and $\theta_4 = 71^{\circ}$.

Table 4-5 Efficiency calculations by taking the effect of background into consideration for $\theta_3 = 40°$ and $\theta_4 = 104°$.

State	No. of Ch.	N_s	$(\bar{N}_s)_b$	N_2	N_1	N_c	$(\bar{N}_c)_b$	$(N_c)_b$	N'_c	$(f)_{exp}$	f'	$\Delta f'$
g.s	8	20,000	15	120	19,880	6,418	0	0	6,418	0.321	0.323	0.005
0.718	4	1,747	44	176	1,571	650	9	36	614	0.372	0.391	0.022
1.74	4	3,098	58	232	2,866	1,711	12	48	1,663	0.552	0.580	0.020
2.15	5	1,908	58	290	1,618	1,040	12	60	980	0.545	0.606	0.031
1.74+2.15	9	5,006	52	468	4,538	2,751	10.5	94	2,657	0.549	0.585	0.018
3.59	4	1,113	59	236	877	561	12	48	513	0.504	0.585	0.043
4.77	4	791	74	296	495	72	10	40	32	0.091	0.064	0.031
5.16	4	3,772	98	392	3,380	2,044	11	44	2,000	0.542	0.592	0.019
6.025	6	12,634	249	1,494	11,140	241	12	72	169	0.019	0.015	0.002
7.47	7	11,502	415	2,907	8,595	196	12	84	112	0.017	0.013	0.003

Table 4-6 Efficiency calculations by taking the effect of background into consideration for $\theta_3 = 40°$ and $\theta_4 = 106°$.

State	No. of Ch.	N_s	$(\bar{N}_s)_b$	N_2	N_1	N_c	$(\bar{N}_c)_b$	$(N_c)_b$	N'_c	$(f)_{exp}$	f'	$\Delta f'$
g.s.	8	32,833	29	231	32,602	23,569	2	16	23,553	0.718	0.722	0.006
0.718	5	2,921	53	265	2,656	2,135	14	71	2,064	0.731	0.777	0.027
1.74	6	5,210	96	577	4,633	4,176	27	162	4,013	0.801	0.866	0.023
2.15	5	3,141	96	480	2,661	2,299	27	135	2,164	0.732	0.813	0.031
1.74+2.15	11	8,351	96	1,056	7,295	6,475	27	297	6,178	0.775	0.847	0.021
3.59	4	1,721	114	458	1,263	702	28	111	591	0.408	0.468	0.035
4.77	4	1,189	124	496	693	102	21	84	18	0.086	0.026	0.030
5.16	5	6,531	184	922	5,608	1,719	19	94	1,625	0.263	0.290	0.010
6.025	6	20,703	470	2,824	17,879	383	18	107	275	0.018	0.015	0.002
7.47	7	18,970	732	5,128	13,842	436	23	164	272	0.023	0.019	0.003

Table 4-7 Efficiency calculations by taking the effect of background into consideration for $\theta_3 = 40°$ and $\theta_4 = 102°$.

State	No. of Ch.	N_s	$(\bar{N}_s)_b$	N_2	N_1	N_c	$(\bar{N}_c)_b$	$(N_c)_b$	N'_c	$(f)_{exp}$	f'	$\Delta f'$
g.s.	8	29,928	28	224	29,704	1,113	0	0	1,113	0.037	0.037	0.001
0.718	5	2,704	110	550	2,154	200	6	30	170	0.074	0.079	0.009
1.74	6	4,945	84	504	4,441	869	7	42	827	0.176	0.186	0.008
2.15	4	2,726	84	336	2,390	577	7	28	549	0.212	0.230	0.012
1.74+2.15	10	7,671	84	840	6,831	1,446	7	70	1,376	0.188	0.201	0.008
3.59	4	1,737	102	408	1,329	446	10	40	406	0.257	0.305	0.023
4.77	4	1,113	110	440	673	76	9	36	40	0.068	0.059	0.022
5.16	5	6,084	173	865	5,219	2,724	18	88	2,636	0.448	0.505	0.015
6.025	6	19,699	236	1,416	18,283	308	26	158	150	0.016	0.008	0.002
7.47	7	17,761	679	4,753	13,008	339	14	101	238	0.019	0.018	0.002

Table 4-8 Efficiency calculations by taking the effect of background into consideration for $\theta_3 = 70°$ and $\theta_4 = 71°$.

State	No. of Ch.	N_s	$(\bar{N}_s)_b$	N_2	N_1	N_c	$(\bar{N}_c)_b$	$(N_c)_b$	N'_c	$(f)_{exp}$	f'	$\Delta f'$
g.s.	7	5,502	29	203	5,299	1,848	1.5	10	1,838	0.336	0.347	0.010
0.718	5	879	49	245	634	365	7	35	330	0.415	0.520	0.052
1.74	5	1,526	55	273	1,253	904	6	30	874	0.592	0.697	0.039
2.15	6	1,434	55	330	1,104	802	6	36	766	0.559	0.694	0.047
1.74+2.15	11	2,960	55	605	2,355	1,706	6	66	1,640	0.576	0.696	0.036
3.59	5	1,367	63	317	1,049	1,022	7	35	987	0.748	0.941	0.059
4.77	5	1,929	164	820	1,109	431	13	65	366	0.223	0.330	0.034
5.16	5	3,043	148	738	2,305	1,854	22	108	1,746	0.609	0.757	0.034
6.025	7	8,880	182	1,272	7,608	197	14	99	98	0.022	0.013	0.004
7.47	7	5,783	431	3,018	2,765	450	17	119	331	0.078	0.120	0.015

FWHM of beam energy spread	0.140 MeV
Half width in the horizontal plane	0.8 mm
Half divergence in the horizontal plane	7.0 mrad
Half width in the vertical plane	1.2 mm
Half divergence in the vertical plane	7.0 mrad
Effective collimator radius of telescope at plane of proportional counter collimator	6.0 mm
Effective radius of recoil detector	7.8 mm

Table 4-9 displays the results obtained from the Monte Carlo simulation for efficiencies at the specified angles. Measured efficiencies (Tables 4-5 through 4-8) can be compared with the above Monte Carlo values (Table 4-9) and both interpreted in light of Figures. 4-28 and 4-29, which represent diagrammatically the coverage provided for different states by the angular range of the detectors. Tables 4-10 and 4-11 show the calculation of the range of the recoil detector at $\theta_3 = 40^\circ$, and 70° based on kinematics at $E_p = 40.45$ MeV.

Table 4-12 indicates the comparison between the experimental and the Monte Carlo efficiencies for the γ-decaying states at the specified angles. The ratios between the two results are calculated. The discrepancy between these calculations is mostly related to background and particularly to the dead time effect which was not included in the calculations. The average ratios for the first three γ-decaying states at the pairs of angles specified below were calculated and the results

are as follows. The g.s. was not included in these calculations due to the background events underlying this state (refer to Fig. 4-30).

Pair of angles	η_{MC}/η_{exp}
$\theta_3 = 40^\circ$, $\theta_4 = 102^\circ$	1.10 ± 0.04
$\theta_3 = 40^\circ$, $\theta_4 = 104^\circ$	1.03 ± 0.02
$\theta_3 = 40^\circ$, $\theta_4 = 106^\circ$	1.01 ± 0.02

The grand average for the above three results was calculated as 1.03 ± 0.01 and this value will be used as the normalization factor for Monte Carlo output when discussing the branching ratios for the particle-decaying states, i.e.,

$$\eta_{MC}(\text{normalized}) = \eta_{MC}(\text{calculated})/\ (1.03 \pm 0.01)$$

It is to be noted that in the above average calculations, the results were weighted according to the corresponding error bars (refer to section 4-6-6, relations (4-2) and (4-3).).

4-6-5 Study of the Existence and the Effect of Impurities in the Target

The different states of ^{10}B from the proper reaction $^{13}C(p,\alpha)^{10}B$ were shown in Fig. 4-10. Existence of impurities in the ^{13}C target could initiate some other reactions and affect the validity

Table 4-9 Monte Carlo Output

State (MeV)	Mode of decay	θ_3 (deg.)	θ_4 (deg.)	Efficiency
g.s.	stable	40	102	0.048 ± 0.001
		40	104	0.354 ± 0.004
		40	106	0.748 ± 0.006
0.718	γ	40	102	0.100 ± 0.002
		40	104	0.444 ± 0.005
		40	106	0.822 ± 0.006
1.74	γ	40	102	0.202 ± 0.003
		40	104	0.580 ± 0.005
		40	106	0.847 ± 0.006
2.15	γ	40	102	0.252 ± 0.003
		40	104	0.636 ± 0.006
		40	106	0.823 ± 0.006
3.59	γ	40	102	0.447 ± 0.005
		40	104	0.797 ± 0.006
		40	106	0.637 ± 0.006
4.77	γ	40	102	0.616 ± 0.005
		40	104	0.779 ± 0.006
		40	106	0.447 ± 0.004
4.77	α	40	102	0.042 ± 0.001
		40	104	0.041 ± 0.001
		40	106	0.045 ± 0.001

Table 4-9 (continued)

State (MeV)	Mode of decay	θ_3 (deg.)	θ_4 (deg.)	Efficiency
5.16	γ	40	102	0.668 ± 0.006
		40	104	0.739 ± 0.006
		40	106	0.384 ± 0.004
5.16	α	40	102	0.019 ± 0.001
		40	104	0.020 ± 0.001
		40	106	0.020 ± 0.001
6.025	γ	40	102	0.742 ± 0.006
		40	104	0.617 ± 0.006
		40	106	0.253 ± 0.003
6.025	α	40	102	0.0110 ± 0.0007
		40	104	0.0110 ± 0.0007
		40	106	0.0110 ± 0.0007
7.47	γ	40	102	0.677 ± 0.006
		40	104	0.366 ± 0.004
		40	106	0.086 ± 0.001
7.47	p	40	102	0.063 ± 0.001
		40	104	0.069 ± 0.001
		40	106	0.082 ± 0.001
g.s.	stable	70	71	0.574 ± 0.005
0.718	γ	70	71	0.629 ± 0.006
1.74	γ	70	71	0.802 ± 0.006
2.15	γ	70	71	0.865 ± 0.006
3.59	γ	70	71	0.978 ± 0.007

Table 4-9 (continued)

State (MeV)	Mode of decay	θ_3 (deg.)	θ_4 (deg.)	Efficiency
4.77	γ	70	71	0.988 ± 0.007
4.77	α	70	71	0.072 ± 0.001
5.16	γ	70	71	0.982 ± 0.007
5.16	α	70	71	0.033 ± 0.001
6.025	γ	70	71	0.929 ± 0.007
6.025	α	70	71	0.017 ± 0.001
7.47	γ	70	71	0.704 ± 0.006
7.47	p	70	71	0.137 ± 0.002

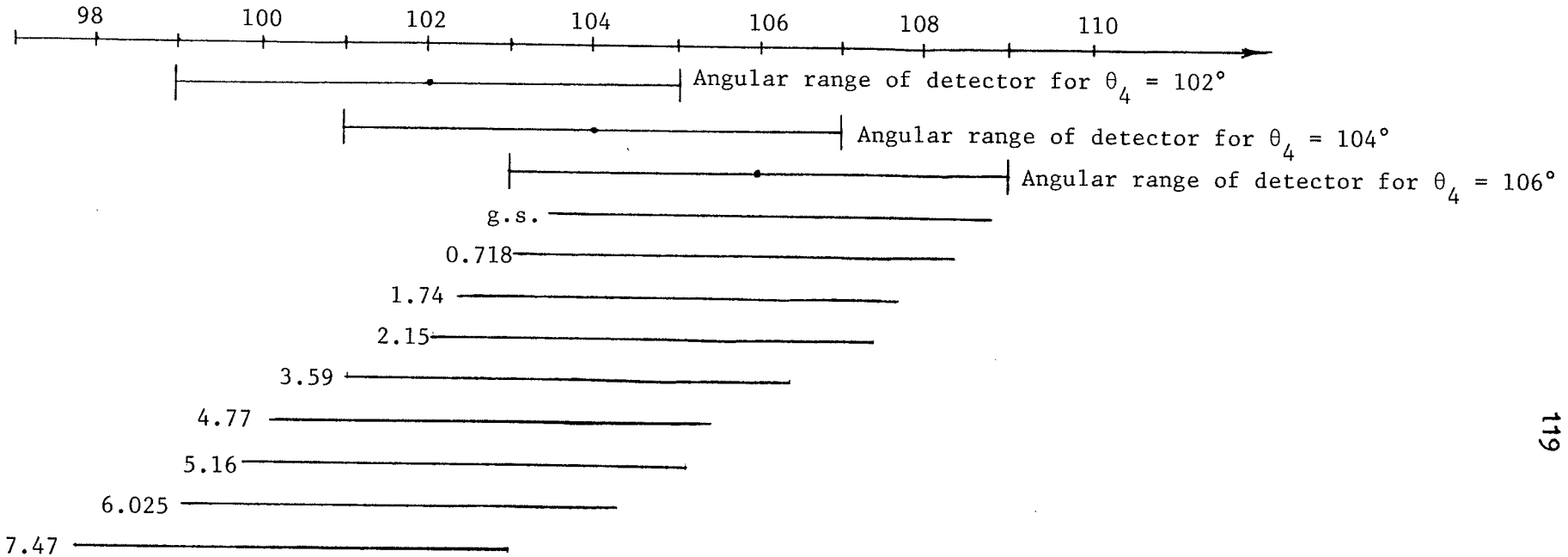

Fig. 4-28 Angular range of recoil ^{10}B events and of recoil detector, $\theta_3 = 40^\circ$.

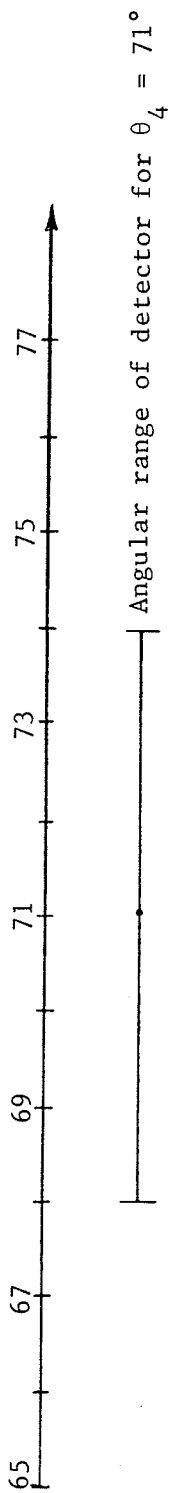

Fig. 4-29 Angular range of recoil events and of recoil detector, $\theta_3 = 70^\circ$.

Table 4-10 Range of θ_4 for $\theta_3 = 40°$, $E_p = 40.45$ MeV.

State	θ_4	$d\theta_4/d\theta_3$	$\Delta\theta_4$ (1)	Range of θ_4 (2)
g.s.	106.18	1.346	2.665	103.51 - 108.84
0.718	105.72	1.344	2.661	103.06 - 108.38
1.74	105.03	1.342	2.657	102.37 - 107.69
2.15	104.74	1.342	2.657	102.08 - 107.40
3.59	103.69	1.338	2.649	101.04 - 106.34
4.77	102.76	1.333	2.639	100.12 - 105.40
5.16	102.45	1.331	2.635	99.81 - 105.08
6.025	101.72	1.327	2.627	99.08 - 104.35
7.47	100.41	1.318	2.609	97.80 - 103.02

(1) $\Delta\theta_4 = (d\theta_4/d\theta_3) \times (\Delta\theta_3)$

where $\Delta\theta_3 = \pm 1.98°$.

(2) Range of $\theta_4 = \theta_4 \pm \Delta\theta_4$

Table 4-11 Range of θ_4 for $\theta_3 = 70°$, $E_p = 40.45$ MeV.

State	θ_4	$d\theta_4/d\theta_3$	$\Delta\theta_4$ (1)	Range of θ_4 (2)
g.s.	73.04	0.925	1.831	71.21 - 74.87
0.718	72.67	0.921	1.823	70.85 - 74.49
1.74	72.12	0.916	1.814	70.31 - 73.93
2.15	71.90	0.914	1.810	70.09 - 73.71
3.59	71.08	0.906	1.794	69.29 - 72.87
4.77	70.36	0.898	1.778	68.58 - 72.14
5.16	70.12	0.895	1.772	68.35 - 71.89
6.025	69.56	0.889	1.760	67.80 - 71.32
7.47	68.58	0.879	1.740	66.84 - 70.32

(1) $\Delta\theta_4 = (d\theta_4/d\theta_3) \times (\Delta\theta_3)$

where $\Delta\theta_3 = \pm 1.98°$.

(2) Range of $\theta_4 = \theta_4 \pm \Delta\theta_4$.

Table 4-12 Comparison between the experimental (η_{exp}) and the Monte Carlo efficiencies (η_{MC}).

State	θ_3 (deg)		θ_4 (deg)				η_{exp} (%)	η_{MC} (%)	$(\eta_{MC})/(\eta_{exp})$
	40	70	102	104	106	71			
0.718	✓		✓				7.9 ± 0.9	10.0 ± 0.2	1.27 ± 0.15
	✓			✓			39.1 ± 2.2	44.4 ± 0.5	1.13 ± 0.06
	✓				✓		77.7 ± 2.7	82.2 ± 0.6	1.06 ± 0.04
		✓				✓	52.0 ± 5.2	62.9 ± 0.6	1.21 ± 0.12
1.74	✓		✓				18.6 ± 0.8	20.2 ± 0.3	1.09 ± 0.05
	✓			✓			58.0 ± 2.0	58.0 ± 0.5	1.00 ± 0.03
	✓				✓		86.6 ± 2.3	84.7 ± 0.6	0.98 ± 0.03
		✓				✓	69.7 ± 3.9	80.2 ± 0.6	1.15 ± 0.06
2.15	✓		✓				23.0 ± 1.2	25.2 ± 0.3	1.09 ± 0.06
	✓			✓			60.6 ± 3.1	63.6 ± 0.6	1.05 ± 0.05
	✓				✓		81.3 ± 3.1	82.3 ± 0.6	1.01 ± 0.04
		✓				✓	69.4 ± 4.7	86.5 ± 0.6	1.25 ± 0.08

of the calculated efficiencies for the proper reaction. As a first step to verify these impurities, different possible (p,α) reactions having comparable alpha energies were investigated by studying the corresponding kinematics. The energies for scattered particles and recoil nuclei related to probable reactions were extracted from kinematics and were compared with those for different possible impurity groups in Fig. 4-10. The information obtained from this study showed that ^{14}N impurity was the dominant one. The different states of ^{11}C from the reaction $^{14}N(p,\alpha)^{11}C$ are shown in Figs. 4-30 and 4-31 for different angles. Alpha fragments resulting from the reaction

$$^{12}C(p,\alpha)^{9}B \longrightarrow p + {}^{8}Be$$

$$^{8}Be \longrightarrow \alpha + \alpha.$$

due to the presence of ^{12}C impurity in the target is also shown in Fig. 4-30. In addition, some states of ^{12}C from the reaction $^{14}N(p,{}^{3}He)^{12}C$ as well as the g.s. of ^{13}N from the reaction $^{16}O(p,\alpha)^{13}N$ due to ^{14}N and ^{16}O impurities respectively were investigated and are shown in Fig. 4-32.

While the number of coincidence events for the above reactions were rather negligible as compared with those for the proper one, nevertheless, Monte Carlo calculations were carried out in order to obtain their efficiencies and determine the corresponding number of single events by performing "inverse calculations". The information

obtained from these Monte Carlo calculations verified that the effect of these impurities could be neglected. For example and in order to clarify the procedure followed, the Monte Carlo efficiency for the reaction $^{14}N(p,\alpha)^{11}C$ was calculated as $\eta = 0.859$ at $\theta_3 = 40^\circ$ and $\theta_4 = 106^\circ$. Referring to Fig. 4-30, the highest number of coincidence events for the same pair of angles was calculated as 45 events for 6.48 MeV state of ^{11}C. Then the number of corresponding single events using the above efficiency of 0.859 becomes 52 which is quite negligible as compared with the proper events. However, as was mentioned in section 4-6-4, the g.s. was not included in normalizing the Monte Carlo output due to the background events underlying this state (refer to Fig. 4-30).

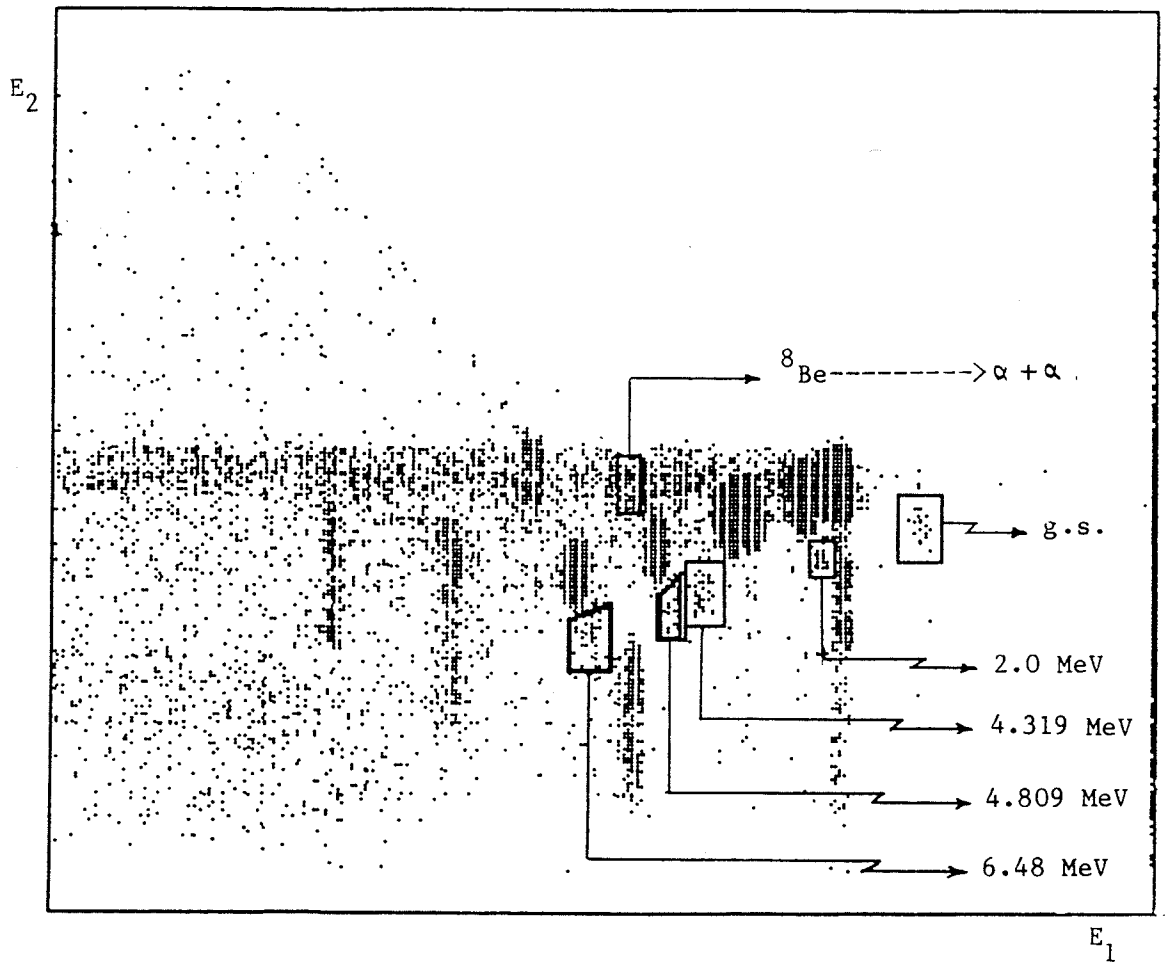

Fig. 4-30 States of ^{11}C from the reaction $^{14}N(p,\alpha)\ ^{11}C$ due to the ^{14}N impurity in the target, ($\theta_3 = 40^\circ$, $\theta_4 = 106^\circ$). Also ^{8}Be fragments resulting from the reaction $^{12}C(p,\alpha)^{9}B$ $\rightarrow p + {}^{8}Be$, is shown.

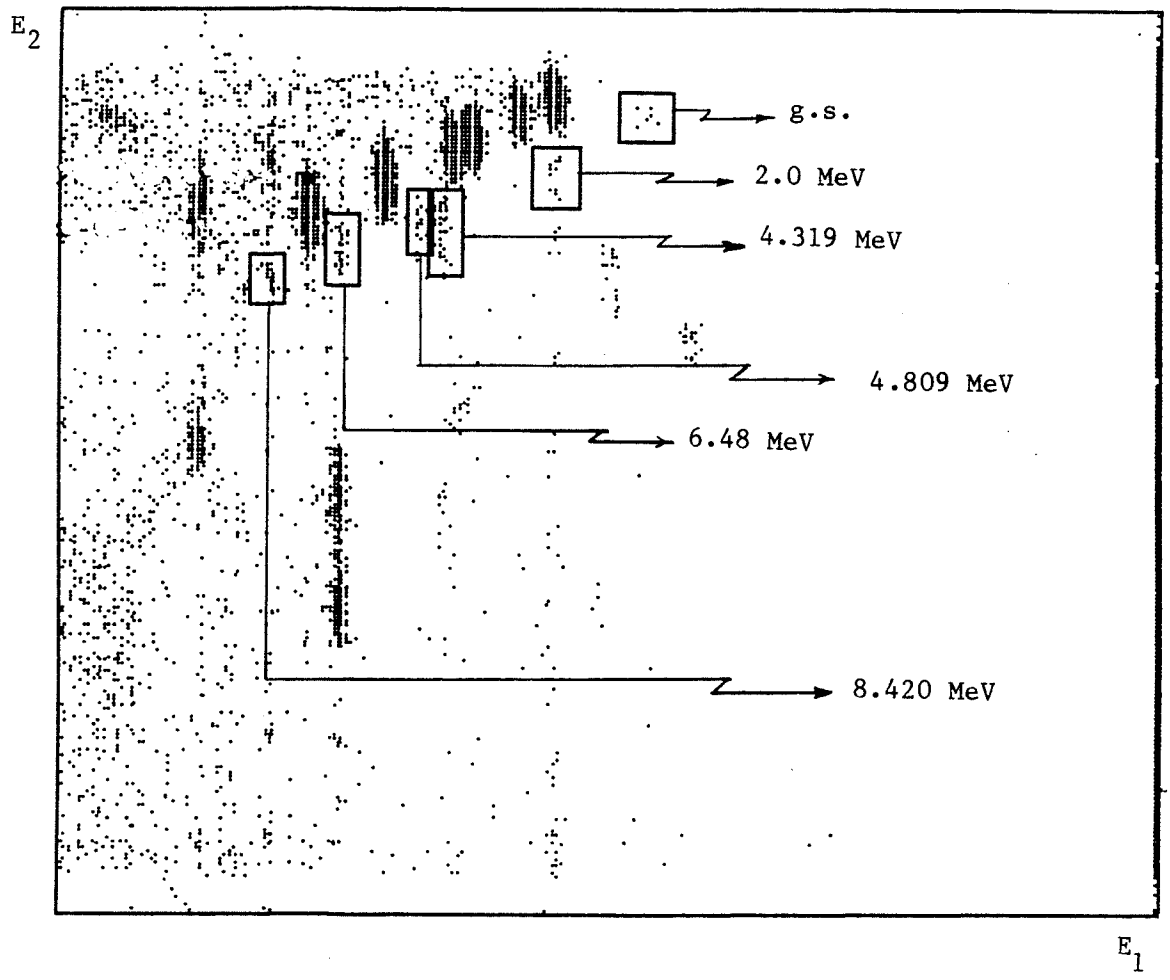

Fig. 4-31 States of ^{11}C from the reaction $^{14}N(p,\alpha)\ ^{11}C$ due to the ^{14}N impurity in the target, ($\theta_2 = 70^\circ$, $\theta_1 = 71^\circ$).

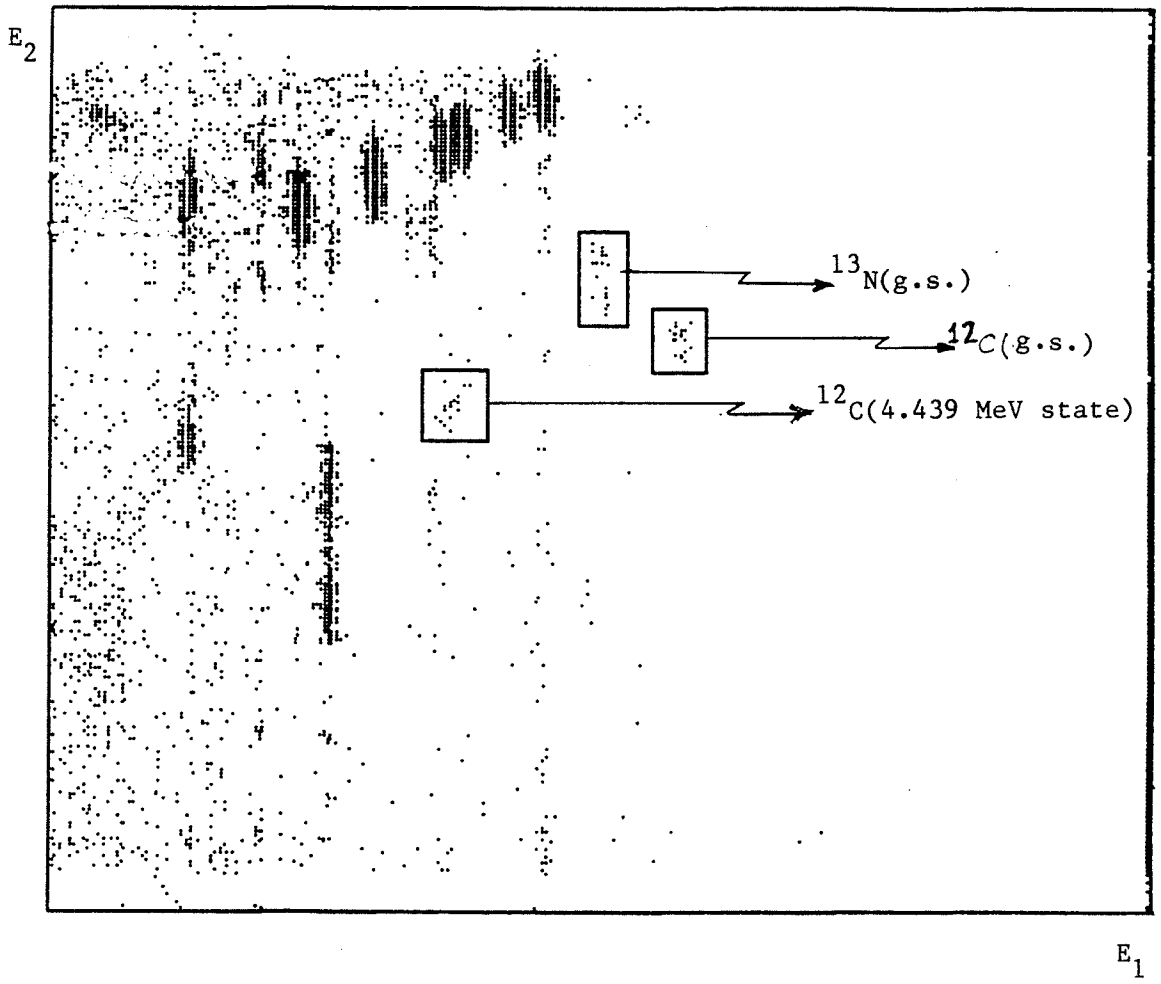

Fig. 4-32 Some states of the ^{12}C from the reaction ^{14}N $(p,^{3}He)^{12}C$ due to the ^{14}N impurity and the g.s. of ^{13}N from the reaction $^{16}O(p,\alpha)^{13}N$ due to the ^{16}O impurity in the target, ($\theta_3 = 70^\circ$, $\theta_4 = 71^\circ$)

4-6-6 Branching Ratios

The excitations, spin-parity assignments and previously reported modes of decay for ^{10}B nuclei are given in table 4-4. Levels of ^{10}B up to 7.47 MeV in excitation were examined and shown in two-dimensional spectra in Figures. 4-10 and 4-11. As was mentioned in section 4-6-2, the low-lying states consisting of 0.718, 1.74, 2.15 and 3.59 MeV, are purely γ-decaying states and these formed a major group in Figures. 4-10 and 4-11. In this section we discuss the particle-decaying states and their branching ratios in more detail.

It is to be noted that the symbol Γ represents full width at half maximum intensity of a resonance excitation function or of a level, and the subscripts when shown, indicate partial widths for decay, via the channel shown by the subscript. In addition, the branching ratios are represented by the symbol β followed by the appropriate subscript identifying the decay mode.

a) 4.77 MeV State

As far as the electromagnetic transitions are concerned, the 4.77 MeV state deexcitation mode in ^{10}B has large probabilities to cascade through the 0.718 MeV first excited state (Ne 85). According to Ajzenberg-Selove (Aj 84),

$$\Gamma\,(\text{total}) = 0.020 \pm 0.004 \text{ eV}$$

$$\beta_\gamma = 0.23 \pm 0.03 \% \ .$$

Fig. 4-33 shows a one-dimensional α-spectrum with a gate on the 4.77 MeV state and, as the result of the gate, the corresponding two-dimensional spectrum shown in Fig. 4-34. The events contained in the middle gate correspond to the locus formed by the purely γ-decaying states described before. Now to measure the branching ratios of this state quantitatively, we refer to our experimental values of the efficiencies (Tables 4-5 through 4-8) and the Monte Carlo efficiencies (Table 4-9).

At $\theta_3 = 40^\circ$ and $\theta_4 = 102^\circ$; from the Table 4-7 the experimental efficiency (f') is equal to 0.059 ± 0.022. Now from the Table 4-9, the Monte Carlo calculated efficiency, for the same angles, assuming the state to be γ-decaying is 0.616 ± 0.005 and the efficiency assuming the state to be α-decaying is 0.042 ± 0.001. Taking the normalization factor for the Monte Carlo efficiencies into account (refer to the section 4-6-4), we have

$$\eta_{MC}(\text{normalized}) = \eta_{MC}(\text{calculated})/(1.03 \pm 0.01)$$

Then the normalized Monte Carlo value for γ-decaying channel will be 0.598 ± 0.007 and that for α-decaying channel will be 0.041 ± 0.001.

Based on the above discussion we have

$$(\beta_\gamma) \times (0.598 \pm 0.007) + (\beta_\alpha) \times (0.041 \pm 0.001) = 0.059 \pm 0.022$$

$$(\beta_\gamma) + (\beta_\alpha) = 1$$

with the constraint $\beta_\gamma \leq 1$ and $\beta_\alpha \leq 1$.

From these equations we get

$$\beta_\alpha = 96.8 \pm 4.3\ \%$$

$$\beta_\gamma = 3.2 \pm 4.3\ \%$$

Following the same procedure, the branching ratios for the 4.77 MeV state at the other pairs of angles were calculated:

For $\theta_3 = 40^\circ$, $\theta_4 = 104^\circ$,

$$\beta_\alpha = 96.6 \pm 4.6\ \%$$

$$\beta_\gamma = 3.4 \pm 4.6\ \%$$

For $\theta_3 = 40^\circ$, $\theta_4 = 106^\circ$,

$$\beta_\alpha = 104.6 \pm 8.1\ \%$$

$$\beta_\gamma = -4.6 \pm 8.1\ \%$$

Noting that the uncertainties in the above results are different, the mean values for the branching ratios, $\overline{\beta}$, should be obtained by weighting the results according to the corresponding error bars. We apply the following equation (Be 69) to calculate the mean values for the branching ratio

$$\mu = \frac{\Sigma\ (x_i/\sigma_i^2)}{\Sigma\ (1/\sigma_i^2)}\ , \qquad (4\text{-}2)$$

where σ_i is the uncertainty in the data point x_i.

The uncertainty, σ_μ, in the mean μ is obtained according to the equation

$$\sigma_{\mu}^{2} = \frac{1}{\Sigma\ (1/\sigma_{i}^{2})} \cdot \qquad (4\text{-}3)$$

By inserting our results in the relation (4-2), we get

$$\overline{\beta}_{\alpha} = [0.968/(0.043)^2 + 0.966/(0.046)^2 + 1.046/(0.081)^2]/$$
$$[1/(0.043)^2 + 1/(0.046)^2 + 1/(0.081)^2]$$

or $$\overline{\beta}_{\alpha} = 0.977$$

From the relation (4-3),

$$\sigma_{\overline{\beta}_{\alpha}} = [1/(0.043)^2 + 1/(0.046)^2 + 1/(0.081)^2]^{-1/2}$$

Or $$\sigma_{\overline{\beta}_{\alpha}} = 0.029$$

Therefore, our final values for the branching ratios of the 4.77 MeV state are,

$$\overline{\beta}_{\alpha} = 97.7 \pm 2.9\ \%$$
$$\overline{\beta}_{\gamma} = 2.3 \pm 2.9\ \%$$

Hence, it is concluded that the 4.77 MeV state is primarily α-decaying ($\beta_{\alpha} \sim \beta_{tot}$). However, by taking the uncertainty of $\pm$ 2.9 % into consideration, an upper limit of $\sim$ 5 % can be assigned to γ-decaying channel.

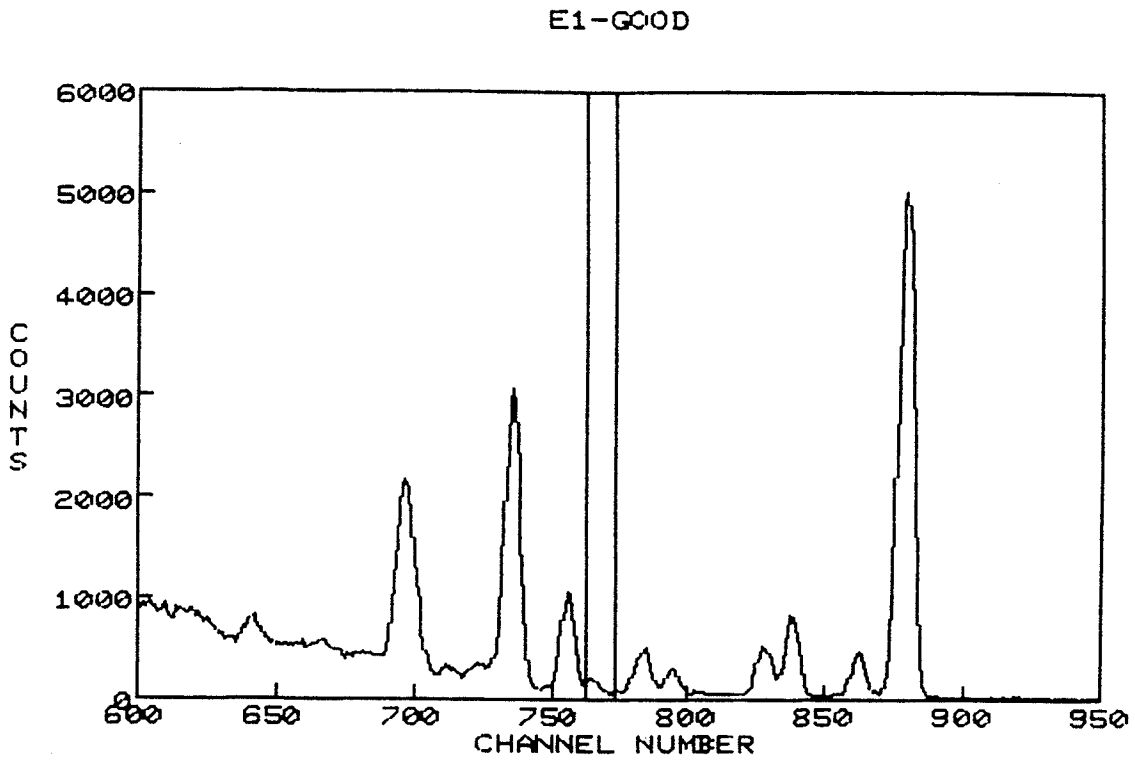

Fig. 4-33 1-D α-spectrum with a gate set on the 4.77 MeV state.

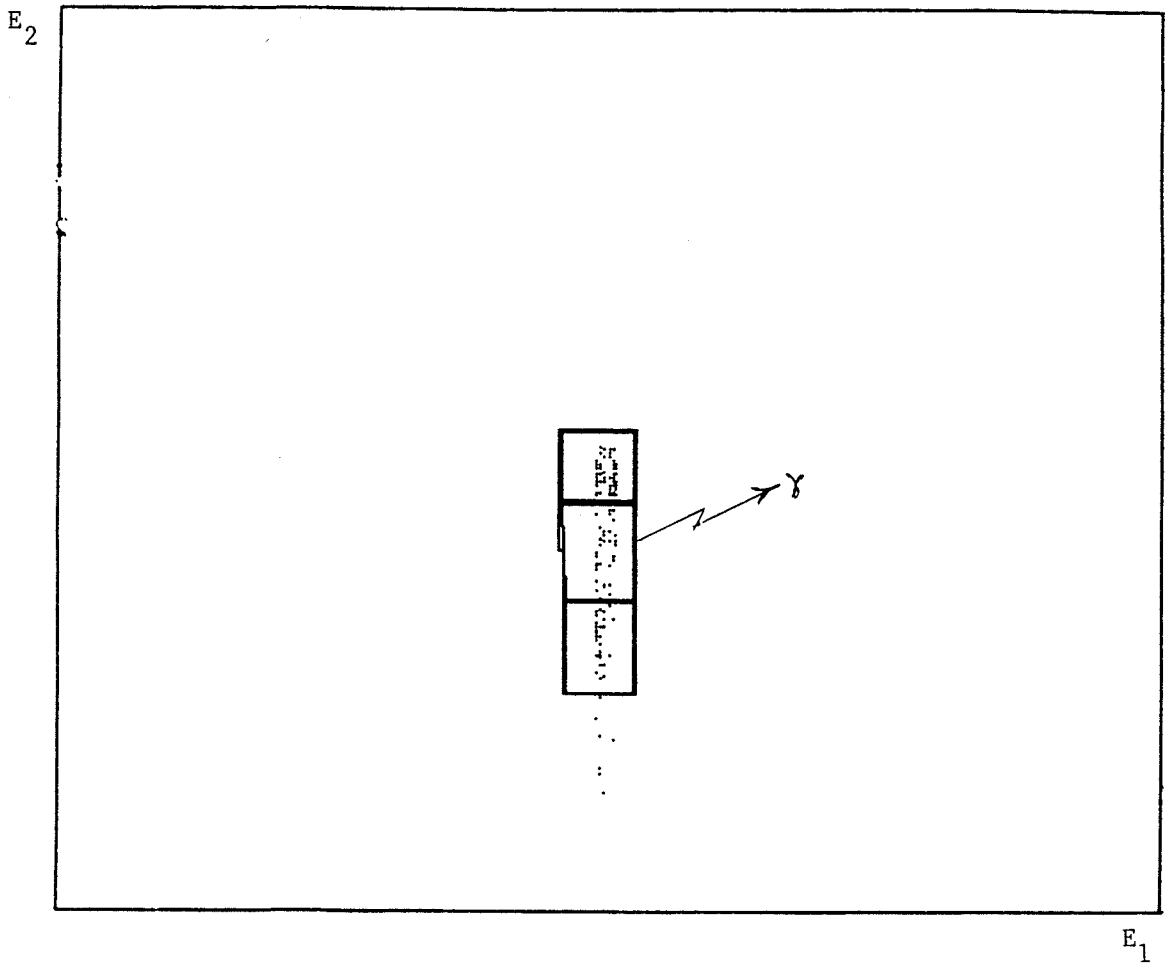

Fig. 4-34 2-D plot of the 4.77 MeV state.

b) 5.16 MeV State

An alpha spectrum with a gate on the 5.16 MeV state is shown in Fig. 4-35 and, as the result of the gate, the corresponding two-dimensional spectrum shown in Fig. 4-36 at $\theta_3 = 40^\circ$ and $\theta_4 = 106^\circ$. Fig. 4-37 shows the projection of the 5.16 MeV state of Fig. 4-36 on the E_2 axis.

The major group at the central portion of Fig. 4-36 represents the γ-decaying channel of the 5.16 MeV state and it is located on the γ-locus formed by low-lying states described before.

At $\theta_3 = 40^\circ$ and $\theta_4 = 102^\circ$, from Table 4-7 the experimental efficiency (f´) is equal to 0.505 ± 0.015. From Table 4-9, the corresponding Monte Carlo efficiency for the above pair of angles assuming the state to be γ-decaying is 0.668 ± 0.006 and the efficiency assuming the state to be α-decaying is 0.019 ± 0.001. Following the same procedure as in a) above and applying the normalization factor for Monte Carlo calculations, we have

$$(\beta_\gamma) \times (0.648 \pm 0.008) + (\beta_\alpha) \times (0.018 \pm 0.001) = 0.505 \pm 0.015$$

$$(\beta_\gamma) + (\beta_\alpha) = 1$$

with the constraint $\beta_\gamma \leqslant 1$ and $\beta_\alpha \leqslant 1$.

By solving the above, we get the following branching ratios for the pair of angles $\theta_3 = 40^\circ$ and $\theta_4 = 102^\circ$,

$$\beta_\alpha = 22.7 \pm 2.8\ \%$$

$$\beta_\gamma = 77.3 \pm 2.8\ \%$$

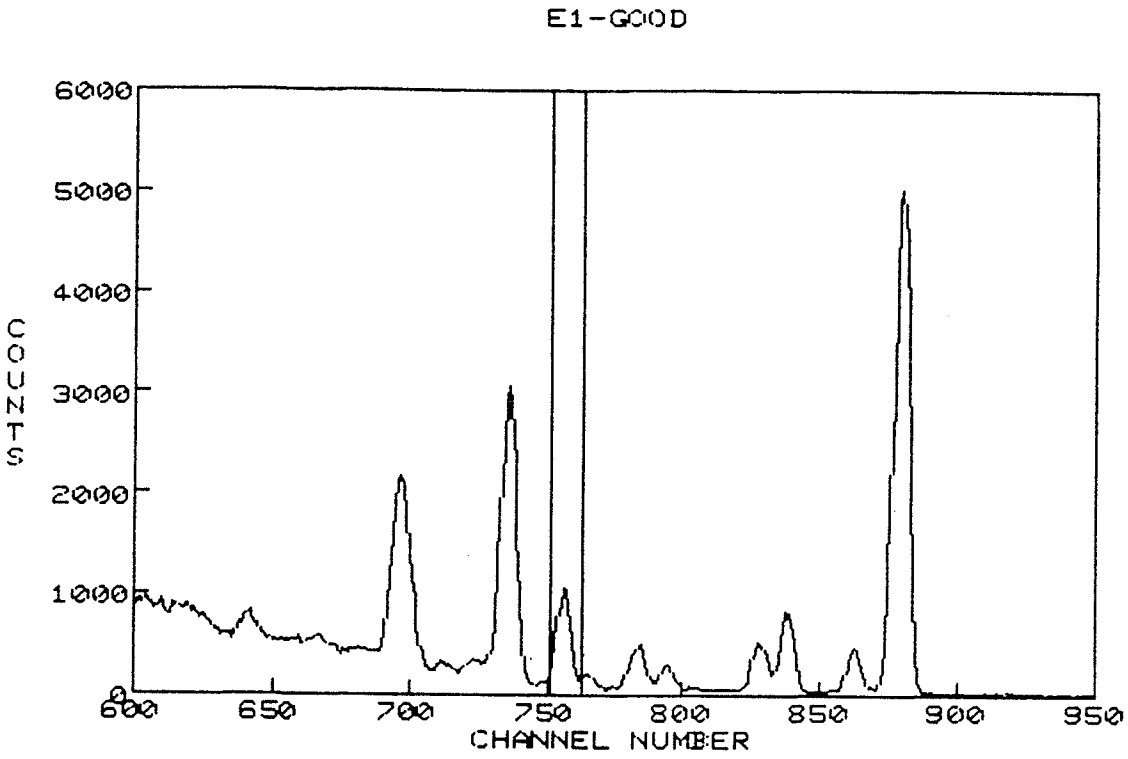

Fig. 4-35 1-D α-spectrum with a gate set on the 5.16 MeV state.

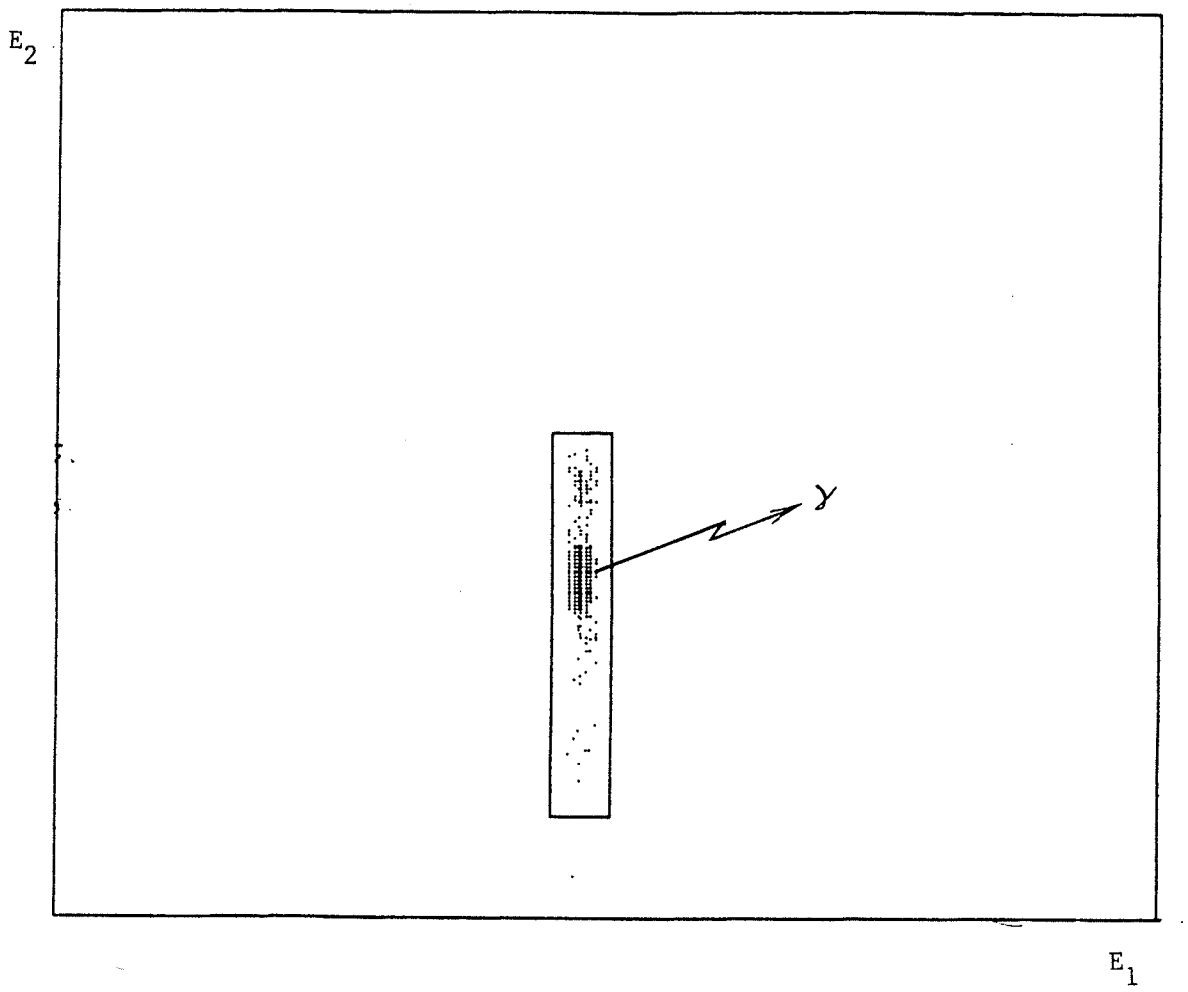

Fig. 4-36 2-D plot of the 5.16 MeV state.

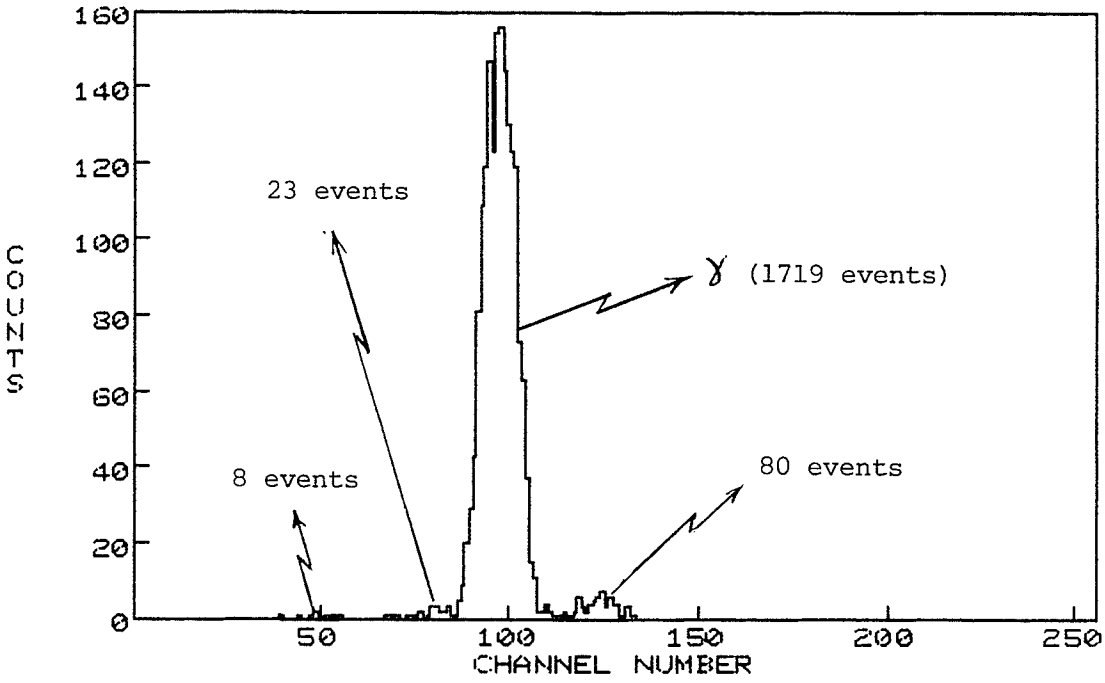

Fig. 4-37 E_2 projection of the 5.16 MeV state of Fig. 4-36

Pursuing the above steps as for $\theta_3 = 40^\circ$ and $\theta_4 = 102^\circ$, the branching ratios for the other pairs of angles were calculated

For $\theta_3 = 40^\circ$ and $\theta_4 = 104^\circ$,

$$\beta_\alpha = 17.9 \pm 3.0\ \%$$

$$\beta_\gamma = 82.1 \pm 3.0\ \%$$

For $\theta_3 = 40^\circ$ and $\theta_4 = 106^\circ$,

$$\beta_\alpha = 23.4 \pm 3.1\ \%$$

$$\beta_\gamma = 76.6 \pm 3.1\ \%$$

Now, we again use the relations (4-2) and (4-3) to calculate the mean value and the corresponding uncertainty of the above results. After inserting the respective values and doing the calculations, the final values for the branching ratios of the 5.16 MeV state were calculated as

$$\bar{\beta}_\alpha = 21.3 \pm 1.7\ \%$$

$$\bar{\beta}_\gamma = 78.7 \pm 1.7\%$$

Previously reported values are (Aj 84), (Ke 79), (Al 66)

$$\Gamma\,(\text{total}) = 1.5 \pm 0.1\ \text{eV}$$

$$\beta_\gamma = 87.0 \pm 4.0\ \%$$

As noted above, there is $\sim$ 8 % discrepancy between the two results and our calculated value for β_γ is by this amount smaller than the reported one. In verifying this discrepancy, similar calculation was carried out for the pair of angles at $\theta_3 = 70^\circ$ and $\theta_4 = 71^\circ$ and the following results were obtained,

$$\beta_\alpha = 21.3 \pm 3.9\ \%$$

$$\beta_\gamma = 78.7 \pm 3.9\ \%$$

which confirms the results obtained for the pairs of angles at $\theta_3 = 40^\circ$.

The above discrepancy is attributed to the two neighbouring, i.e. the 5.11 and 5.18 MeV states. These states are very closely spaced with respect to the 5.16 MeV state and are nearly 100 % alpha-decaying. If we assume the previously reported value of $\beta_\gamma = 87.0 \pm 4.0\ \%$, we can calculate the contribution due to the 5.11 and 5.18 MeV states as follows:

Let f be the fraction of contribution due to the 5.16 MeV state and f-1 be the fraction of contribution due to the 5.11 +5.18 MeV states. Assuming the 5.11 and 5.18 MeV states to be 100 % alpha decaying we have (for $\theta_3 = 40^\circ$ and $\theta_4 = 102^\circ$)

$$f \times (0.87 \pm 0.04) \times (0.648 \pm 0.008) + [f \times (0.13 \pm 0.04) + (1 - f)] \times (0.018 \pm 0.001) = 0.505 \pm 0.015.$$

From the above we get

$$f = 0.888 \pm 0.039$$

By carrying out the similar calculation for the other pairs of angles and taking the average, the average value ($\bar{f}$) of the fraction of the contibution due to the 5.16 MeV state is $\bar{f} = 0.899 \pm 0.027$ and the fraction of the contribution due to the 5.11 + 5.18 MeV states is $1 - f = 0.101 \pm 0.027$.

Then it is concluded that these alpha-decaying states contribute approximately 10 % to the excitation in the region of the 5.16 MeV state.

c) 6.025 MeV State

A two-dimensional spectrum with a gate on the 6.025 MeV state is shown in Fig. 4-38 at $\theta_3 = 40^\circ$ and $\theta_4 = 106^\circ$, and the projection showing the corresponding peaks is represented in Fig. 4-39. The weak group of events at the central portion of the gate in Fig. 4-38 is due to the γ-decaying channel of the state and the energy of the peak labelled gamma in Fig. 4-39 is consistent with the energy calculated from kinematics for ^{10}B decay to the final g.s. The strong group is related to the particle-decaying channel and the energies of the two distinct peaks in Fig. 4-39 correspond very closely with the max. energies obtained for α, (5.318 MeV), and ^6Li, (5.901 MeV), from the kinematics for the breakup:

$$^{10}B_{(6.025\ \text{MeV state})} \dashrightarrow {}^6Li + \alpha .$$

At $\theta_3 = 40^\circ$ and $\theta_4 = 102^\circ$, from Table 4-7 the experimental efficiency (f´) is equal to 0.008 ± 0.002. From Table 4-9, the corresponding Monte Carlo efficiency for the above pair of angles assuming the state to be γ-decaying is 0.742 ± 0.006 and the efficiency assuming the state to be α-decaying is 0.0110 ± 0.0007. Following the same procedure as in a) above and applying the normalization factor to the above Monte Carlo efficiencies we have

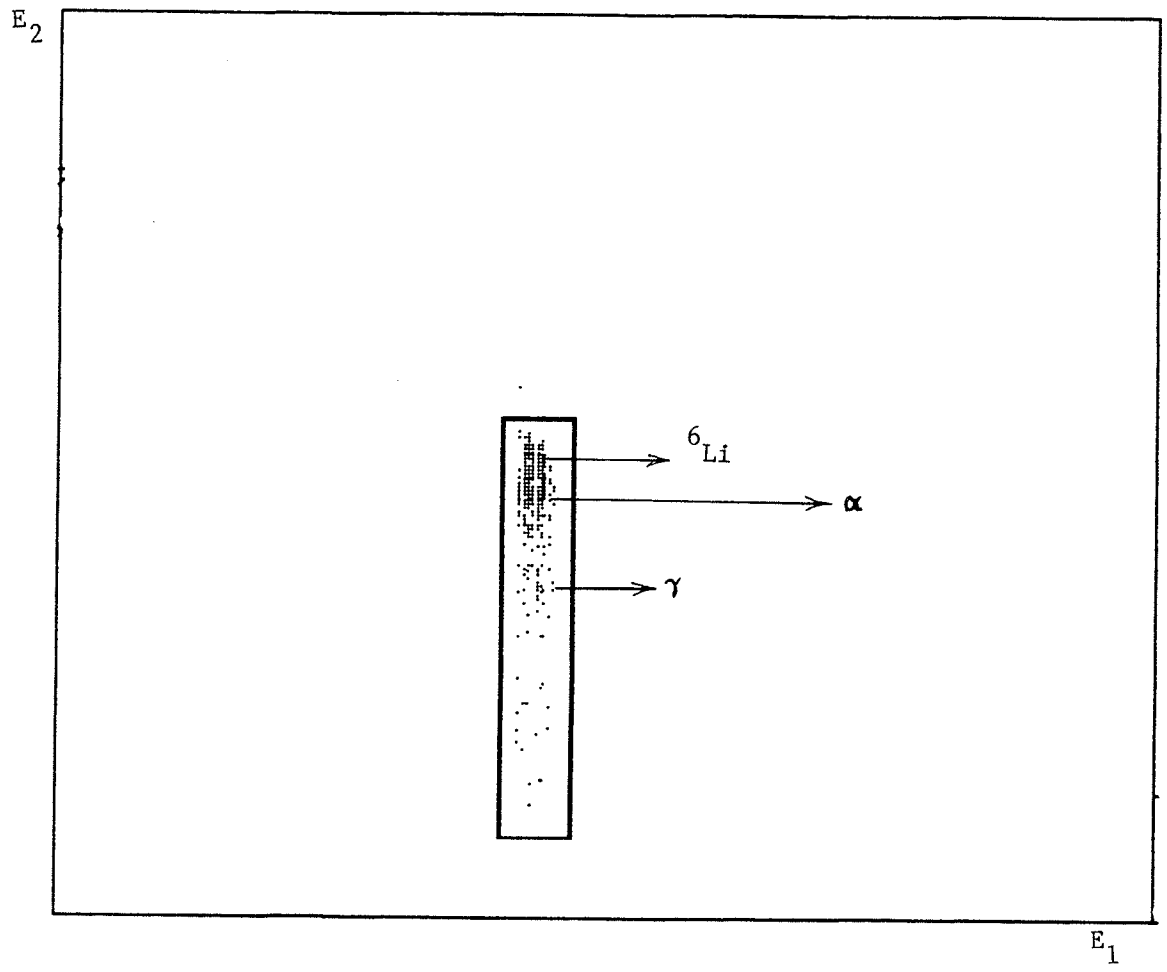

Fig. 4-38 2-D spectrum of the 6.025 MeV state.

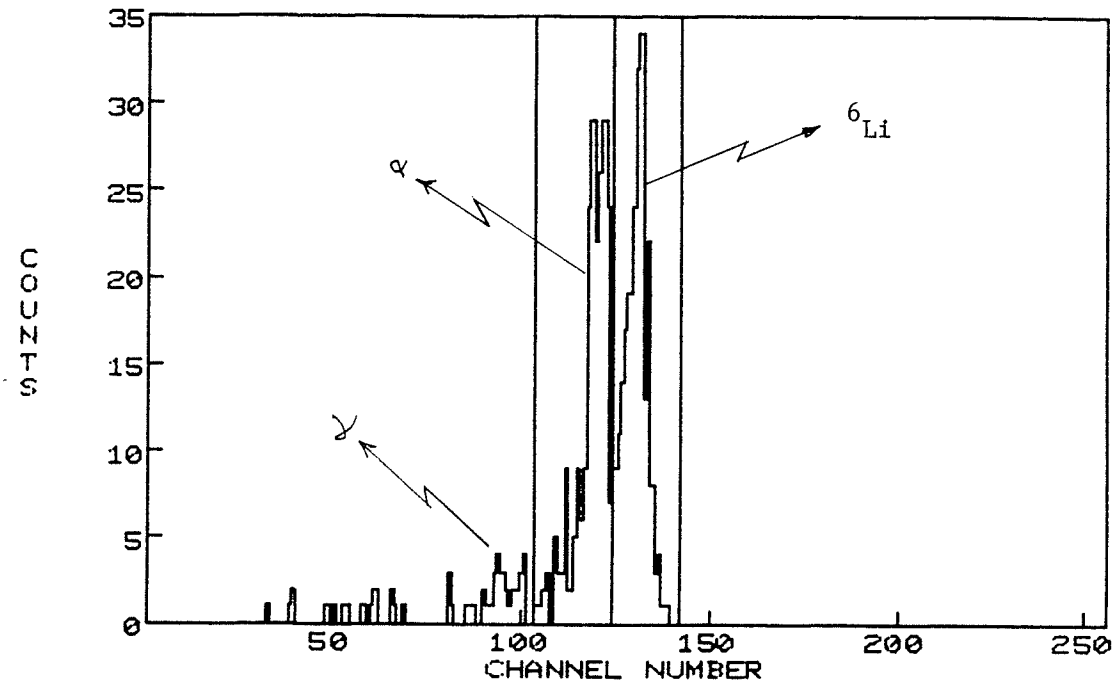

Fig. 4-39 E_2 projection of the 6.025 MeV state of Fig. 4-38 on the E_2 axis.

$(\beta_\gamma) \times (0.720 \pm 0.009) + (\beta_\alpha) \times (0.0107 \pm 0.0007) = 0.008 \pm 0.002$

$(\beta_\gamma) + (\beta_\alpha) = 1.$

with the constraint $\beta_\gamma \leq 1$ and $\beta_\alpha \leq 1$.

By solving the above, we get the following branching ratios for the pair of angles $\theta_3 = 40^\circ$ and $\theta_4 = 102^\circ$

$$\beta_\alpha = 100.4 \pm 1.8 \%$$

$$\beta_\gamma = -0.4 \pm 1.8 \%$$

Following the previous procedure, the branching ratios for the other pairs of angles were calculated

For $\theta_3 = 40^\circ$ and $\theta_4 = 104^\circ$,

$$\beta_\alpha = 99.3 \pm 1.9 \%$$

$$\beta_\gamma = 0.7 \pm 1.9 \%$$

For $\theta_3 = 40^\circ$ and $\theta_4 = 106^\circ$,

$$\beta_\alpha = 98.2 \pm 2.4 \%$$

$$\beta_\gamma = 1.8 \pm 2.4 \%$$

By using the relations (4-2) and (4-3), the mean value and the corresponding uncertainty of the above results were calculated as follows

$$\overline{\beta_\alpha} = 99.5 \pm 1.1 \%$$

$$\overline{\beta_\gamma} = 0.5 \pm 1.1 \%$$

Similar calculation was made for the pair of angles $\theta_3 = 70^\circ$ and $\theta_4 = 71^\circ$ and the following results were obtained.

$$\beta_\alpha = 100 \pm 7.3 \%$$

$$\beta_\gamma = 0.0 \pm 7.3\ \%$$

Hence, the 6.025 MeV state is primarily ($\sim$100 %) a α-decaying state. It should also be noted that since there are other closely spaced levels in the neighbourhood of the 6.025 MeV state (refer to Fig. 4-6), the above branching ratios can be attributed to the region of the 6.025 MeV state rather than purely to the 6.025 MeV state.

Previously reported values are (Aj 84)

$$\Gamma\,(\text{total}) = 0.11 \pm 0.02\ \text{eV}$$
$$\beta_\gamma \leqslant 0.9\ \%$$

d) 7.47 MeV State

A two-dimensional spectrum of the 7.47 MeV state is shown in Fig. 4-40 at $\theta_3 = 40^\circ$, $\theta_4 = 106^\circ$; and the projection showing the corresponding peaks is represented in Fig. 4-41. By comparing the corresponding efficiencies assuming the state to be γ-decaying and those assuming the state to be p-decaying (refer to Table 4-9) with the experimental efficiencies (refer to Table 4-5 to Table 4-8), it is noticed that the experimental efficiencies are much lower than the former ones. Hence it can be concluded another process providing a lower efficiency might be involved. The results obtained from the Monte Carlo calculation as well as the energy analysis of the spectrum confirm the α-decay to be the third process.

Table 4-13 shows the Monte Carlo calculation for the α- and p-decays. In this table η_{tot} represents the total coincidence efficiency for the process concerned and the η_{low} and η_{high} indicate the backward and forward scattering efficiencies for the breakup fragments.

The branching ratios for the γ-, p- and α-decay for the 7.47 MeV state are calculated as follows:

$$(\beta_\gamma \times \eta_\gamma) + (\beta_p \times \eta_p) + (\beta_\alpha \times \eta_\alpha) = \eta_{exp}.$$

The group labelled (3) in Fig. 4-41 represents the α-decay and energetically it corresponds to the forward scattering of the α and ^{6}Li (g.s.) fragments. By using Table 4-6 and Table 4-13 we have

$$\beta_\alpha \times [(0.0043 \pm 0.001) + (0.0028 \pm 0.001)] = N_3/\text{singles}.$$

$$= (6 \pm 2)/(13842 \pm 118).$$

$$\therefore \quad (\beta_\alpha)(^6\text{Li to the g.s.}) = 5.6 \pm 2.7\ \%. \qquad (1)$$

The group labelled (1) in Fig. 4-41 represents the p-decay and it corresponds to the backward scattering of ^{9}Be. By using Table 4-6 and Table 4-13 we have

$$(\beta_p \times \eta_p) = N_1/\text{singles}.$$

$$\beta_p \times (0.0324 \pm 0.001) = (211 \pm 14)/(13842 \pm 118)$$

$$= 0.015 \pm 0.001.$$

$$\therefore \quad \beta_p = 0.463 \pm 0.034. \qquad (2)$$

The group labelled (2) in Fig. 4-41 represents the p-decay (forward scattered ^{9}Be), α-decay with both α and ^{6}Li (first excited state) forward scattered and possibly γ-decay.

By using the Tables 4-6, 4-9 and 4-13 we have

$$\beta_\gamma \times (0.086 \pm 0.001) + \beta_p(0.0475 \pm 0.001) + \beta_\alpha[(0.0097 \pm 0.001) + (0.0048 \pm 0.001)] = (430 \pm 21)/(13842 \pm 118) \quad (3)$$

The constraint is

$$\beta_\gamma + \beta_p + \beta_\alpha(^{6}Li \text{ to the g.s.}) + \beta_\alpha(^{6}Li \text{ to the first excited state}) = 1. \quad (4)$$

From (1), (2), (3) and (4) above, for $\theta_3 = 40^\circ$, $\theta_4 = 106^\circ$, we get

$\beta_p \sim 46.3 \pm 3.4$ %

β_α (^{6}Li to the g.s.) $\sim 5.6 \pm 2.7$ %

β_α (^{6}Li to the first excited state) $\sim 46.9 \pm 1.6$ %

$\beta_\gamma \sim$ an upper limit of 2 %.

Similar calculations are made for the other pairs of angles and the results are as follows

For $\theta_3 = 40^\circ$ and $\theta_4 = 102^\circ$

$\beta_p \sim 60.0 \pm 5.8$ %

β_α (^{6}Li to the g.s.) $\sim 6.2 \pm 2.6$ %

β_α (^{6}Li to the first excited state) $\sim 35.7 \pm 6.4$ %

$\beta_\gamma \sim 0.$

For $\theta_3 = 40^\circ$ and $\theta_4 = 104^\circ$

$\beta_p \sim 55.8 \pm 4.9$ %

β_α (^{6}Li to the g.s.) $\sim 4.1 \pm 1.4$ %

β_α (^{6}Li to the first excited state) $\sim 43.6 \pm 5.6$ %

$\beta_\gamma \sim 0.$

Finally, the grand average for the above results is calculated with the following results:

$\bar{\beta}_p \sim 51.3 \pm 2.5$ %

$\bar{\beta}_\alpha$ (^{6}Li to the g.s.) $\sim 4.7 \pm 1.1$ %

$\bar{\beta}_\alpha$ (^{6}Li to the first excited state) $\sim 46.0 \pm 1.5$ %

Considering the uncertainties in the above values, an upper limit of 1 to 2 % can be assigned to the γ-decaying process.

No previous information seems to be available for the branching ratios of the 7.47 MeV state, but the previously reported values for the neighbouring 7.479 MeV state measured at $E_p = 0.992$ MeV in the reaction ^{9}Be(p,γ)^{10}B are as follows (Aj 84)

$$\beta_p = 65 \text{ \%}$$
$$\Gamma = 25.8 \text{ eV.}$$

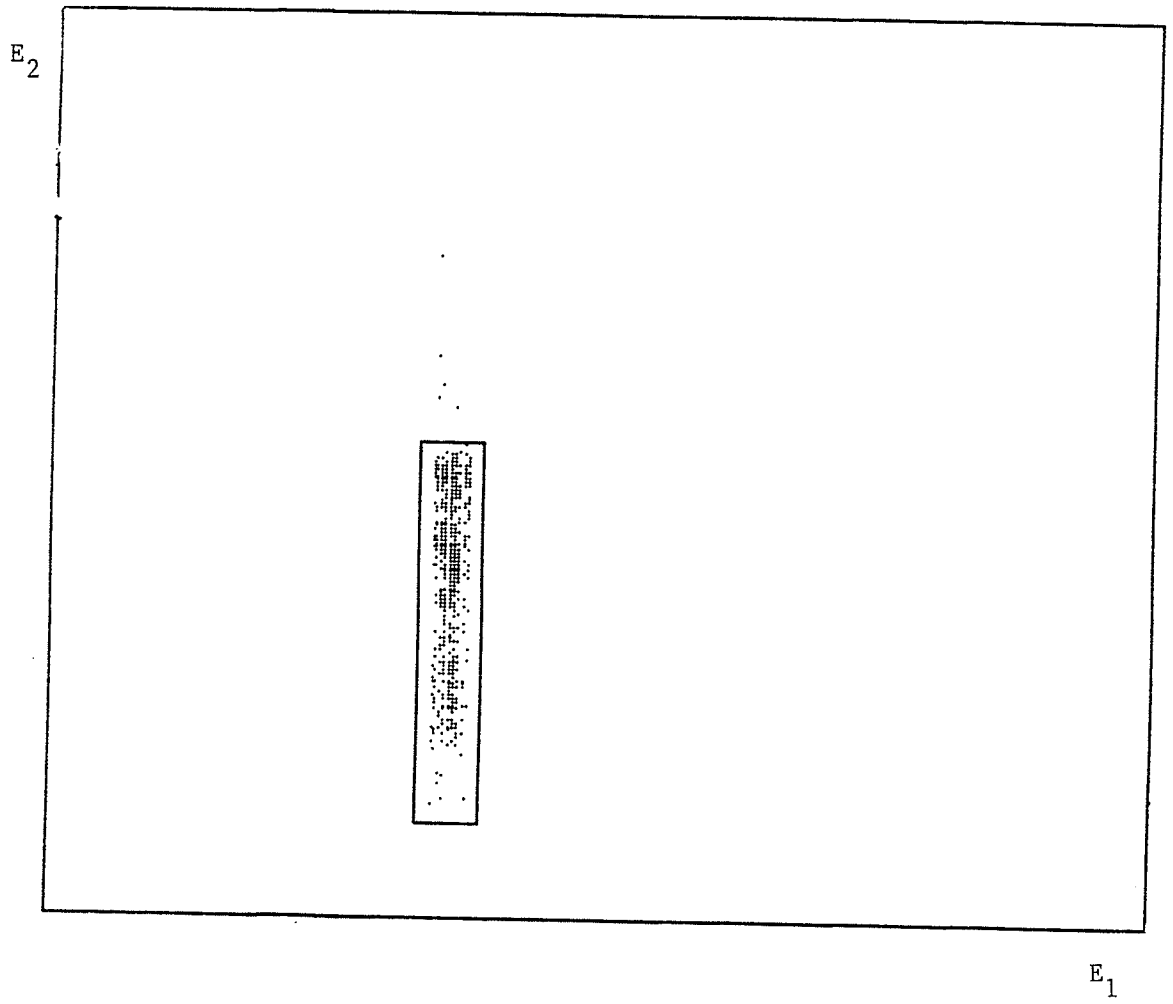

Fig. 4-40 2-D spectrum of the 7.47 MeV state at $\theta_3 = 40^\circ$ and $\theta_4 = 106^\circ$.

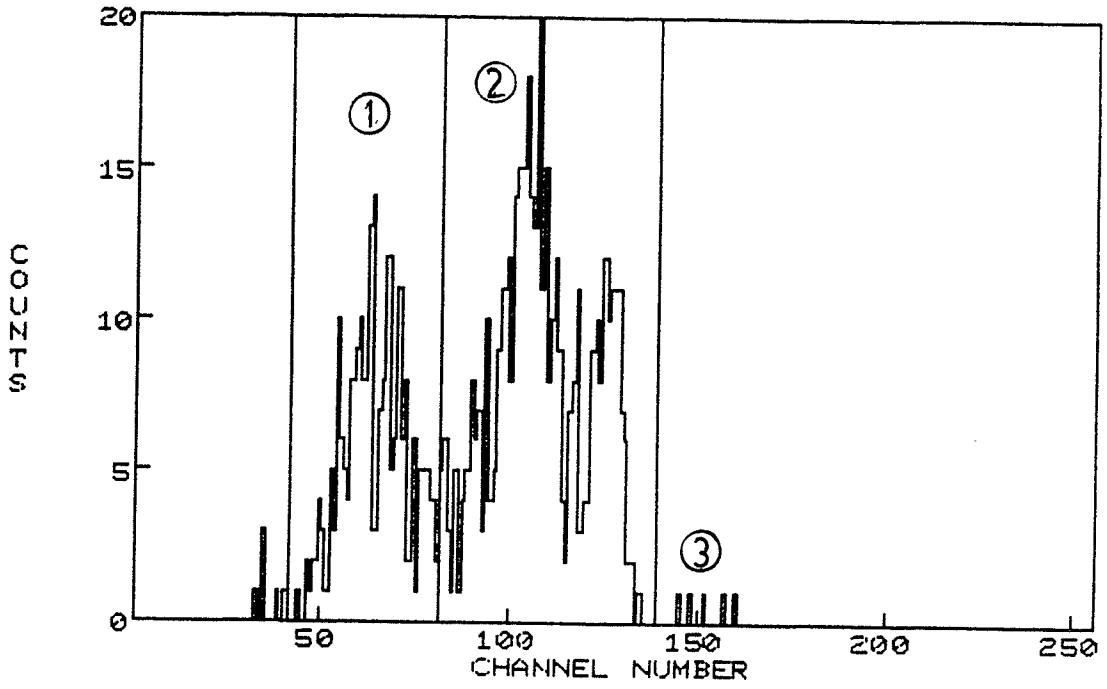

Fig. 4-41 E_2 projection of the 7.47 MeV state.

Table 4-13 Monte Carlo calculation for the α- and p-decays (7.47 MeV state)

	θ_4	η_{tot}	$\eta(^6Li)^{g.s.}$		η_α	
			low	high	low	high
α-decay	102	0.0083	0.0001	0.0046	0	0.0034
Li^6(g.s.)	104	0.0075	0.0001	0.0040	0	0.0032
	106	0.0071	0.00005	0.0043	0	0.0028
α-decay	102	0.0162	0.0011	0.0081	0.0002	0.0051
^{6}Li(1st	104	0.0169	0.0016	0.0094	0.0004	0.0049
excited	106	0.0170	0.0020	0.0097	0.0004	0.0048
state						
	θ_4	η_{tot}	$\eta(^9Be)$		η_p	
			low	high	low	high
p-decay	102	0.0628	0.0200	0.0398	0.0001	0.0012
	104	0.0688	0.0233	0.0424	0.00005	0.0024
	106	0.0823	0.0324	0.0475	0.00005	0.0024

CHAPTER 5

Conclusion

The X-Y position sensitive proportional counter, having a simple construction and low cost, provided an acceptable position resolution in two dimensions. The measured intrinsic position resolution of the counter in vertical and horizontal directions was as 1.4 and 1.3 mm respectively which were quite satisfactory for our experiment. In order to obtain a good position resolution it was necessary to calculate and experimentally to optimize the reduced electric field, E/P. The gas pressure of 0.16 atm and bias voltage between 680 and 720 volts were optimum values in the case of our counter. The position resolution of proportional counters can get worse in use where some conditions such as normal incident particles are not present. The explanation for this effect probably is that energy loss fluctuations can lead to position fluctuations for non-normal particles. The energy-loss fluctuations as well as multiple scattering in the entrance window and counter gas could have deteriorated the resolution up to 0.7 mm. In addition to position information, it was possible to measure the drift velocity of electrons in the counter as $v_d = 3.87 \pm 0.04$ cm/μ sec.

The proportional counter was succesfully used in a coincidence study of the breakup of states in ^{10}B to measure the branching ratios for γ- and particle (alpha and proton)-decay.

The energy resolution in the reaction $^{13}C(p,\alpha)^{10}B$ was greatly improved by calculating the scattering angle and applying the kinematic correction. The FWHM of the g.s. which was 0.356 MeV in the raw spectra, was improved to 0.215 MeV.

In this work, the levels of ^{10}B were examined up to 7.47 MeV in excitation and it was possible to separate the γ-decaying states from the particle- decaying ones. The summary of the results for branching ratios are shown in Table 5-1.

Table 5-1 The summary of the results for the branching ratios of ^{10}B

State	Branching ratios (β), %			Previously reported values (β_γ), %
	γ	α	p	(Aj 84), (Ke 79), (A1 66)
0.718	100			100
1.74	100			100
2.15	100			100
3.59	100			100
4.77	2.3±2.9	97.7±2.9		0.23±0.03
5.16	78.7±1.7	21.3±1.7*		87.0±4.0
6.025	0.5±1.1	99.5±1.1		⩽0.9
7.47	~2.0	50.7±1.8	51.3±2.5	-

* ~10% contribution from the 5.11 and 5.18 MeV neighbouring states.

APPENDIX 1

a) BTEN.COM;

```
$ASSIGN/GROUP MTB0: TA
$ASSIGN/GROUP MTB1: TB
$DMEM ALL
$CL FLAGS
$CL ALL
$AMEM 1    512      I*4 1D E-RIGHT
$AMEM 2    512      I*4 1D E-LEFT
$AMEM 3    512      I*4 1D E-SUM
$AMEM 4    1024     I*4 1D E1
$AMEM 5    1024     I*4 1D E2
$AMEM 6    1024     I*4 1D R-TAC
$AMEM 7    1024     I*4 1D L-TAC
$AMEM 8    1024     I*4 1D E2-TAC
$AMEM 9    2048     I*4 1D ER/S1
$AMEM 10   256     I*4 1D ER/S              !S MEANS E-SUM
$AMEM 11   2048     I*4 1D EL/S1
$AMEM 12   256      I*4 1D EL/S
$AMEM 13   64       I*4 1D BREG             !THIS IS THE BIT REG SPECTRA
$AMEM 14   1024     I*4 1D E1-GOOD          !FOR ALPHAS IMPROVED
$AMEM 15   1024     I*4 1D ET0-NORM         !for ALPHA singles, normal res.
$AMEM 17   256      I*4 1D S-DIF
$AMEM 18   256      I*4 1D Z-DIF
$AMEM 20   256 256  I*2 2D E1-V-E2
$AMEM 21   64  64   I*2 2D ER-EL
$AMEM 22   64  64   I*2 2D ER/ES-S
$AMEM 23   64  64   I*2 2D EL/ES-S
$AMEM 24   64  64   I*2 2D ER/S-TR
$AMEM 25   64  64   I*2 2D EL/S-TL
$AMEM 26   64  64   I*2 2D TLTR
$AMEM 28   16  16   I*4 2D ZS-V-SS          !Z for single vs. S for single
$AMEM 29   16  16   I*4 2D ZC-V-SC          !Z for coin. vs. S for coin
$AMEM 35   256 256  I*2 2D E1G-V-E2         !With improved E1 for gating purposes
$AMEM 60   256      I*4 1D P1E2
$AMEM 61   1024     I*4 1D E2-GOOD
$AMEM 62   1024     I*4 1D E2-TAC-GOOD
$AMEM 63   128      I*4 1D XDIF
$AMEM 64   128      I*4 1D YDIF
$AMEM 65   1024     I*4 1D E2-IMPROVED
$AMEM 66   1024     I*4 1D E2-IMPR-GOOD
$AMEM 67    256     I*4 1D P2E2
$AMEM 68    256     I*4 1D P3E2
$AMEM 70    256     I*4 1D E,SING,COMPRESSED
$AMEM 71    256     I*4 1D E,COIN,COMPRESSED
```

```
$! **** 1-D GATES ****
$!
$GATE NEW
$GATE 4 9
$GATE 8 1
$GATE 14 7
$GATE 62 1
$GATE 70 1
$GATE 71 1
$!
$! **** 2-D GATES ****
$!
$TDG ALL 1   256 256 RECL1
$TDG ALL 2   256 256 RECL2
$TDG ALL 3   256 256 RECL3
$TDG ALL 4   256 256 RECL4
$TDG ALL 5   256 256 RECL5
$TDG ALL 6   256 256 RECL6
$TDG ALL 7   256 256 RECL7
$TDG ALL 8   256 256 RECL8
$TDG ALL 9   256 256 RECL9
$TDG ALL 10  256 256 RECL10
$TDG ALL 11  64  64    TEST
$TDG ALL 15  64  64    PX1
$TDG ALL 16  64  64    PX2
$TDG ALL 17  64  64    PX3
$TDG ALL 18  64  64    PX4
$TDG ALL 19  64  64    PX5
$TDG ALL 20  64  64    PY1
$TDG ALL 21  64  64    PY2
$TDG ALL 22  64  64    PY3
$TDG ALL 23  64  64    PY4
$TDG ALL 24  64  64    PY5
$!
$EVOP SE B10
$SCAL START
$SCAL NEW
$SCAL CLEAR
$SCAL BEGIN 1 2 3
$SCAL HEAD 1 CRM1 PU1 SCA1 CRMR PUR SCAR
$SCAL HEAD 2 CRM2 PU2 SCA2 CRML PUL SCAL
$SCAL HEAD 3 COINC1 MSTROBE COINC2 TIME F.CUP BLANK
$SCR LEFT 1 CURRENT
$SCR LEFT 2 NA-HR
$SCR REPEAT 2
$EXIT
```

b) BTEN.EVL;

```
C Sorting routine for 13C(P,ALPHA)10B* -----) ALPHA + 6Li exprimant.
C This file is accessed by "EVDP Sq B10" in Bten.COM
C                                          ALI: JUNE,1986
C MODIFIED JULY,1986
C
C
DATA EVSIZ 9      !Eight parameters per event;4 words from AD811 ,3 from TDC and
C                 !1 from I.R.
C
C **** Declare Spectra ****
C
SPEC SR     1
SPEC SL     2
SPEC SS     3
SPEC SE1    4
SPEC SE2    5
SPEC STR    6
SPEC STL    7
SPEC STE2   8
SPEC R/S1   9
SPEC R/S    10
SPEC L/S1   11
SPEC L/S    12
SPEC SIR    13
SPEC SE1G   14
SPEC ETAN   15
SPEC SDIF   17
SPEC ZDIF   18
SPEC E1E2   20
SPEC RL     21
SPEC RSS    22
SPEC LSS    23
SPEC RST    24
SPEC LST    25
SPEC TLTR   26
SPEC ZSSS   28
SPEC ZCSC   29
SPEC S1G    35
SPEC SE2G   61
SPEC TE2G   62
SPEC XDIF   63
SPEC YDIF   64
SPEC SE2I   65
SPEC E2GI   66
SPEC SES    70
SPEC SEC    71
```

```
C
C **** Define Formats ****
C * ADC Formats *
FORMAT FR     1 11 3
FORMAT FR2D   1 11 6
FORMAT FL     2 11 3
FORMAT FL2D   2 11 6
FORMAT FE1    3 11 2
FORMAT E12D   3 11 6
FORMAT FE2    4 11 2
FORMAT E22D   4 11 6
C * TDC Formats *
FORMAT FTR    5 11 2
FORMAT FTR2   5 11 6
FORMAT FTL    6 11 2
FORMAT FTL2   6 11 6
FORMAT FTE2   7 11 2
FORMAT TE22   7 11 6
FORMAT BREG   8 6  1              This is the Bi Rm 2351 Bit Register
FORMAT BR3    8 3  3
FORMAT BR4    8 4  4
C
C **** Define Gates ****
C * 2-D Gates *
TDG GR0   1
TDG GR1   2
TDG GR2   3
TDG GR3   4
TDG GR4   5
TDG GR5   6
TDG GR6   7
TDG GR7   8
TDG GR8   9
TDG GR9   10
TDG TEST  11
C * 1-D Gates *
GATE AL0   4  1           !q.s. alpha gate
GATE AL1   4  2
GATE AL2   4  3
GATE AL3   4  4
GATE AL4   4  5
GATE AL5   4  6
GATE AL6   4  7
GATE AL7   4  8
GATE AL8   4  9
GATE GL0   14 1           !q.s. alpha gate on good resolution spec.
GATE GL1   14 2
GATE GL2   14 3
GATE GL3   14 4
```

```
GATE GL4   14 5
GATE GL5   14 6
GATE GL6   14 7
GATE GL7    8 1
GATE GL8   62 1
GATE GL9   70 1
GATE GL10 71 1
C
C **** Executable stuff follows ****
VARIABLE  CON1=256
VARIABLE  CON2=512
VARIABLE  CON3=2048
VARIABLE  CON4=750
VARIABLE  ZERO=0
VARIABLE  CON5=70
VARIABLE  CON6=100
VARIABLE  ONE=1
VARIABLE  CON7=150
VARIABLE  CON8=7
C
C       VARIABLE TALX is set to 1 if event is within X-window
C       VARIABLE GAL0 is set to 1 if event is within q.s. window
C
      GET  BREG
      TINC SIR
      GET  FR
      TINC SR
      STA  FRVL
      GET  FL
      TINC SL
      STA  FLVL
      ADD  FRVL
      TINC SS
      STA  SVV            !SUM 1024 CH
      LSH  -3
      STA  SV2           !Variable sum for 2-D spectra,64 CH.EL+ER
      GET  FE1
      STA  VE1
      TINC SE1
      STA  SE1V          !Variable E1,1024 CH.
      SUB  512
      LSH  -1
      STA  SE1V2         !VARIABLE E1,256 CH,FOR 2-D SPECTRA WITH 50% OFFSET
      GET  FTR
      TINC STR
      GET  FTL
      TINC STL
      GET  FL2D
      TTDI FR2D RL       !ER VS. EL
```

```
      INC   RL
      LDA   SVV                          !check if SVV is zero
       IF   LT 1
            LDA CON2
            STA SVV
       ENDIF
      LDA FRVL
      FLOAT
      DIV SVV
      MUL CON3
      FIX
      TINC R/S1
      SUB CON4
      LSH -1
      TINC R/S          !XL
      LSH -2            !64 CH. VERSION OF XL
      STA  RS2D         ! variable R/S for 2D spectra
      LDA SV2
      TTDI RS2D  RSS
      INC  RSS
      GET FTR2
      STA TR2V
      STA NZ3R
      TTDI RS2D  RST
      INC  RST
      LDA FLVL
      FLOAT
      DIV SVV
      MUL CON3
      FIX
      TINC L/S1
      SUB CON4
      LSH -1
      TINC L/S        !XR
      LSH -2
      STA  LS2D       ! variable L/S for 2D spectra
      LDA SV2
      TTDI LS2D  LSS
      INC  LSS
      GET  FTL2
      STA  NZ3L
      TTDI LS2D  LST
      INC  LST
C     KINEMATIC CORRECTION FOR ALPHA SPECTRUM(#4)
      LDA  RS2D
      STA  NS3L
      LDA  LS2D
      STA  NS3R
```

```
      LDA  0
      STA  Z
      STA  S
      STA  NDS
      STA  NDZ
      STA  GAL0
      LDA VE1
      STA VE1C
      CALL 1 VE1C NZ3R NS3R NZ3L NS3L Z S NDS NDZ
      TINC VE1C SE1G           !SPEC#14
           IF GL0
                LDA ONE
                STA GAL0
           ENDIF
C  ***************************************************************************
       LDA NS3R
       SUB NS3L
       ADD CON5
       TINC XDIF          !Spec#63
       LDA NZ3R
       SUB NZ3L
       ADD CON5
       TINC YDIF          !Spec#64
C  Alpha singles only
                          GET BR3
                          IF EQ 1
                             IF GAL0 EQ 1
                                LDA VE1C
                                SUB 512
                                LSH -1
                                STA E1V2G
                             ENDIF
                          ENDIF
C  ***************************************************************************
      LDA NDS
      ADD CON6
      TINC SDIF           !spec# 17
      LDA NDZ
      ADD CON7
      TINC ZDIF           !spec# 18
C
      CALL 2 NS3R NS3L NZ3R NZ3L
```

```
      IF GAL0 EQ 1
         LDA S
         ADD CON8
         STA SS1
         LDA Z
         ADD CON8
         STA SZ1
         LDA SS1
         TTDI SZ1 ZSSS            !spec # 28; x singles, s singles
         INC ZSSS
      ENDIF
      LDA TR2V
      TTDI FTL2 TLTR
      INC  TLTR
C
      LDA VE1C
      SUB S12
      LSH -1
      STA SE1V2G
      TINC SES            !SPEC#70;E;sing;256 ch.

C
      GET  BR4
        IF EQ 1
           GET FTE2
           TINC STE2
        IF GL7
           LDA ONE
           STA GAL7
        IF GAL7 EQ 1
           LDA  SE1V2G
           TINC SEC       !Spec#71;E-Coinc;256 ch
           GET  FE2
           TINC SE2
           LSH  -2          !256 CH. E2 FOR 2-D
           STA  SE2V2       !Y
           LDA  SE1V2G        !X
           TTDI SE2V2 E1E2
           INC  E1E2
        ENDIF
        ENDIF
```

```
C Coincidences:
        IF GAL0 EQ 1
                LDA  E1V2G                  !X
                TTDI  SE2V2 S1G             !SPEC #35
                INC S1G
C
            IF GR0
                LDA S
                ADD CON8
                STA SS2
                LDA Z
                ADD CON8
                STA SZ2
                LDA SS2
                TTDI SZ2 ZCSC    !Spec#29; z coin, s coin.
                INC ZCSC
            ENDIF
C
                GET FE2
                TINC SE2G        !Spec#61
C
                GET FTE2
                TINC TE2G        !Spec#62
        IF GL8
                LDA ONE
                STA GAL1
C
        IF GAL1 EQ 1
                GET FE2
                TINC SE2I        !Spec#65
        ELSE
                GET FE2
                TINC E2GI        !Spec66
         ENDIF
         ENDIF
         ENDIF
       ENDIF
    END
```

c) BTEN.DAP;

```
B10
5
90
INIT
1  18  12  11                !EVAL CODE NAME
1  17  12  26                !MBD CHANNEL NUMBER
1  13   0   9                !BUFFERSIZE(SHOULD BE MULTIPLE OF EVSIZ)
1   2   0   2                !INITIALIZE THE CNAF'S
1  30  10  26                !ONE INIT CNAF
LAM                           !ENABLE LECROY LAMS
1  18   1   2                !TDC CLEAR
1  18   2   2                !INPUT REG.
1  18   3   2                !ENABLE CRATE LAMS
1  18   7   2
1  13   5   2                !ER(PORT 1;ORTEC 811 ADC)
1  13   6   2                !EL
1  13   7   2                !E1
1   2   0   0                !E2(MUST READ THE LAST PORT TO CLEAR)
1  17   0   2                !TR(PORT 5;LECROY 2228A TDC)
END                           !TL
                              !TE2(MUST READ THE LAST PORT TO CLEAR)
                              !BI RA 2351 INPUT REGISTER
```

d) Subroutine EVLSUB1

```
C
C*****************************************************************
C       THIS SUBROUTINE, EVLSUB1, IS CALLED FROM XSYS EVAL PROGRAM,
C       13C(P,ALPHA)10B.
C*****************************************************************
C
        SUBROUTINE EVLSUB1(NT3,NZ3R,NS3R,NZ3L,NS3L,Z,S,NDS,NDZ)
        COMMON /KIN/W1,W2,W3,W4,W5,W6,EXB,BEB
        DOUBLE PRECISION W1,W2,W3,W4,W5,W6,EXB,BEB
        INTEGER Z,S,DSS
C       READ REST MASSES OF PARTICLES, EXCITATION ENERGY OF B*,
C       BREAKUP ENERGY OF B*, AND BOMBARDING ENERGY, ALL IN MEV.
C                13C(p,ALPHA)10B*
C                             ------) ALPHA+6Li
C                  2 1   3     4         5     6
C       DPHID=ANGLE OF PROPORTIONAL COUNTER WITH RESPECT TO BEAM
C       D1=DISTANCE FROM TARGET TO PROPORTIONAL COUNTER
        Z3R=12.587-(0.36971*NZ3R)
        S3R=11.630-(0.32527*NS3R)
        Z3L=9.3852-(0.35192*NZ3L)
        S3L=-10.385+(0.32724*NS3L)
        Z1=(Z3R+Z3L)/2
        S1=(S3R+S3L)/2
        Z3=Z1-0.48
        S3=S1+0.308
        DPHID=40.
        D1=172.364
        PI=3.141592654
        RAD=180.0/PI
        IF(NT3.EQ.0) GO TO 9
        PHID=DPHID/RAD
        CPHID=COS(PHID)
        SPHID=SIN(PHID)
C       D3DTH IS THE PARTICLE 3 ENERGY CHANGE AS A FUNCTION OF ANGLE (MEV/RAD)
        D3DTH=-7.2026
        DS=S3R-S3L
        IF(DS.LT.0) NDS=(DS*100)-0.5
        IF(DS.GE.0) NDS=(DS*100)+0.5
        DZ=Z3R-Z3L
        IF(DZ.LT.0) NDZ=(DZ*20)-0.5
        IF(DZ.GE.0) NDZ=(DZ*20)+0.5
C       WRITE(4,6)NDS,NDZ
C6      FORMAT(' ',I5,3X,I5,//)
C7      WRITE(4,7)Z3R,Z3L,DZ,S3R,S3L,DS
C7      FORMAT(' ',F10.4,2X,F10.4,2X,F10.4,2X,F10.4,2X,F10.4,2X,F10.4,//)
C       Coordinates of particle 3
        X3=D1*CPHID+S3*SPHID
        Y3=D1*SPHID-S3*CPHID
        Z3=Z3
        R3=SQRT(X3*X3+Y3*Y3+Z3*Z3)
        THET3=ACOS(X3/R3)
```

```
C         Spectrum kinematics correction
          DTHETA=THET3-PHID
          COR=DTHETA*D3DTH
          IF(COR.LT.0) NCOR=(COR*29.4057)-0.5
          IF(COR.GE.0) NCOR=(COR*29.4057)+0.5
          NT3=NT3-NCOR
          GO TO 9
9         CONTINUE
          IF(Z3.LT.0) Z=(Z3*1)-0.5
          IF(Z3.GE.0) Z=(Z3*1)+0.5
          IF(S3.LT.0) S=(S3*1)-0.5
          IF(S3.GE.0) S=(S3*1)+0.5
          RETURN
          END
C*************************************************************************
          SUBROUTINE KINEMAT(I,T,THET3,T3,THET4,T4,V4)
          COMMON /KIN/W1,W2,W3,W4,W5,W6,EXB,BEB
          DOUBLE PRECISION W1,W2,W3,W4,W5,W6,EXB,BEB,S0,W4X,
          1 E1,E0,P1,P1C,S,E3,P3,P4S,P4,E4
          IF(I.GE.1) GO TO 5
          S0=(W1*W1+W2*W2+W3*W3)/2.0
          W4X=W4+EXB
5         E1=T+W1
          E0=E1+W2
          P1=SQRT(E1*E1-W1*W1)
          CTH3=COS(THET3)
          P1C=P1*CTH3
          S=S0-W4X**2/2.0+E1*W2
          E3=(E0*S+P1C*SQRT(S*S+W3*W3*(P1C**2-E0**2)))/(E0**2-P1C**2)
          T3=E3-W3
          P3=SQRT(E3*E3-W3*W3)
          IF(I.LE.1) GO TO 30
          P4S=P1*P1-2.0*P3*P1C+P3*P3
          P4=SQRT(P4S)
          E4=SQRT(P4S+W4X*W4X)
          T4=E4-W4X
          V4=SQRT(2.0*T4/W4X)
          THET4=ACOS((P1-P3*CTH3)/P4)
30        CONTINUE
          RETURN
          END
C
C*************************************************************************
          SUBROUTINE EVLSUB2 (NS3R,NS3L,NZ3R,NZ3L)
          IDS=NS3R-NS3L
          IDZ=NZ3R-NZ3L
C         WRITE(4,40)NS3R,NS3L,NZ3R,NZ3L,IDS,IDZ
40        FORMAT(' ',I6,3X,I6,3X,I6,3X,I6,3X,I6,3X,I6,//)
          CONTINUE
          RETURN
          END
```

APPENDIX 2 Channel by Channel Data

Ch.	SING1	COIN1	R1	DR1	SING2	COIN2	R2	DR2	SING3	COIN3	R3	DR3	SING4	COIN4	R4	DR4
1	1517	5	0.003	0.002	2842	14	0.005	0.001	2952	19	0.006	0.002	823	28	0.034	0.008
2	1641	14	0.009	0.002	3766	13	0.003	0.001	4893	21	0.004	0.001	752	22	0.029	0.007
3	2234	14	0.006	0.002	6007	13	0.002	0.001	7574	21	0.003	0.001	711	22	0.031	0.008
4	4482	24	0.005	0.001	7694	18	0.002	0.001	7064	15	0.002	0.001	714	23	0.032	0.008
5	5246	17	0.003	0.001	6499	14	0.002	0.001	3935	19	0.005	0.001	659	24	0.036	0.009
6	2771	14	0.005	0.001	3813	22	0.006	0.001	2509	13	0.005	0.002	731	22	0.030	0.008
7	1573	8	0.005	0.002	2607	16	0.006	0.002	2276	14	0.006	0.002	694	23	0.033	0.008
8	1455	16	0.011	0.003	2414	14	0.006	0.002	2243	15	0.007	0.002	654	23	0.035	0.009
9	1328	9	0.007	0.002	2393	16	0.007	0.002	2205	19	0.009	0.002	685	30	0.044	0.010
10	1361	13	0.010	0.003	2404	20	0.008	0.002	2223	14	0.006	0.002	659	22	0.033	0.008
11	1403	15	0.011	0.003	2359	10	0.004	0.001	2129	20	0.009	0.002	706	28	0.040	0.009
12	1332	11	0.008	0.003	2277	18	0.008	0.002	2185	22	0.010	0.002	782	27	0.035	0.008
13	1387	14	0.010	0.003	2376	15	0.006	0.002	2097	19	0.009	0.002	1015	31	0.031	0.006
14	1221	14	0.011	0.003	2282	15	0.007	0.002	2176	24	0.011	0.002	1402	32	0.023	0.005
15	1319	19	0.014	0.004	2323	22	0.009	0.002	2174	21	0.010	0.002	1146	28	0.024	0.005
16	1304	11	0.008	0.003	2328	12	0.005	0.002	2152	20	0.009	0.002	803	31	0.039	0.008
17	1317	9	0.007	0.002	2439	26	0.011	0.002	2455	20	0.008	0.002	729	31	0.043	0.009
18	1469	10	0.007	0.002	2734	25	0.009	0.002	2629	16	0.006	0.002	694	24	0.035	0.008
19	1562	20	0.013	0.003	3078	20	0.006	0.002	3088	28	0.009	0.002	693	24	0.035	0.008
20	1918	11	0.006	0.002	3251	40	0.012	0.002	3429	22	0.006	0.001	532	18	0.034	0.009
21	2051	13	0.006	0.002	3529	18	0.005	0.001	3215	38	0.012	0.002	526	19	0.036	0.010
22	2136	29	0.014	0.003	3190	24	0.008	0.002	2692	16	0.006	0.002	459	11	0.024	0.008
23	1789	24	0.013	0.003	2764	30	0.011	0.002	2337	25	0.011	0.002	475	19	0.040	0.011
24	1489	10	0.007	0.002	2350	24	0.010	0.002	2098	20	0.010	0.002	446	7	0.016	0.007
25	1320	12	0.009	0.003	2327	18	0.008	0.002	2183	29	0.013	0.003	460	17	0.037	0.011
26	1434	12	0.008	0.003	2473	24	0.010	0.002	2367	17	0.007	0.002	429	18	0.042	0.012
27	1504	12	0.008	0.003	2563	22	0.009	0.002	2312	29	0.013	0.003	447	14	0.031	0.010
28	1470	13	0.009	0.003	2238	22	0.010	0.002	1942	12	0.006	0.002	453	19	0.042	0.012
29	1170	10	0.009	0.003	2041	32	0.016	0.003	1896	24	0.013	0.003	486	22	0.045	0.012
30	1114	17	0.015	0.004	1895	25	0.013	0.003	1851	24	0.013	0.003	562	11	0.020	0.007
31	1130	16	0.014	0.004	2007	22	0.011	0.003	1924	24	0.012	0.003	696	44	0.063	0.012
32	1170	22	0.019	0.005	2160	26	0.012	0.003	2192	34	0.016	0.003	953	89	0.093	0.013
33	1243	15	0.012	0.003	2389	21	0.009	0.002	2357	27	0.011	0.002	1362	137	0.101	0.011

34	1436	16	0.011	0.003	2484	23	0.009	0.002	2319	27	0.012	0.002	1074	87	0.081	0.011
35	1565	18	0.012	0.003	2344	24	0.010	0.002	1900	19	0.010	0.003	650	60	0.092	0.016
36	1227	7	0.006	0.002	1920	21	0.011	0.003	1617	16	0.010	0.003	426	20	0.047	0.013
37	1064	11	0.010	0.003	1727	18	0.010	0.003	1620	15	0.009	0.003	413	14	0.034	0.011
38	963	5	0.005	0.002	1730	19	0.011	0.003	1595	15	0.009	0.003	703	23	0.033	0.008
39	973	18	0.018	0.005	1699	26	0.015	0.003	1608	21	0.013	0.003	1385	17	0.012	0.003
40	992	8	0.008	0.003	1727	24	0.014	0.003	1611	26	0.016	0.004	1642	17	0.010	0.003
41	1021	15	0.015	0.004	1568	21	0.013	0.003	1630	17	0.010	0.003	1127	21	0.019	0.005
42	985	12	0.012	0.004	1750	21	0.012	0.003	1673	19	0.011	0.003	591	21	0.036	0.009
43	1015	14	0.014	0.004	1804	23	0.013	0.003	1646	23	0.014	0.003	448	17	0.038	0.011
44	1037	15	0.014	0.004	1772	28	0.016	0.003	1714	22	0.013	0.003	397	24	0.060	0.015
45	1032	14	0.014	0.004	1832	19	0.010	0.003	1677	20	0.012	0.003	257	12	0.047	0.016
46	1132	13	0.011	0.004	1858	33	0.018	0.004	1799	27	0.015	0.003	223	10	0.045	0.017
47	1083	20	0.018	0.005	1809	19	0.011	0.003	1654	16	0.010	0.003	371	16	0.043	0.013
48	1038	9	0.009	0.003	1737	20	0.012	0.003	1637	20	0.012	0.003	1073	24	0.022	0.005
49	1023	20	0.020	0.005	1808	21	0.012	0.003	1643	21	0.013	0.003	2336	45	0.019	0.003
50	906	10	0.011	0.004	1669	31	0.019	0.004	1581	18	0.011	0.003	2607	51	0.020	0.003
51	996	18	0.018	0.005	1701	34	0.020	0.004	1586	22	0.014	0.003	1673	41	0.025	0.004
52	962	13	0.014	0.004	1741	21	0.012	0.003	1532	21	0.014	0.003	608	14	0.023	0.007
53	962	16	0.017	0.005	1699	21	0.012	0.003	1656	17	0.010	0.003	212	6	0.028	0.013
54	1019	18	0.018	0.005	1764	17	0.010	0.003	1653	25	0.015	0.003	118	13	0.110	0.041
55	979	16	0.016	0.005	1667	23	0.014	0.003	1602	20	0.012	0.003	129	13	0.101	0.037
56	949	15	0.016	0.005	1556	20	0.013	0.003	1448	20	0.014	0.003	123	26	0.211	0.061
57	867	12	0.014	0.004	1519	24	0.016	0.004	1358	29	0.021	0.005	297	170	0.572	0.077
58	828	13	0.016	0.005	1379	23	0.017	0.004	1264	17	0.013	0.004	717	485	0.676	0.056
59	801	15	0.019	0.005	1263	20	0.016	0.004	1179	20	0.017	0.004	1072	704	0.657	0.045
60	692	13	0.019	0.006	1212	38	0.031	0.006	1123	17	0.015	0.004	697	396	0.568	0.050
61	694	11	0.016	0.005	1199	19	0.016	0.004	1147	22	0.019	0.005	260	99	0.381	0.062
62	665	8	0.012	0.005	1144	23	0.020	0.005	1150	22	0.019	0.005	172	26	0.151	0.041
63	615	11	0.018	0.006	1312	34	0.026	0.005	1321	24	0.018	0.004	263	20	0.076	0.022
64	767	22	0.029	0.007	1462	40	0.027	0.005	1521	32	0.021	0.004	283	38	0.134	0.030
65	951	20	0.021	0.005	1626	63	0.039	0.006	1500	35	0.023	0.005	427	88	0.206	0.032
66	965	32	0.033	0.007	1451	72	0.050	0.007	1225	34	0.028	0.006	558	152	0.272	0.034

67	768	43	0.056	0.011	1295	65	0.050	0.008	1107	21	0.019	0.005	457	103	0.225	0.033
68	705	30	0.043	0.009	1151	49	0.043	0.007	1053	20	0.019	0.005	204	50	0.245	0.052
69	623	14	0.022	0.007	1084	31	0.029	0.006	1069	24	0.022	0.005	67	6	0.090	0.048
70	625	13	0.021	0.007	1062	21	0.020	0.005	993	19	0.019	0.005	47	5	0.106	0.063
71	644	21	0.033	0.008	1089	29	0.027	0.006	971	23	0.024	0.006	74	1	0.014	0.015
72	671	12	0.018	0.006	1068	15	0.014	0.004	1020	16	0.016	0.004	69	8	0.116	0.055
73	705	21	0.030	0.008	1052	26	0.025	0.006	1075	19	0.018	0.005	70	8	0.114	0.054
74	646	9	0.014	0.005	1107	18	0.016	0.004	1031	19	0.018	0.005	107	42	0.393	0.099
75	622	6	0.010	0.004	1032	25	0.024	0.006	998	20	0.020	0.005	268	194	0.724	0.096
76	680	14	0.021	0.006	1101	11	0.010	0.003	1121	21	0.019	0.005	449	389	0.866	0.085
77	653	20	0.031	0.008	1110	26	0.023	0.005	1168	22	0.019	0.005	381	291	0.764	0.084
78	690	12	0.017	0.006	1169	27	0.023	0.005	1027	14	0.014	0.004	162	106	0.654	0.115
79	652	14	0.021	0.007	1031	20	0.019	0.005	964	21	0.022	0.005	71	22	0.310	0.103
80	564	9	0.016	0.006	972	33	0.034	0.007	944	16	0.017	0.005	60	5	0.083	0.048
81	554	12	0.022	0.007	933	24	0.026	0.006	836	16	0.019	0.005	54	3	0.056	0.040
82	504	11	0.022	0.008	837	20	0.024	0.006	761	14	0.018	0.006	61	5	0.082	0.047
83	492	17	0.035	0.010	843	21	0.025	0.006	845	18	0.021	0.006	36	3	0.083	0.062
84	490	11	0.022	0.008	894	17	0.019	0.005	775	11	0.014	0.005	52	9	0.173	0.082
85	521	12	0.023	0.008	910	32	0.035	0.007	817	15	0.018	0.005	71	5	0.070	0.040
86	497	11	0.022	0.008	884	16	0.018	0.005	758	18	0.024	0.006	75	8	0.107	0.050
87	490	9	0.018	0.007	867	17	0.020	0.005	808	11	0.014	0.005	75	6	0.080	0.042
88	463	12	0.026	0.009	842	24	0.029	0.007	797	11	0.014	0.005	106	11	0.104	0.041
89	477	5	0.010	0.005	929	26	0.028	0.006	989	21	0.021	0.005	109	28	0.257	0.073
90	516	12	0.023	0.008	1488	23	0.015	0.004	1996	20	0.010	0.002	151	63	0.417	0.087
91	850	6	0.007	0.003	2733	37	0.014	0.002	3715	36	0.010	0.002	287	190	0.662	0.087
92	2062	17	0.008	0.002	4011	44	0.011	0.002	4165	55	0.013	0.002	441	298	0.676	0.071
93	3221	25	0.008	0.002	4256	84	0.020	0.002	3215	78	0.024	0.003	340	212	0.624	0.077
94	2312	44	0.019	0.003	3166	96	0.030	0.004	2317	77	0.033	0.004	194	94	0.485	0.085
95	1562	56	0.036	0.006	2099	96	0.046	0.006	1364	52	0.038	0.006	229	144	0.629	0.094
96	979	36	0.037	0.007	1217	56	0.046	0.007	714	17	0.024	0.007	392	258	0.658	0.074
97	434	18	0.041	0.012	675	27	0.040	0.009	476	17	0.036	0.010	501	329	0.657	0.066
98	313	12	0.038	0.013	518	19	0.037	0.010	497	11	0.022	0.008	290	142	0.490	0.070
99	276	11	0.040	0.014	543	26	0.048	0.011	540	9	0.017	0.006	114	31	0.272	0.074

100	326	11	0.034	0.012	633	28	0.044	0.010	643	16	0.025	0.007	63	8	0.127	0.061
101	402	11	0.027	0.010	581	25	0.043	0.010	579	18	0.031	0.009	35	5	0.143	0.088
102	361	6	0.017	0.008	537	19	0.035	0.010	438	14	0.032	0.010	43	0	0.000	0.000
103	254	6	0.024	0.011	441	15	0.034	0.010	425	15	0.035	0.011	50	4	0.080	0.051
104	220	11	0.050	0.018	526	10	0.019	0.007	550	12	0.022	0.007	45	3	0.067	0.048
105	332	8	0.024	0.010	605	14	0.023	0.007	658	7	0.011	0.004	49	13	0.265	0.111
106	425	9	0.021	0.008	695	26	0.037	0.009	627	15	0.024	0.007	105	54	0.514	0.120
107	351	12	0.034	0.012	620	14	0.023	0.007	573	17	0.030	0.008	190	103	0.542	0.093
108	286	8	0.028	0.012	630	22	0.035	0.009	698	13	0.019	0.006	278	125	0.450	0.067
109	370	15	0.041	0.013	839	22	0.026	0.006	1099	17	0.015	0.004	212	65	0.307	0.059
110	468	14	0.030	0.009	2021	50	0.025	0.004	3078	50	0.016	0.003	94	18	0.191	0.065
111	1509	28	0.019	0.004	4249	69	0.016	0.002	6001	102	0.017	0.002	45	3	0.067	0.048
112	3790	84	0.022	0.003	6013	92	0.015	0.002	5814	90	0.015	0.002	57	14	0.246	0.098
113	4268	64	0.015	0.002	5135	98	0.019	0.002	2810	36	0.013	0.002	124	68	0.548	0.116
114	2249	44	0.020	0.003	2515	51	0.020	0.003	897	13	0.014	0.005	494	255	0.516	0.056
115	647	12	0.019	0.006	770	23	0.030	0.007	319	10	0.031	0.012	1311	605	0.461	0.032
116	171	9	0.053	0.022	269	15	0.056	0.018	185	13	0.070	0.025	1836	602	0.328	0.021
117	110	8	0.073	0.033	201	8	0.040	0.017	182	10	0.055	0.021	1226	265	0.216	0.019
118	111	7	0.063	0.030	236	25	0.106	0.028	201	23	0.114	0.032	407	50	0.123	0.023
119	124	10	0.081	0.033	274	18	0.066	0.019	293	76	0.259	0.045	104	3	0.029	0.019
120	146	22	0.151	0.045	539	74	0.137	0.022	804	350	0.435	0.039	21	1	0.048	0.058
121	387	124	0.320	0.045	1285	267	0.208	0.019	1864	872	0.468	0.027	23	0	0.000	0.000
122	1053	534	0.507	0.038	1939	471	0.243	0.017	2096	1005	0.479	0.026	28	0	0.000	0.000
123	1578	939	0.595	0.034	1885	596	0.316	0.020	998	416	0.417	0.034	23	0	0.000	0.000
124	754	447	0.593	0.050	883	311	0.352	0.032	322	81	0.252	0.042	30	0	0.000	0.000
125	181	74	0.409	0.078	361	66	0.183	0.032	256	26	0.102	0.026	30	1	0.033	0.039
126	164	30	0.183	0.048	348	40	0.115	0.024	372	23	0.062	0.016	19	3	0.158	0.127
127	269	22	0.082	0.022	399	27	0.068	0.016	305	19	0.062	0.018	33	4	0.121	0.082
128	234	12	0.051	0.018	272	14	0.051	0.017	180	8	0.044	0.019	40	2	0.050	0.043
129	124	8	0.065	0.029	170	21	0.124	0.036	91	6	0.066	0.034	47	4	0.085	0.055
130	65	10	0.154	0.068	124	21	0.169	0.052	124	14	0.113	0.040	44	7	0.159	0.084
131	65	9	0.138	0.063	150	25	0.167	0.047	114	7	0.061	0.029	28	2	0.071	0.064
132	78	8	0.103	0.048	150	29	0.193	0.052	143	13	0.091	0.033	16	0	0.000	0.000

133	87	13	0.149	0.057	210	36	0.171	0.040	290	29	0.100	0.024	18	0	0.000	0.000
134	125	10	0.080	0.032	435	56	0.129	0.023	747	112	0.150	0.020	16	0	0.000	0.000
135	258	45	0.174	0.037	795	109	0.137	0.018	1157	168	0.145	0.015	24	1	0.042	0.050
136	522	67	0.128	0.021	963	145	0.151	0.017	1006	120	0.119	0.015	16	1	0.063	0.078
137	540	83	0.154	0.023	695	109	0.157	0.021	396	55	0.139	0.026	21	0	0.000	0.000
138	230	38	0.165	0.038	383	62	0.162	0.029	198	30	0.152	0.038	26	2	0.077	0.069
139	96	18	0.188	0.063	238	54	0.227	0.046	309	96	0.311	0.049	22	0	0.000	0.000
140	148	70	0.473	0.095	435	150	0.345	0.045	574	176	0.307	0.036	29	1	0.034	0.041
141	345	194	0.562	0.071	561	246	0.439	0.046	573	124	0.216	0.028	17	0	0.000	0.000
142	383	207	0.540	0.065	469	214	0.456	0.052	281	50	0.178	0.036	19	0	0.000	0.000
143	237	90	0.380	0.065	256	92	0.359	0.060	142	15	0.106	0.036	16	0	0.000	0.000
144	74	14	0.189	0.073	134	33	0.246	0.064	135	18	0.133	0.043	25	0	0.000	0.000
145	59	16	0.271	0.103	140	34	0.243	0.062	111	12	0.108	0.041	24	1	0.042	0.050
146	78	20	0.256	0.086	139	29	0.209	0.056	117	12	0.103	0.039	23	3	0.130	0.103
147	92	16	0.174	0.062	131	31	0.237	0.063	97	5	0.052	0.028	25	6	0.240	0.146
148	60	9	0.150	0.069	97	28	0.289	0.084	81	5	0.062	0.034	14	6	0.429	0.290
149	51	8	0.157	0.077	110	20	0.182	0.058	101	10	0.099	0.041	24	4	0.167	0.117
150	52	9	0.173	0.082	108	26	0.241	0.070	95	13	0.137	0.052	19	2	0.105	0.099
151	65	13	0.200	0.080	95	33	0.347	0.096	89	8	0.090	0.041	18	0	0.000	0.000
152	49	10	0.204	0.094	116	25	0.216	0.063	95	7	0.074	0.035	7	0	0.000	0.000
153	54	9	0.167	0.078	99	23	0.232	0.072	78	4	0.051	0.031	16	0	0.000	0.000
154	40	9	0.225	0.111	91	24	0.264	0.081	81	11	0.136	0.056	17	0	0.000	0.000
155	41	11	0.268	0.123	156	55	0.353	0.076	175	41	0.234	0.054	17	0	0.000	0.000
156	79	38	0.481	0.132	314	196	0.624	0.080	535	151	0.282	0.035	14	0	0.000	0.000
157	196	122	0.622	0.101	763	534	0.700	0.056	1031	224	0.217	0.021	14	0	0.000	0.000
158	620	378	0.610	0.056	1035	812	0.785	0.052	985	161	0.163	0.018	11	0	0.000	0.000
159	706	368	0.521	0.047	873	702	0.804	0.058	466	55	0.118	0.021	9	0	0.000	0.000
160	307	134	0.436	0.063	468	354	0.756	0.075	311	93	0.299	0.048	13	0	0.000	0.000
161	144	71	0.493	0.100	553	389	0.703	0.066	842	236	0.280	0.028	8	0	0.000	0.000
162	407	302	0.742	0.079	1211	965	0.797	0.049	1652	317	0.192	0.015	10	0	0.000	0.000
163	1097	658	0.600	0.041	1622	1358	0.837	0.044	1458	178	0.122	0.012	12	0	0.000	0.000
164	1181	590	0.500	0.035	1228	1029	0.838	0.050	520	37	0.071	0.015	13	0	0.000	0.000
165	413	161	0.390	0.050	479	380	0.793	0.077	162	8	0.049	0.021	15	0	0.000	0.000

166	83	18	0.217	0.075	117	55	0.470	0.107	62	2	0.032	0.027	12	0	0.000	0.000
167	33	4	0.121	0.082	67	19	0.284	0.100	57	5	0.088	0.051	7	0	0.000	0.000
168	32	8	0.250	0.133	60	13	0.217	0.088	65	6	0.092	0.049	3	0	0.000	0.000
169	42	5	0.119	0.072	64	20	0.313	0.109	73	1	0.014	0.015	2	0	0.000	0.000
170	37	3	0.081	0.060	68	17	0.250	0.091	61	3	0.049	0.035	4	0	0.000	0.000
171	36	7	0.194	0.106	99	31	0.313	0.088	75	6	0.080	0.042	8	0	0.000	0.000
172	51	10	0.196	0.089	108	58	0.537	0.122	152	27	0.178	0.049	10	0	0.000	0.000
173	53	21	0.396	0.141	296	212	0.716	0.091	451	54	0.120	0.022	12	0	0.000	0.000
174	208	108	0.519	0.086	625	459	0.734	0.064	879	70	0.080	0.012	8	0	0.000	0.000
175	558	252	0.452	0.048	911	700	0.768	0.055	815	36	0.044	0.009	8	0	0.000	0.000
176	683	223	0.327	0.034	767	564	0.735	0.058	407	13	0.032	0.010	10	0	0.000	0.000
177	298	67	0.225	0.040	322	200	0.621	0.079	151	7	0.046	0.021	11	0	0.000	0.000
178	74	17	0.230	0.082	146	75	0.514	0.102	159	8	0.050	0.022	5	0	0.000	0.000
179	68	16	0.235	0.087	149	71	0.477	0.096	213	12	0.056	0.020	12	0	0.000	0.000
180	103	31	0.301	0.084	433	302	0.697	0.074	571	91	0.159	0.023	11	0	0.000	0.000
181	211	103	0.488	0.082	1612	1262	0.783	0.042	2560	230	0.090	0.008	12	0	0.000	0.000
182	1072	681	0.635	0.044	4929	3864	0.784	0.024	7544	419	0.056	0.003	8	0	0.000	0.000
183	4137	2024	0.489	0.018	8902	6568	0.738	0.017	10529	276	0.026	0.002	5	0	0.000	0.000
184	7721	2412	0.312	0.010	9527	6767	0.710	0.016	6503	79	0.012	0.002	10	0	0.000	0.000
185	5363	1040	0.194	0.009	5745	3803	0.662	0.019	1753	6	0.003	0.001	7	0	0.000	0.000
186	1273	114	0.090	0.011	1494	897	0.600	0.036	255	0	0.000	0.000	4	0	0.000	0.000
187	120	13	0.108	0.040	191	106	0.555	0.094	42	0	0.000	0.000	9	0	0.000	0.000
188	29	1	0.034	0.041	43	10	0.233	0.109	26	0	0.000	0.000	5	0	0.000	0.000
189	15	0	0.000	0.000	33	4	0.121	0.082	34	0	0.000	0.000	6	0	0.000	0.000
190	13	0	0.000	0.000	33	4	0.121	0.082	37	0	0.000	0.000	6	0	0.000	0.000
191	10	0	0.000	0.000	27	0	0.000	0.000	19	0	0.000	0.000	12	0	0.000	0.000
192	18	0	0.000	0.000	27	1	0.037	0.044	40	0	0.000	0.000	6	0	0.000	0.000
193	14	0	0.000	0.000	21	2	0.095	0.088	27	0	0.000	0.000	6	0	0.000	0.000
194	14	0	0.000	0.000	36	0	0.000	0.000	25	0	0.000	0.000	9	0	0.000	0.000
195	10	0	0.000	0.000	24	0	0.000	0.000	20	0	0.000	0.000	4	0	0.000	0.000
196	16	0	0.000	0.000	19	0	0.000	0.000	14	0	0.000	0.000	10	0	0.000	0.000
197	7	0	0.000	0.000	26	1	0.038	0.046	24	0	0.000	0.000	1	0	0.000	0.000
198	15	0	0.000	0.000	14	0	0.000	0.000	28	0	0.000	0.000	10	0	0.000	0.000

199	13	0	0.000	0.000	37	0	0.000	0.000	18	0	0.000	0.000	4	0	0.000	0.000
200	11	0	0.000	0.000	31	1	0.032	0.038	18	0	0.000	0.000	0	0	0.000	0.000
201	10	0	0.000	0.000	33	3	0.091	0.068	37	2	0.054	0.047	5	0	0.000	0.000
202	22	2	0.091	0.084	29	7	0.241	0.136	49	3	0.061	0.044	4	0	0.000	0.000
203	29	4	0.138	0.095	56	13	0.232	0.095	37	1	0.027	0.031	5	0	0.000	0.000
204	35	3	0.086	0.064	37	6	0.162	0.093	28	2	0.071	0.064	4	0	0.000	0.000
205	23	2	0.087	0.080	28	3	0.107	0.082	21	0	0.000	0.000	4	0	0.000	0.000
206	9	0	0.000	0.000	21	0	0.000	0.000	15	0	0.000	0.000	5	0	0.000	0.000
207	9	0	0.000	0.000	21	0	0.000	0.000	17	0	0.000	0.000	2	0	0.000	0.000
208	8	0	0.000	0.000	23	0	0.000	0.000	15	0	0.000	0.000	3	0	0.000	0.000
209	12	0	0.000	0.000	12	0	0.000	0.000	17	0	0.000	0.000	1	0	0.000	0.000
210	12	0	0.000	0.000	7	0	0.000	0.000	13	0	0.000	0.000	4	0	0.000	0.000
211	10	0	0.000	0.000	15	0	0.000	0.000	21	0	0.000	0.000	1	0	0.000	0.000
212	11	0	0.000	0.000	12	0	0.000	0.000	14	0	0.000	0.000	0	0	0.000	0.000
213	9	0	0.000	0.000	16	0	0.000	0.000	15	0	0.000	0.000	5	0	0.000	0.000
214	6	0	0.000	0.000	19	0	0.000	0.000	17	0	0.000	0.000	2	0	0.000	0.000
215	10	0	0.000	0.000	11	0	0.000	0.000	12	0	0.000	0.000	1	0	0.000	0.000
216	10	0	0.000	0.000	13	0	0.000	0.000	12	0	0.000	0.000	2	0	0.000	0.000
217	13	0	0.000	0.000	19	0	0.000	0.000	19	0	0.000	0.000	2	0	0.000	0.000
218	15	0	0.000	0.000	19	0	0.000	0.000	18	0	0.000	0.000	5	0	0.000	0.000
219	17	0	0.000	0.000	13	0	0.000	0.000	17	0	0.000	0.000	5	0	0.000	0.000
220	11	0	0.000	0.000	22	1	0.045	0.055	7	0	0.000	0.000	2	0	0.000	0.000
221	5	0	0.000	0.000	22	1	0.045	0.055	21	0	0.000	0.000	6	0	0.000	0.000
222	14	0	0.000	0.000	10	0	0.000	0.000	10	0	0.000	0.000	0	0	0.000	0.000
223	6	0	0.000	0.000	13	0	0.000	0.000	13	0	0.000	0.000	3	0	0.000	0.000
224	9	0	0.000	0.000	18	0	0.000	0.000	10	0	0.000	0.000	5	0	0.000	0.000
225	9	0	0.000	0.000	23	0	0.000	0.000	12	0	0.000	0.000	3	0	0.000	0.000
226	5	0	0.000	0.000	11	0	0.000	0.000	7	0	0.000	0.000	1	0	0.000	0.000
227	3	0	0.000	0.000	12	0	0.000	0.000	10	0	0.000	0.000	1	0	0.000	0.000
228	9	0	0.000	0.000	12	0	0.000	0.000	7	0	0.000	0.000	2	0	0.000	0.000
229	7	0	0.000	0.000	15	0	0.000	0.000	15	0	0.000	0.000	4	0	0.000	0.000
230	11	0	0.000	0.000	11	0	0.000	0.000	11	0	0.000	0.000	3	0	0.000	0.000
231	6	0	0.000	0.000	14	1	0.071	0.091	9	0	0.000	0.000	2	0	0.000	0.000

232	8	0	0.000	0.000	16	0	0.000	0.000	7	0	0.000	0.000	1	0	0.000	0.000
233	4	0	0.000	0.000	8	0	0.000	0.000	14	0	0.000	0.000	4	0	0.000	0.000
234	7	0	0.000	0.000	18	0	0.000	0.000	9	0	0.000	0.000	2	0	0.000	0.000
235	3	0	0.000	0.000	15	0	0.000	0.000	10	0	0.000	0.000	0	0	0.000	0.000
236	8	0	0.000	0.000	7	0	0.000	0.000	10	0	0.000	0.000	0	0	0.000	0.000
237	6	0	0.000	0.000	7	0	0.000	0.000	10	0	0.000	0.000	3	0	0.000	0.000
238	4	0	0.000	0.000	4	0	0.000	0.000	8	0	0.000	0.000	3	0	0.000	0.000
239	4	0	0.000	0.000	13	0	0.000	0.000	11	0	0.000	0.000	1	0	0.000	0.000
240	7	0	0.000	0.000	13	0	0.000	0.000	9	0	0.000	0.000	4	0	0.000	0.000
241	6	0	0.000	0.000	8	0	0.000	0.000	4	0	0.000	0.000	0	0	0.000	0.000
242	3	0	0.000	0.000	7	0	0.000	0.000	7	0	0.000	0.000	0	0	0.000	0.000
243	7	0	0.000	0.000	11	0	0.000	0.000	9	0	0.000	0.000	0	0	0.000	0.000
244	7	0	0.000	0.000	10	0	0.000	0.000	12	0	0.000	0.000	1	0	0.000	0.000
245	6	0	0.000	0.000	6	0	0.000	0.000	12	0	0.000	0.000	0	0	0.000	0.000
246	6	0	0.000	0.000	9	0	0.000	0.000	3	0	0.000	0.000	0	0	0.000	0.000
247	3	0	0.000	0.000	4	0	0.000	0.000	6	0	0.000	0.000	0	0	0.000	0.000
248	5	0	0.000	0.000	6	0	0.000	0.000	6	0	0.000	0.000	1	0	0.000	0.000
249	8	0	0.000	0.000	6	0	0.000	0.000	11	0	0.000	0.000	1	0	0.000	0.000
250	2	0	0.000	0.000	6	0	0.000	0.000	7	0	0.000	0.000	2	0	0.000	0.000
251	3	0	0.000	0.000	10	0	0.000	0.000	6	0	0.000	0.000	2	0	0.000	0.000
252	8	0	0.000	0.000	7	0	0.000	0.000	5	0	0.000	0.000	1	0	0.000	0.000
253	4	0	0.000	0.000	7	0	0.000	0.000	4	0	0.000	0.000	4	0	0.000	0.000
254	1	0	0.000	0.000	8	1	0.125	0.169	2	0	0.000	0.000	0	0	0.000	0.000
255	1	0	0.000	0.000	3	0	0.000	0.000	3	0	0.000	0.000	1	0	0.000	0.000
256	61790	373	0.006	0.000	*****	528	0.005	0.000	99164	589	0.006	0.000	39174	879	0.022	0.001

REFERENCES

(Aj 79) F. Ajzenberg-Selove, Nucl. Phys. A320, (1979) 175-177.

(Aj 84) F. Ajzenberg-Selove, Nucl. Phys. A413, (1984) 140-151.

(Al 66) D.E. Alberger et al, Phys. Rev. 143, (1966) 692.

(Ar 86) R.A. Aryainejad, Annual Research Report 1985-86, University of Manitoba Cyclotron Laboratory, Winnipeg, Canada.

(Au 69) L.S. August et al, Phys. Rev. Lett. 23, (1969) 537.

(Be 69) P.R. Bevington, "Data Reduction and Error Analysis for the Physical Sciences", McGraw-Hill, New York, (1969).

(Bl 63) H.R. Bleiden, Phys. Lett. 3, (1963) 257.

(Bo 57) T.E. Bortner et al, Rev. Sci. Instr. 28, (1957) 103.

(Ch 79) G. Charpak and F. Sauli, Nucl. Instr. Meth. 162, (1979) 405.

(Ch 84) G. Charpak and F. Sauli, "High Resolution Electronic Particle Detectors", CERN, 1984.

(Gl 71) J.E. Glenn et al, Phys. Rev. Lett. 26, (1971) 328.

(Gl 61) A. Glassner, "Introduction to Nuclear Science", 1961.

(Gu 71) P. Guazzoni et al, Phys. Rev. c4, (1971) 1092.

(Hi 67) S. Hinds et al, Phys. Lett. 24B, (1967) 34.

(Ja 66) J.F. Janni, "Calculations of Energy Loss, Range, Pathlength, Straggling, Multiple Scattering, and the Probability of Inelastic Nuclear Collisions for 0.1-to 1000-MeV Protons", Air Force Weapons Laboratory, Kirtland Air Force Base, New Mexico, (1966).

(Ke 79) J. Keinonen and A. Anttila, Nucl. Phys. A330, (1979) 397.

(Kl 71) O. Klemperer, "Electron Optics", 1971.

(Ko 68) E.J. Kobetich and R. Katz, Phys. Rev. 170, (1968) 391.

(Ma 75a) R.G. Markham and R.G.H. Robertson, Nucl. Instr. Meth. 129, (1975) 131-140.

(Ma 75b) R.G. Markham et al, Nucl. Instr. Meth. 129, (1975) 141-145.

(Ma 71) C.C. Maples, "Systematics of the Direct (p,) Reactions", Ph.D. Thesis, Lawrence Berkeley Laboratory, UCLA, (1971).

(Ne 85) J.E. Nelson et al, Phys. Rev. C31, (1985) 2295.

(Pr 64) W.J. Price, "Nuclear Radiation Detection", Office of Aerospace Research, USAF, 1964.

(Sa 84) D.C. Santry and R.D. Werner, Nucl. Instr. Meth. B1, (1984).

(Sa 75) H. Sann et al, Nucl. Instr. Meth. 124,(1975) 509-519.

(Sa 64) G.R. Satchler, Nucl. Phys. 55, (1964) 1.

(Sa 77) F. Sauli, "Principles of Operation of Multiwire Proportional and Drift Chambers", CERN, 1977.

(Se 77) E. Segre`, "Nuclei and Particles", second edition, 1977.

(Se 67) A. Septier, "Focusing of Charged Particles", volume 1, (1967).

(Va 75) P. Vavilov, Zh. Eksp. Theor. Fis. 32, (1975)920.